Poly(glycoamidoamine)s: Understanding Their Structure and Structure-Bioactivity Relationships

Vijay P. Taori

Dissertation submitted to the faculty of the Virginia Polytechnic Institute and State University in partial fulfillment of the requirements for the degree of

Doctor of Philosophy
In
Chemistry

Theresa M. Reineke, Chair
Timothy E. Long, Member
Robert B. Moore, Member
Abby W. Morgan, Member
Judy S. Riffle, Member
Garth L. Wilkes, Member

July 7, 2010
Blacksburg, Virginia

Keywords: Non-viral DNA Delivery, Poly(glycoamidoamine), Polymer degradation, amide Hydrolysis, Layer-by-layer, Sustained release, Guanidine, Structure-bioactivity relationship

Poly(glycoamidoamine)s: Understanding their Structure and Structure-Bioactivity Relationships

Vijay P. Taori

ABSTRACT

In order to achieve effective therapeutic effects, it is essential to understand the structure of biomaterials that are intended for use in therapeutic delivery systems. This study investigated the hydrolysis patterns of plasmid DNA (pDNA) delivery vehicles comprised of poly(glycoamidoamine)s (PGAAs) under physiological conditions, as well as how subtle changes in the chemical structure of the PGAAs could impact their biological performance.

The unusual hydrolysis behaviors of tartarate- and galactarate-based PGAAs were investigated by studying the hydrolysis of small model molecules that mimic the repeat unit of the respective polymers. In the case of tartarate-and galactarate-based molecules with terminal amines, faster hydrolysis of the amide bonds was observed. Additionally, for the tartarate-based compounds, we confirmed that terminal amine functionality was necessary for intramolecular hydrolysis to occur. The model compounds used in this study consisted of two amide bonds, which were designed to be symmetric. However, we showed that the amide bond on only one side of the tartarate moiety underwent hydrolysis. Further studies revealed that one side of the amine facilitated the hydrolysis of the amide bond on the other side of the tartarate moiety.

Degradation studies of poly(L-tartaramidopentaethylenetetramine) (**T4**) were used to investigate the sustained release of pDNA from the layer-by-layer constructs of **T4**/pDNA. The thickness of the constructs was characterized by ellipsometry, while UV-visible spectroscopy was used to characterize the loading capacity of the pDNA constructs. The indirect sustained release of pDNA under physiological conditions with respect to time was characterized by cellular uptake studies using HeLa cells. Specifically, an increase in the uptake of Cy5 labeled

pDNA was observed over a period of eleven days. The integrity of the sustained released pDNA for the transgene expression was characterized via an assay in order to observe the expression of the green fluorescent protein (GFP) from the **T4**/GFP-pDNA layer-by-layer constructs.

This research also confirmed that PGAAs can facilitate the efficient delivery of pDNA in a non-toxic manner. We found that the chemical structure of the polymer impacts both pDNA binding behavior, as well as the release of pDNA from polymer-pDNA complexes. In order to better understand the fundamentals of nucleic acid delivery—and therefore the design of nucleic acid delivery vehicles—subtle changes in the chemical structure of PGAAs were designed and studied for their biological activity. The effect of charge type was investigated by designing and synthesizing guanidine-based polymer series analogues to galactarate- and tartarate-based PGAAs (**G1** and **T1**), which incorporate secondary amines as the charge type on the polymer backbone. The guanidine-based polymer series, poly(glycoamidoguanidine)s (PGAGs), showed highly non-toxic behaviors in HeLa cells at the various polymer-to-pDNA ratios (*N/P* ratio) studied. Interestingly, PGAGs are the only non-toxic, guanidine-containing polymers that have been reported in the literature to date. This investigation also confirmed that the cellular uptake of pDNA assisted by PGAGs was a little higher compared to the PGAAs studied —although both series of polymers showed similar transgene expression. The transgene expression of the PGAGs we investigated also implies the release of polymer-pDNA complexes from the endosome. In another study that looked at the structure-bioactivity relationship based on the degree of polymerization (DP) of poly(galactaramidopentaethylenetetramine) (**G4**), it was found that an increase in the DP of the G4 increased the toxicity of polymers in HeLa cells.

ACKNOWLEDGEMENTS

I would foremost like to thank my advisor, Dr. Theresa M. Reineke, for her guidance and inspiration throughout my doctoral career. She has built a tremendous environment that encourages collaborative work, while at the same time fostering independent and critical thinking. Dr. Reineke's direction over the years has helped me excel as an independent scientist. I would also like to thank my committee members here at Virginia Tech—Dr. Timothy E. Long, Dr. Robert B. Moore, Dr. Abby W. Morgan and Dr. Judy S. Riffle—for their direction and support. My gratitude also goes to Dr. Joseph A. Caruso and Dr. James E. Mack at the University of Cincinnati for their advice. In addition, I thank Dr. Garth L. Wilkes at Virginia Tech for substituting for one of my committee members in my defense. I am grateful to all my committee members for their comments and suggestions—and for challenging me to think more critically.

I would also like to thank Dr. James Tanko and Dr. Paul Carlier at Virginia Tech for taking an interest in my research and for their useful comments and suggestions about how to experimentally validate my theories. I would like to thank Dr. Timothy Long and Ms. Mana Tamami for their help in polymer characterization using GPC. A special thanks goes to the mass spec facilities at both Virginia Tech and the University of Cincinnati—and in particular Dr. Stephen Macha, Dr. Larry Sallans, Dr. Mehdi Ashraf-Khorassani and Mr. William Bebout—for their assistance in characterizing small molecules, and Dr. Carla Slebodnick for X-ray crystallography.

I am especially grateful to senior members of the Reineke group (Dr. Chris Gulgas, Dr. Sathya Srinivasachari and Dr. Yemin Liu) for their guidance in helping me to transition from engineering to the pure sciences. I also thank Dr. Lisa E. Prevette and Dr. Patrick McLendon

who have become two of my best friends during my during my doctoral years. I am thankful to Dr. Chen-Chang Lee and Antons Sizovs for their insightful discussions about science and philosophy. I would also like to thank Dr. Adam Smith and Dr. Nilesh Ingle for their input—I am fortunate to have had a chance to interact with them. Special thanks go to Hao Lu for very interesting discussions, collaboration, and help in my research endeavors. I would be remiss if I did not acknowledge the friendship and support of Ms. Giovanna Grandinetti—I will always remember her help on New Year's Eve 2009 to get a paper published!

Most importantly, I would like to thank my family for always believing in me and their support in my every decision. I especially acknowledge my mother (Jamuna), my father (Purushottam), and my grandmother (Gaurabai) for their sacrifices and for teaching me the importance of science. I also want to thank my brothers, Shyam and Anand, who have always been there for me when I needed them and are two of my best friends. I am also thankful to my family and friends, Harsha, Preeti, and Sarika, for their significant support—and especially for helping to look out for my parents when I was thousands of miles away from them.

Finally, I would like to give a special thanks to my brother, Sudhir, who has not only helped me in my early life but also, taught me how to lead by example. He showed me what a positive attitude can do, and his unwavering trust in me helped to make this achievement possible.

Table of Contents

List of Figures

List of Tables

List of Schemes

Chapter 1

Introduction

Over the last few decades, a variety of novel biocompatible materials (biomaterials) have found increasing applications in the area of therapeutics. The ability of biomaterials to cross various barriers in biological systems in order to achieve specific therapeutic effects makes them noteworthy for advanced fundamental studies. For example, non-viral nucleic acid delivery and drug delivery are two of the most important fields for which scientists are designing medicines of the future. In order to achieve efficient therapeutic effects, however, one must be able to control the specificity and structural architecture of these materials, thereby facilitating the development of multi-functional therapeutic carriers.

This dissertation is dedicated towards understanding the structure and structure-bioactivity relationships of poly(glycoamidoamine)s (PGAAs), a very well established group of biomaterials with potential for DNA delivery vehicles. In addition to designing more effective DNA delivery vehicles, these materials could be used to design a new class of biomaterials with improved selectivity and biodegradability.

The dissertation is organized in distinct sections that focus on the different research efforts conducted during this Ph.D. study. Chapter 2 represents a thorough literature review of cationic polymer-based DNA delivery, biodegradable polymers as biomaterials, and layer-by-layer technology for achieving the sustained release of therapeutics. Chapter 3 discusses the biodegradability of poly(L-tartaramidoamine)s and poly(*meso*-galactaramidoamine)s, two polymer series based upon tartarate and *meso*-galactarate carbohydrate moieties, respectively. This chapter also details the inspiration for and importance of this study, the design of the project and associated experiments that were developed to answer the various research questions, as well as one of the most

important inventions that emerged from this study. Chapter 4 is based on one of the applications connected to the biodegradibility of poly(L-tartaramidopentaethylenetetramine) (**T4**) for the sustained release of pDNA from the layer-by-layer constructs of **T4**/pDNA. This chapter, which points to the multi-disciplinary nature of this research, also investigates the non-viral delivery vehicle, **T4.** Chapter 4 also explains the design, manufacture, and characterization of **T4**/pDNA bilayer constructs. The biological experiments discussed herein were designed to characterize the sustained release of pDNA from the bilayer constructs under physiological conditions, as well as to corroborate the integrity of pDNA for transgene expression after its release.

Chapter 5 investigates the structure-bioactivity relationships of various PGAAs. In this chapter, a second generation polymer series of PGAAs were designed, synthesized and characterized. These polymers differ in their very subtle chemical compositions, which is associated with the charge type (i.e., amine versus guanidine). The aim of this chapter is to understand if there are any effects on biological activity with respect to the chemical composition of the delivery vehicle. It includes a detailed explanation of the rationale, design, synthesis and characterization of small molecules, the synthesis and characterization of polymers, characterization of polymer-pDNA complexes (polyplexes), as well as a discussion of the biological activity of the polyplexes in HeLa cells. Finally, Chapter 6 addresses the implications of this research—and in particular how it can be applied toward the design and development of more effective biomaterials for various applications.

Chapter 2

Next generation therapeutic carriers: Controlled release, selectivity, and biodegradability

2.1 - Therapeutic materials

Over the last few decades, medical research has expanded into new and interesting fields in the area of therapeutics [1-7]. In fact, collaborations in chemistry, biology, pharmacokinetics, medicine, materials science, and engineering are pushing the field in revolutionary directions [1, 5-8]. Currently, various studies in the fields of drug delivery [2], nucleic acid delivery [9-11], and tissue engineering [2, 6] look very promising and have already resulted in documented achievements [10, 11] and interesting prospects [10, 12]. Although a variety of chemical compounds, proteins and biomacromolecules have the potential to be used as therapeutics, efficient delivery systems are needed to achieve specific therapeutic effects at the desired target. For this reason, this study investigates various materials that have been used as delivery vehicles to understand and to better design of new materials.

Numerous factors need to be considered when designing the new delivery systems since the intended therapeutic effect may be compromised by a number of factors, such as the hydrophobicity of the drug [13], enzymatic degradation [14], and various other biological barriers [15]. Materials such as cyclodextrin [16], poly(ethylene glycol) (PEG) [17], copolymers [8], hydrogels [18], dendrimers [19] are strategically designed to compact and deliver specific therapeutic compounds into biological systems. The design of these systems has used various different rationales for increasing certain bioactivity aspects of the vehicles. These design considerations include the complexing of delivery vehicles with therapeutics by ionic interaction [20-25], or the incorporation of cytotoxic drugs in the core of the copolymeric micelles [8]. In order to increase the circulation time of the conjugates in a biological system, PEGylation is often used, which involves

incorporating hydrophilic PEG groups on the surface of the bioconjugates to avoid non-specific uptake or clearance of bioconjugates via reticuloendothelial system (RES). The ability of the acetal functionality to hydrolyze at lower pH levels has inspired scientists to use acetal polymers for faster hydrolysis in lysosomes (pH 5.5) and endosomes (pH 6.0)—as compared to physiological pH (7.4)—for improved release of conjugates in a cellular environment [26, 27]. Similarly, Szoka *et al.* reviewed a variety of biomaterials for drug and gene delivery, which can be triggered by changes in pH, redox potential and temperature [28]. As documented in a related study, an enzymatic trigger can be incorporated in the architecture of the biomaterial (Figure 2.1), which can result in the release of conjugates based on the level of enzyme to achieve the desired specificity [29].

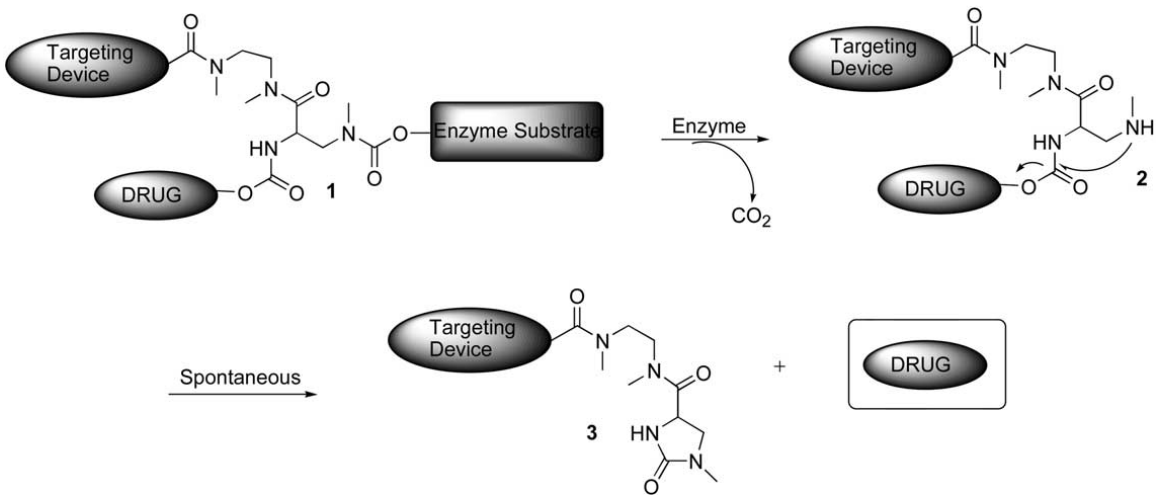

Figure 2.1 General mechanism of drug release starting with specific enzymatic cleavage. Figure adapted from Gopin et al. (Bioorganic & Medicinal Chemistry12 (2004) 1853–1858)

Specific delivery of bioconjugates to the target cell or tissue type is preferred, which is due to the fact that non-specific delivery is more likely to result in the elimination of conjugates by reticuloendothelial system (RES) clearance. Hence, Different targeting moieties such as sugar

residues [30], PEGpeptides [31], and antibodies [32] can be incorporated in the architecture of a delivery vehicle, which can then be recognized by the specific cell surface receptor in order to increase delivery efficacy. Figure 2.2 shows a schematic diagram explaining cell-specific targeted delivery and non-specific delivery in breast cancer tumors [13].

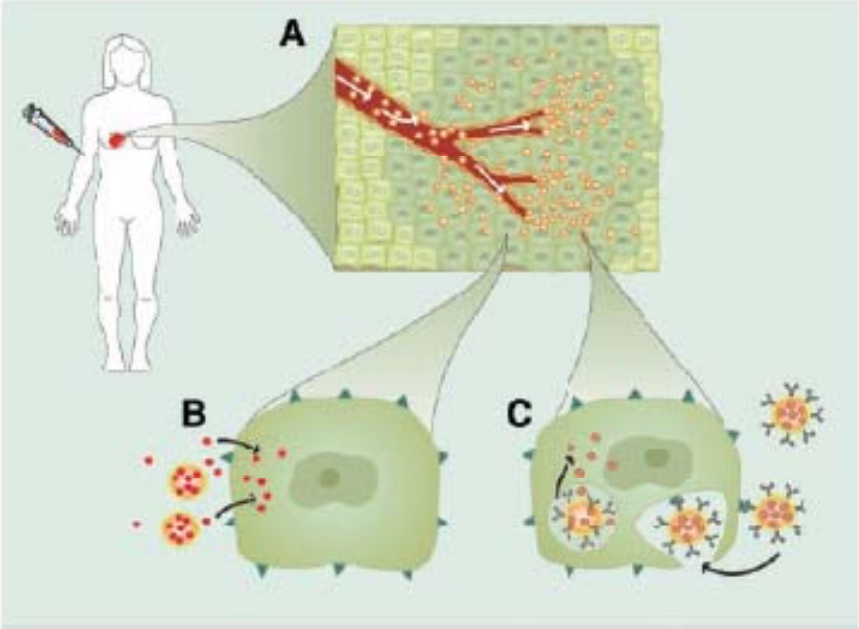

Figure 2.2 Schematic diagram for the delivery system depicting the cell specific targeted delivery and non-specific delivery. Figure adapted from Allen et al.

. As shown in the figure, bioconjugates incorporating anticancer therapeutics in the blood stream enter the tumor tissue area (dark green) from the gaps in vascular endothelial cells (A). The bioconjugates are subsequently taken up by the cell surface via non-specific interactions, after which the therapeutic is released in the cells (B). Then, in case of cell-specific targeted drug delivery, bioconjugates with a targeting moiety (antibody or carbohydrate based) bind to the receptors (dark green triangles) on the cell surface. This will increase the internalization of the bioconjugates, thereby highly

influencing the results [13]. Imaging techniques in the area of therapeutic delivery are very important since they help the researcher visualize and document the various processes that occur, as well as afford a more detailed understanding of the biological systems that are impacted by drug delivery. The delivery vehicle plays the central role in therapeutic drug delivery, although a little is known about how the delivery vehicle functions inside a biological system [33]. For example, theranostic materials afford the ability to image and track the delivery of therapeutics. Lanthanide based biomaterials [33] and quantum dots (QDs) [34] are currently used as theranostic biomaterials. Figure 2.3a depicts a very interesting smart delivery vehicle that incorporates different important capabilities for therapeutic delivery. QDs offer more surface area, which can also be functionalized to link the therapeutic agents. The PEG groups on the QDs provide sheathing from the RES clearance. This delivery vehicle also incorporates affinity ligands, such as antibodies, which can actively target tumor cells [34]. The lack of a tumor-targeting antibody result in low uptake of the functionalized QDs (Figure 2.3-b,c). The goal drug delivery design, therefore, is to understand and overcome every hurdle that can compromise the desired therapeutic effect in various biological systems.

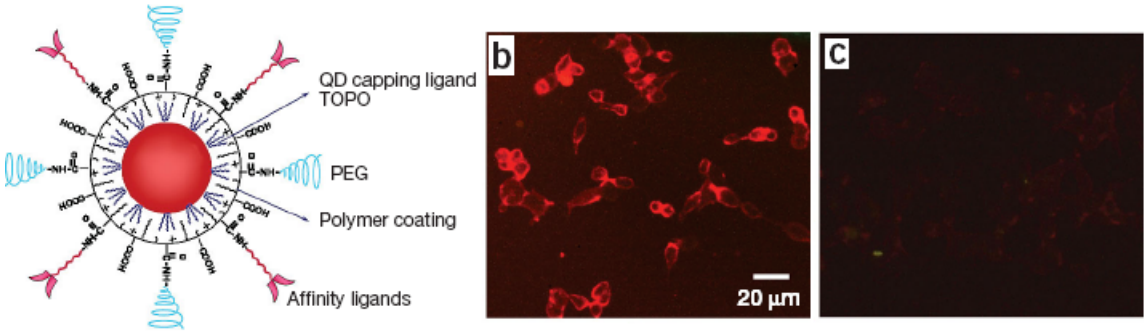

Figure 2.3 Smart biomaterial. a) Delivery vehicle based on quantum dots (QDs) offers active tumor targeting, sheathing offered by PEG groups to avoid RES clearance and imaging capability. b) QDs functionalized with PEG groups and prostate-specific membrane antigen (PSMA) monoclonal antibody (Ab). c) QDs functionalized with PEG groups but lack PSMA-Ab. Figure adapted from Gao *et al.*

2.2 - Degradable biomaterials

Biomaterials play an essential role in therapeutic delivery since they assist the therapeutic agent in crossing various biological barriers so that it can reach the target tissue or cell type in order to achieve a specific therapeutic effect. In addition to delivering the biomaterial, it is also important to consider how to eliminate a biomaterial from a biological system since it can interact with different cellular components based on certain parameters (e.g., ionic, hydrophophic, hydrophilic, etc.). A macromolecule or a polymer can offer multi-functionality and is preferred as a smart biomaterial over small molecules. However, the elimination the polymer is a significant issue due to size and, in many cases, its non-degradability. As a result of the cooperativity effect from polymers, their interaction with cellular components can be significant. Therefore, the degradability of the polymeric biomaterial is an important consideration in a biological system due to the threat of bioaccumulation [35, 36] in various organs, thereby resulting in cytotoxicity.

Because they have evolved over billions of years, complex cellular mechanisms are capable of metabolizing various small molecules such as carbohydrates, oligoamines (e.g., spermine, spermidine), urea, and ammonium ions present in certain concentrations. Certain types of polymers which can be disintegrated into small molecules that do not increase cytotoxicity may possess advantages over the polymers that are incapable of biodegradation. Figure 2.4 summarizes various different biodegradable plasmid delivery vehicles. Poly(4-hydroxy-L-proline ester) (PHP) was the first-ever water soluble, biodegradable, cationic polymer that was reported by two different groups (Langer and co-workers, and Park and co-workers) [37, 38] in 1999.

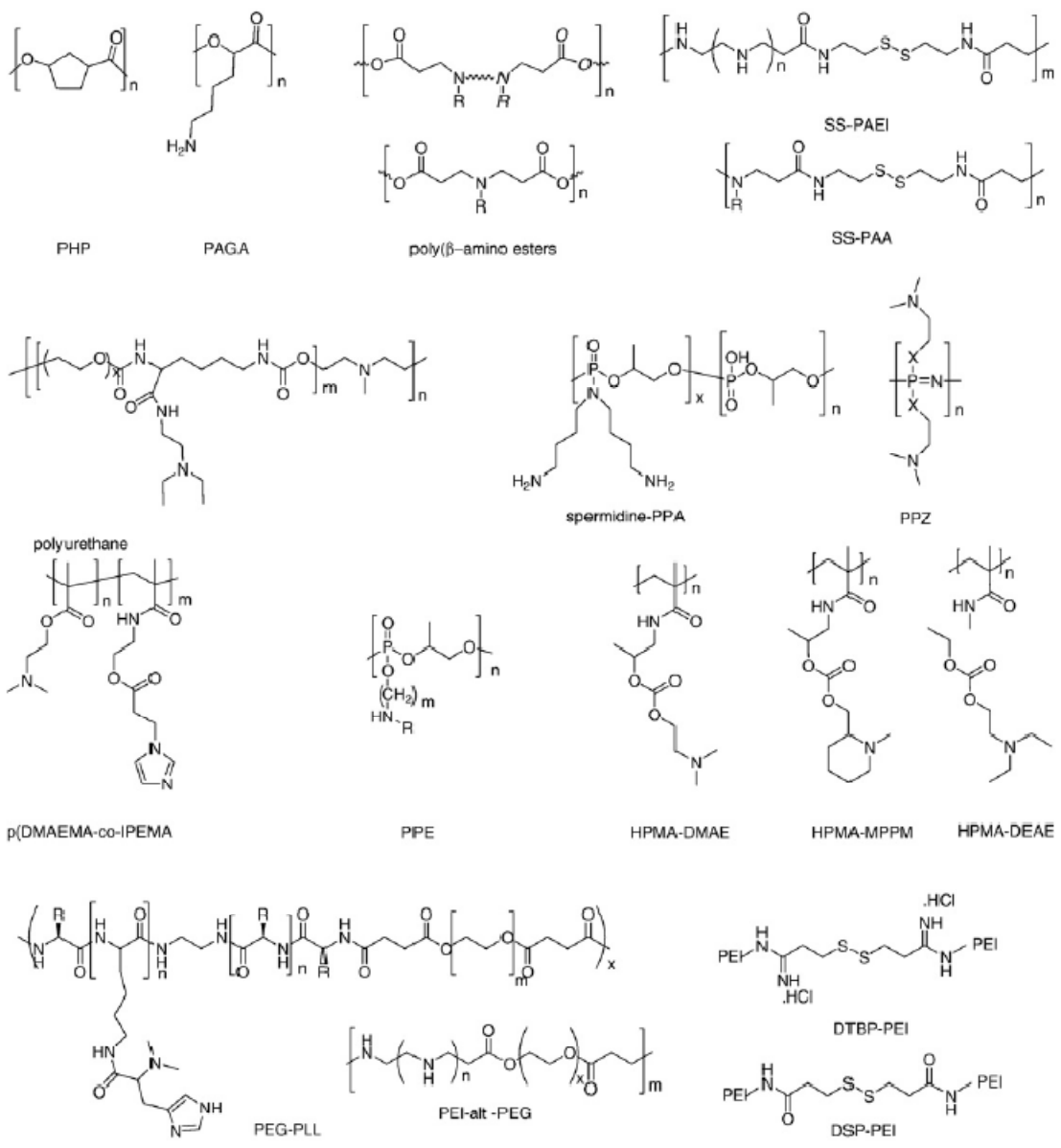

Figure 2.4 Different degradable drug or gene delivery vehicles reviewed by Hennink and co-workers. Figure adapted from Luten et al.

As reported by Kim *et al*, Poly(γ-(4-aminobutyl)-L-glycolic acid)s (PAGAs) show faster hydrolysis initially, but then degrade to one third of their original molecular weight in first 100 minutes. However, they then take as long as six months to completely degrade [39]. A library of over 2000 poly(amino esters) [40-42] were synthesized based

on substituents and degree of branching of the polymers. Typically, the half lives of these polymers vary from days to months [43-47]. Phosphore-containing polymers, poly(phosphazenes) (PPZ), poly(phosphoesters) (PPE) and poly(phosphoramidates) (PPA) have been synthesized and the degradative half life of these polymers under physiological conditions varied from 4 to 20 days [48-50]. The design of some of the polymers was based on the disulfide bond in the polymer chain, which is susceptible to reductive cleavage in a cellular environment, and can thus lower the cytotoxicity of the original polymer. The polymers described in this review were all capable of reducing cytotoxicity—thereby reinforcing the importance of biodegradability in these systems.

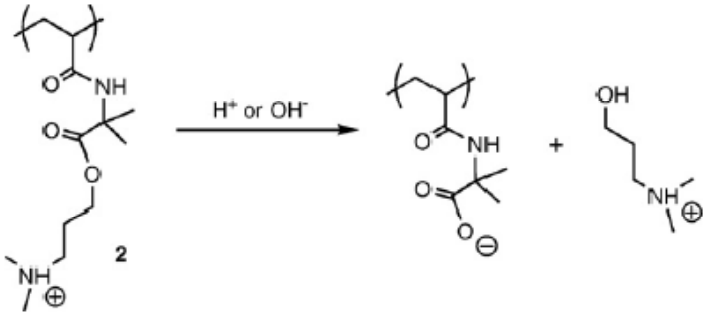

Figure 2.5 A cationic polymer synthesized from radical polymerization technique for the sustained release of the pDNA from polymer/pDNA constructs. As the pendant hydrolyzes the polymer character changes from cationic to less cationic to anionic. Reproduced with permission. Figure adapted from Lynn et al.

The choice of polymerization technique is important, especially since radical polymerization can be utilized to synthesize a polymer with a hydrolyzable pendant. As shown in Figure 2.5, a polymer with a charged pendant in each repeat unit can be designed in order to build a layer-by-layer (lbl) construct of a polymer/pDNA. As the hydrolyzable link in the polymer pendant starts degrading, the charge shift in the polymer has been observed from cationic to less cationic to anionic. These lbl constructs were

designed in order to achieve the extended long-term release of plasmid DNA (pDNA) from the surfaces [51, 52]. Nonetheless, the polymer backbone can still cause concerns in biological delivery systems; hence, radical polymerization might not offer the best solution for designing degradable polymer materials—although radical polymerization can be used to achieve sustained release as described herein. Similarly, radical polymerization was used to synthesize a series of polymer structures based on poly(N-2-hydroxypropyl methacrylamide) (HPMA), as shown Figure 2.4. As discussed in the literature, the final degradation product, the pHPMA polymer, is biocompatible [53].

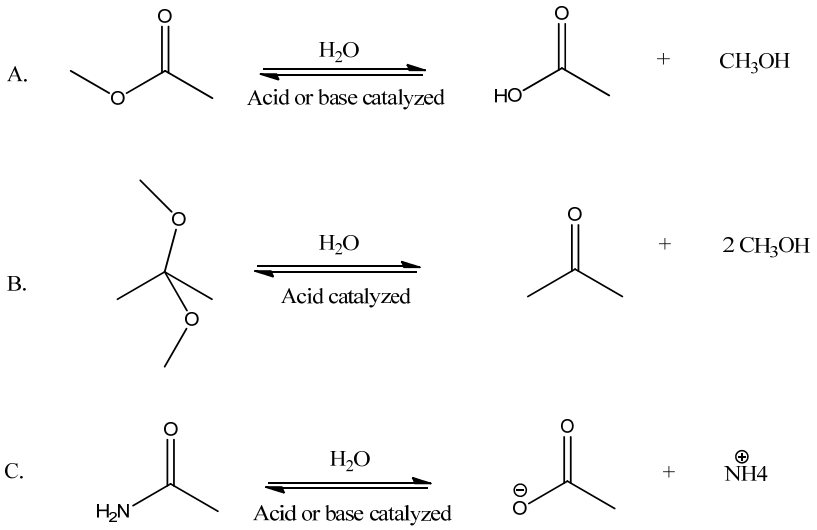

Figure 2.6 Different hydrolyzable functionalities. A) Esters hydrolyze easily in acidic or basic conditions. B) Acetals hydrolyze slower at pH 7 and faster at pH 5.5 C) Amides need very harsh conditions for hydrolysis (e.g., high temperature and high pH)

Step growth polymerization is an effective route for achieving degradability in a polymer structure. The most straightforward step growth polymerization technique involves two different difunctional molecules which can react to afford long chain polymers. The reaction usually involves the formation of new functional groups, which can be predetermined depending on the hydrolysis properties it should provide to the polymer structure. For example, by incorporating a hydrolysable linkage in each repeat

unit, one can enhance the biodegradability of the polymer. As shown in Figure 2.6, ester and acetal functional groups enhance hydrolysis and thus are key functional groups for the design of biodegradable delivery vehicles [26, 54-58]. As discussed earlier, various polymers based on ester linkage have been synthesized and used in either DNA delivery, or in the controlled release of DNA from surfaces [51, 52, 59, 60]. Interestingly, the hydrolysis rate of acetals is pH dependant. Figure 2.7 shows the degradation product of the acetal-based polymers (**1**) (Figure 2.7 a) and the degradation rate (Figure 2.7 b) at pH 7.4 (physiological pH), 6.5 (endosomal pH) and 5.5 (lysosomal pH) [26].

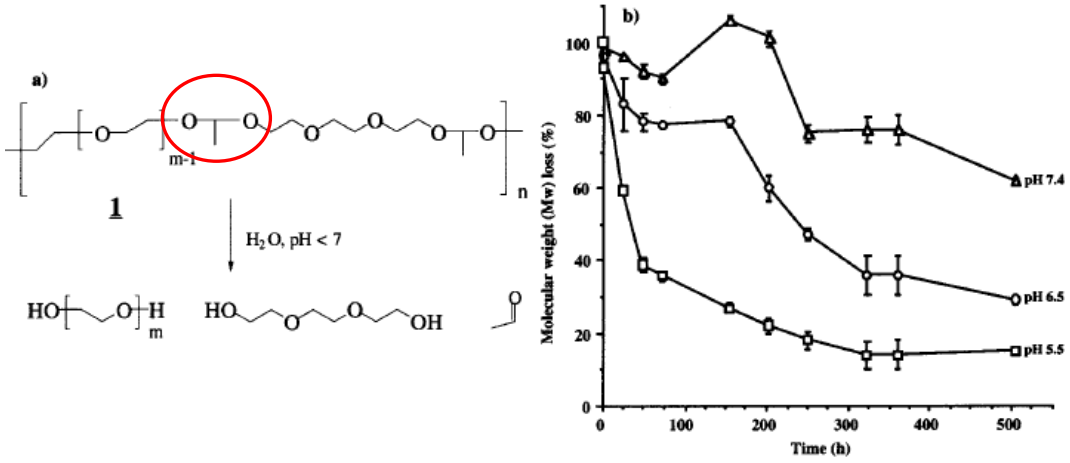

Figure 2.7 Degradation products and degradation profile at different pH for acetal- (shown by the red ellipse) based polymer. Figure adapted from Tomlinson et al.

To enhance therapeutic effects, biomaterials have often been used for conjugatation with therapeutics. The release of therapeutics from conjugates with high selectivity over time and under a number of physiological conditions has been described for several materials with varying functionalities [61]. Biomaterials incorporating ester or acetal functionalities that undergo hydrolysis have been studied as biodegradable nucleic acid delivery and/or as controlled release vehicles [26, 51, 52, 59, 60]. However, the

hydrolysis rate of these biomaterials is highly dependent on pH, which can prove to be a disadvantage for certain systems. Conversely, amide functionality is very versatile due to ease of synthesis, in addition to the fact that it and allows the incorporation of various other functional groups for selectivity and targeting. Amides are very stable, but require harsh conditions (e.g., high temperature and very low or high pH) for hydrolysis to occur (Figure 2.6 C). Therefore, very few studies have reported the hydrolysis of amide functionality groups under physiological conditions [62-65]. Typically, tertiary amides with highly stained structures fall into this category, while none of the other amides have been shown to hydrolyze under physiological conditions. In contrast, a new class of materials poly(glycoamidoamine)s (PGAAs) has displayed markedly different degradation chemistry [66, 67], as described in the following section.

2.3 Polyglycoamidoamines (PGAAs): Efficient biodegradable therapeutic delivery vehicles

Several different viruses, including adenoviruses and rhinoviruses, are proven DNA delivery vehicles. Specifically, viruses use a built-in molecular machinery called capsid to enter the cells, after which it can insert the foreign DNA sequence into the gene. Approximately 75% of clinical trials in the area of gene delivery have utilized viral vectors for the delivery of nucleic acids [68, 69], although various disadvantages such as immunogenicity [70], random genome integration, and systemic inflammatory response [71] have resulted in serious health concerns [69]. Nonetheless, some success has been reported with viral drug delivery—although the death of the patient to due to multiple organ failure [71] has delayed significant advances in this area. Despite that setback, that trial inspired the scientific community to further explore non-viral vehicles for similar or

improved results. For example, various cationic polymers have been used in the past for complexation with DNA for delivery to mammalian cells. Moreover, a large body of research can be found on the synthetic polymer, polyethyleneimene (PEI), and naturally occurring polysaccharide chitosan. Linear PEI (Figure 2.8) contains secondary amines in each repeat unit of the polymer. Studies have shown that one out of every two secondary amines is protonated at a physiological pH [72]. Due to the cationic behavior of PEI, it is shown to complex DNA in an efficient manner since it condenses DNA into nanoparticles. These polymer-DNA complexes, also known as polyplexes, show a high transgene expression upon incubating with different mammalian cell lines. These polyplexes, however, also show high cytotoxicity, which increased with increasing concentrations of PEI [23, 73].

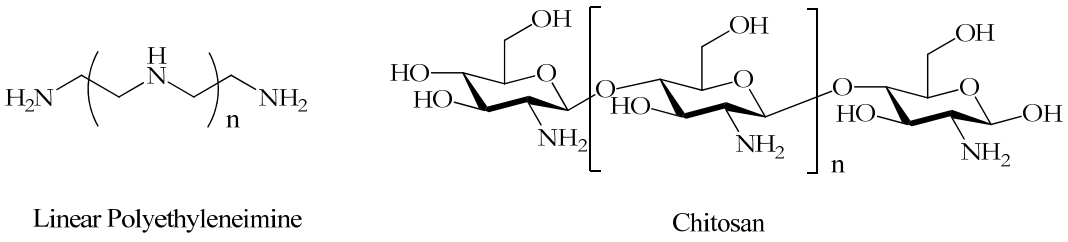

Figure 2.8 Structures of linear polyethyleneimine and chitosan, two widely studied polymers for DNA delivery.

Conversely, chitosan is a naturally occurring polymer that has been shown to be biocompatible in various applications [74-76]. Chitosan, which consists of a glucosamine group in each repeat unit, can complex with DNA [74]. Chitosan-based polyplexes exhibit very low toxicity at different concentrations of chitosan; however, these polyplexes also display very low transgene expression.

After studying the structure-biological activity relationship of these two widely studied vehicles (i.e., PEI and Chitosan), Reineke and coworkers systematically designed

a polymer with a carbohydrate and an oligoethyleneamine moiety in the repeat unit that is linked via amide [20, 24, 73, 77] or triazole [78] functional groups. Inspired by previous reports on ammonolysis chemistry [79-84], a library of 16 different polymers—which are known as poly(glycoamidoamine)s (PGAAs)—were synthesized (Figure 2.9) by reacting four different oligoamines and four different "activated" diesters [20, 24, 73, 85].

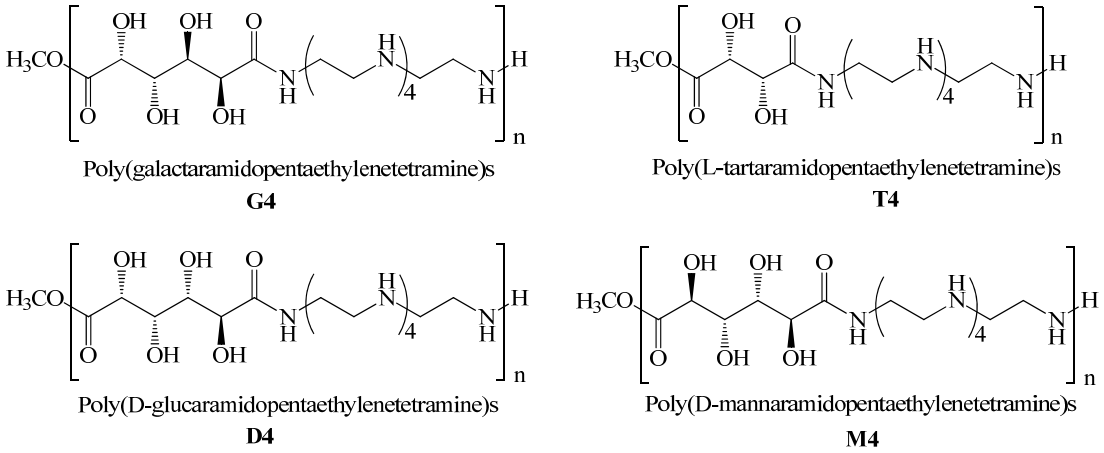

Figure 2.9 Structures of four representative poly(glycoamidoamine)s from a series of 16 differnt polymers.

Polymerization conditions were optimized to control the degree of polymerization (DP) in the range of 11 to 14 in order to eliminate any adverse structural effects on the biological activity of the PGAAs. The polymer and DNA were mixed based on the molar ratio of protonatable amines (*N*) to the molar ratio of the phosphate groups (*P*)—which is known as the *N/P* ratio. As shown in Figure 2.10, different interactions between the PGAAs and the pDNA enhanced their binding ability to form polyplexes. As we determined, PGAAs bind DNA at a low *N/P* ratio of three or less. Furthermore, dynamic light scattering (DLS) and transmission electron microscopy (TEM) revealed that the complexation of the DNA by PGAAs resulted in nanoparticles of ~100 nm. Zeta potential

measurements revealed a positive charge on the surface of the polymer-pDNA complexes (polyplexes).

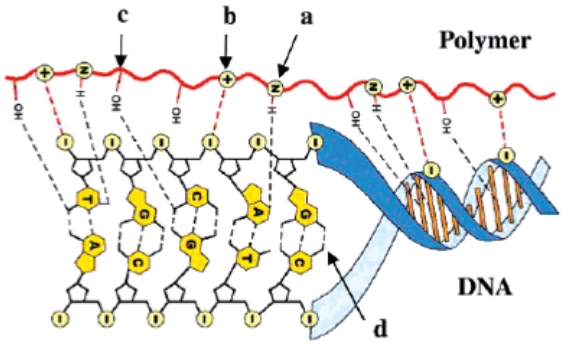

Figure 2.10 Schematic diagram of different interactions that can affect pDNA-PGAA binding. (a) Hydrogen bond between the polymer amine and base, (b) electrostatic interaction between the protonated amine and phosphate group, (c) hydrogen bond between the carbohydrate hydroxyl group and base, and (d) hydrogen bonds between base pairs [86]. Figure adapted from Prevette *et al*.

The PGAAs were then characterized for binding with DNA via complexation at different *N/P* ratios. Subsequent biological characterization studies revealed high transgene expression with PGAAs while retaining high cell viability in different mammalian cell lines. These studies confirmed that the polymers with four secondary amines showed higher biological activity in terms of transgene expression and toxicity. In particular, Poly(galactaramidopetaethylenetetramine) (**G4**) and poly(tartaramidopentaethylenetetraamine) (**T4**) proved to be the most efficient and mostly easily synthesized compounds, which is why they are now commercially available (**G4** = *Glycofect*^{TM}) from Techulon, Inc.

2.4 Structure-bioactivity relationship

Second-generation PGAAs were synthesized in an attempt to further study the effects of increasing the number of secondary amines in the repeat unit of the polymer. Although the delivery vehicles in this study did not appreciably increase transgene

expression, the toxicity of the polyplexes was found to be higher than polymers synthesized previously [87]. Thus, very subtle changes in a polymer's structure can affect its binding with biological macromolecules such as DNA or RNA. Moreover, structural changes can affect other biological mechanisms such as cellular uptake, transgene expression and cytotoxicity. As such, different chemical, physical or morphological aspects of the "expendable" polymer have to be taken under consideration in the design of a delivery vehicle. For example, the specific chemical behavior of the polymer will contribute to its affinity towards negatively charged DNA. This results in the packaging of the DNA, which can protect it from nucleases that are a part of the direct or indirect intracellular digestive system. Due to ionic interactions between the negatively charged DNA and the positively charged polymers, the rigidity of the DNA backbone attenuates [88] and smaller complexes (usually called polyplexes) can form—preferably in the range of 50 to 200 nm.

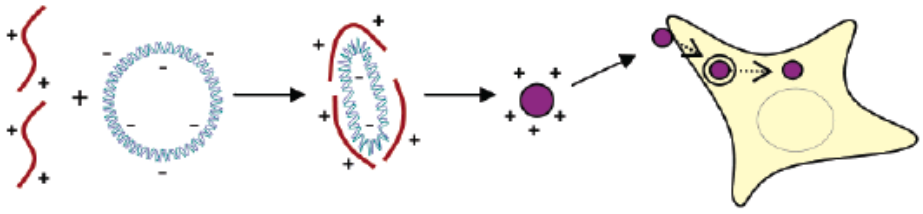

Figure 2.11 Schematic representation of different stages or barriers for the DNA delivery involves polyplex formation, cellular uptake of the polyplexes and its cellular transport to release the DNA for translation and transcription. Figure adopted from Liu *et al*.

The process of DNA delivery using cationic polymers involves specific processes (Figure 2.11). In order to describe these processes and the complex behaviors that each process involves, one typically classifies five different stages that polyplexes pass through: (1) binding of the polymer with DNA to form nanoparticle complexes (termed polyplexes), cellular internalization of the polyplexes via endocytic pathway, (3)

endosomal release of the polyplexes into the cytoplasm, (4) transport of the polyplexes to the nucleus, and (5) release of the DNA from the polyplexes to undergo transcription and translation to produce the required protein. Once the DNA is released from the polyplex, it is very important to determine the "fate" of the polymer, as well as ascertain mechanism it uses to either degrade in the cellular matrix or be recycled out of the cellular matrix. The degradation of the polymer is directly dependent on the availability of the hydrolysable linkage in its chemical structure. This is a very interesting aspect of the polymer, as well as a design feature that enhances degradation behavior in the physiological range of pH 7.4 and at a temperature of about 37^{0}C. The degraded product can then be metabolized by either intracellular or extracellular mechanisms. Understanding each of these processes is vital for designing an ideal therapeutic delivery vehicle that can perform the abovementioned tasks in the most efficient manner. Another chemical property of the polymer can directly impact the efficacy of the therapeutic delivery system is the availability and accessibility of targeting groups for the intended cell or tissue type. Therefore, in order to synthesize next-generation polymers for use in drug delivery, one must understand their structure-bioactivity relationships. Also important to this process is a greater comprehension of the various related processes, such as DNA binding, cellular uptake, and release of DNA from the complexes. The studies described herein involved the extensive synthesis of functional monomers that could be used to generate polymers with subtle structural changes. Subsequent characterization of these second-generation polymers will be essential for comparing and contrasting the different biological processes for which they might be useful—and in particular for the efficient design of new delivery vehicle systems.

2.5 - References

[1] Hench LL, Polak JM. Third-generation biomedical materials. Science's STKE 2002;295:1014.

[2] Langer R. Biomaterials in drug delivery and tissue engineering: one laboratory's experience. Acc. Chem. Res 2000;33:94-101.

[3] Saltzman WM, Olbricht WL. Building drug delivery into tissue engineering. Nature Reviews Drug Discovery 2002;1:177-186.

[4] Bonadio J. Tissue engineering via local gene delivery. Journal of molecular medicine 2000;78:303-311.

[5] Siddik ZH, Newell DR, Boxall FE, Harrap KR. The comparative pharmacokinetics of carboplatin and cisplatin in mice and rats. Biochemical pharmacology 1987;36:1925-1932.

[6] Griffith LG, Naughton G. Tissue engineering--current challenges and expanding opportunities. Science 2002;295:1009.

[7] Langer R, Tirrell DA. Designing materials for biology and medicine. NATURE 2004;428:487-492.

[8] Kataoka K, Harada A, Nagasaki Y. Block copolymer micelles for drug delivery: design, characterization and biological significance. Advanced Drug Delivery Reviews 2001;47:113-131.

[9] Wu SY, McMillan NAJ. Lipidic Systems for In Vivo siRNA Delivery. The AAPS Journal 2009;11:639-652.

[10] Whitehead KA, Langer R, Anderson DG. Knocking down barriers: advances in siRNA delivery. Nature Reviews Drug Discovery 2009;8:129-138.

[11] Davis ME, Zuckerman JE, Choi CHJ, Seligson D, Tolcher A, Alabi CA, Yen Y, Heidel JD, Ribas A. Evidence of RNAi in humans from systemically administered siRNA via targeted nanoparticles. NATURE;464:1067-1070.

[12] Atala A. Tissue engineering of artificial organs. Journal of endourology 2000;14:49-58.

[13] Allen TM, Cullis PR. Drug delivery systems: entering the mainstream. Science 2004;303:1818.

[14] Remaut K, Lucas B, Raemdonck K, Braeckmans K, Demeester J, De Smedt SC. Protection of oligonucleotides against enzymatic degradation by pegylated and nonpegylated branched polyethyleneimine. Biomacromolecules 2007;8:1333-1340.

[15] Kaneda Y. Gene therapy: a battle against biological barriers. Current Molecular Medicine 2001;1:493-499.

[16] Davis ME, Brewster ME. Cyclodextrin-based pharmaceutics: past, present and future. Nature Reviews Drug Discovery 2004;3:1023-1035.

[17] Mishra S, Webster P, Davis ME. PEGylation significantly affects cellular uptake and intracellular trafficking of non-viral gene delivery particles. European journal of cell biology 2004;83:97-111.

[18] Qiu Y, Park K. Environment-sensitive hydrogels for drug delivery. Advanced Drug Delivery Reviews 2001;53:321-339.

[19] Esfand R, Tomalia DA. Poly (amidoamine)(PAMAM) dendrimers: from biomimicry to drug delivery and biomedical applications. Drug Discovery Today 2001;6:427-436.

[20] Liu Y, Reineke TM. Hydroxyl stereochemistry and amine number within poly(glycoamidoamine)s affect intracellular DNA delivery. J. Am. Chem. Soc. 2005;127:3004-3015.

[21] Liu Y, Reineke TM. Poly(glycoamidoamine)s for gene delivery. Stability of polyplexes and efficacy with cardiomyoblast cells. Bioconjugate Chem. 2006;17:101-108.

[22] Liu Y, Wenning L, Lynch M, Reineke TM. Gene delivery with novel poly(L-tartaramidoamine)s. In: Svenson S, editor. Polymeric Drug Delivery Volume I - Particulate Drug Carriers, vol. 923. Washington DC: American Chemical Society, 2006.

[23] Liu YM, Reineke TM. Hydroxyl stereochemistry and amine number within poly(glycoamidoamine)s affect intracellular DNA delivery. Journal of the American Chemical Society 2005;127:3004-3015.

[24] Reineke TM. Poly(glycoamidoamine)s: Cationic glycopolymers for DNA delivery. Journal of Polymer Science Part a-Polymer Chemistry 2006;44:6895-6908.

[25] Srinivasachari S, Liu Y, Zhang G, Prevette L, Reineke TM. Trehalose click polymers inhibit nanoparticle aggregation and promote pDNA delivery in serum. J. Am. Chem. Soc 2006;128:8176-8184.

[26] Tomlinson R, Klee M, Garrett S, Heller J, Duncan R, Brocchini S. Pendent chain functionalized polyacetals that display pH-dependent degradation: a platform for the development of novel polymer therapeutics. Macromolecules 2002;35:473-480.

[27] Knorr V, Russ V, Allmendinger L, Ogris M, Wagner E. Acetal linked oligoethylenimines for use as pH-sensitive gene carriers. Bioconjugate Chem 2008;19:1625-1634.

[28] Guo X, Szoka Jr FC. Chemical approaches to triggerable lipid vesicles for drug and gene delivery. Acc. Chem. Res 2003;36:335-341.

[29] Gopin A, Pessah N, Shamis M, Rader C, Shabat D. A chemical adaptor system designed to link a tumor-targeting device with a prodrug and an enzymatic trigger. Angewandte Chemie 2003;115:341-346.

[30] Seymour LW, Duncan R, Kopeckova P, Kopecek J. Potential of Sugar Residues Attached to N-(2-Hydroxypropyl) methacryl amide Copolymers as Targeting Groups for the Selective Delivery of Drugs. Journal of Bioactive and Compatible Polymers 1987;2:97.

[31] Chen C, Kim J, Liu D, Rettig GR, McAnuff MA, Martin ME, Rice KG. Synthetic PEGylated glycoproteins and their utility in gene delivery. Bioconjugate Chemistry 2007;18:371.

[32] Chiu SJ, Ueno NT, Lee RJ. Tumor-targeted gene delivery via anti-HER2 antibody (trastuzumab, Herceptin®) conjugated polyethylenimine. Journal of Controlled Release 2004;97:357-369.

[33] Bryson JM, Fichter KM, Chu WJ, Lee JH, Li J, Madsen LA, McLendon PM, Reineke TM. Polymer beacons for luminescence and magnetic resonance imaging of DNA delivery. Proceedings of the National Academy of Sciences 2009;106:16913.

[34] Gao X, Cui Y, Levenson RM, Chung LWK, Nie S. In vivo cancer targeting and imaging with semiconductor quantum dots. Nature Biotechnology 2004;22:969-976.

[35] de Wolf HK, Luten J, Snel CJ, Oussoren C, Hennink WE, Storm G. In vivo tumor transfection mediated by polyplexes based on biodegradable poly(DMAEA)-phosphazene. Journal of Controlled Release 2005;109:275-287.

[36] Luten J, van Nostrum CF, De Smedt SC, Hennink WE. Biodegradable polymers as non-viral carriers for plasmid DNA delivery. Journal of Controlled Release 2008;126:97-110.

[37] Putnam D, Langer R. Poly (4-hydroxy-L-proline ester): Low-temperature polycondensation and plasmid DNA complexation. Macromolecules 1999;32:3658-3662.

[38] Lim YB, Choi YH, Park JS. A self-destroying polycationic polymer: Biodegradable poly(4-hydroxy-L-proline ester). Journal of the American Chemical Society 1999;121:5633-5639.

[39] Lim Y, Kim C, Kim K, Kim SW, Park J. Development of a Safe Gene Delivery System Using Biodegradable Polymer, Poly [[alpha]-(4-aminobutyl)-l-glycolic acid]. J. Am. Chem. Soc 2000;122:6524-6525.

[40] Akinc A, Lynn DM, Anderson DG, Langer R. Parallel synthesis and biophysical characterization of a degradable polymer library for gene delivery. Journal of the American Chemical Society 2003;125:5316.

[41] Anderson DG, Lynn DM, Langer R. Semi-automated synthesis and screening of a large library of degradable cationic polymers for gene delivery. Angewandte Chemie 2003;115:3261-3266.

[42] Green JJ, Shi J, Chiu E, Leshchiner ES, Langer R, Anderson DG. Biodegradable polymeric vectors for gene delivery to human endothelial cells. Bioconjugate Chem 2006;17:1162-1169.

[43] Kim T, Seo HJ, Choi JS, Yoon JK, Baek J, Kim K, Park JS. Synthesis of Biodegradable Cross-Linked Poly ([beta]-amino ester) for Gene Delivery and Its Modification, Inducing Enhanced Transfection Efficiency and Stepwise Degradation. Bioconjugate Chem 2005;16:1140-1148.

[44] Wu D, Liu Y, Jiang X, Chen L, He C, Goh SH, Leong KW. Evaluation of hyperbranched poly (amino ester) s of amine constitutions similar to polyethylenimine for DNA delivery. Biomacromolecules;6:3166.

[45] Lim Y, Kim SM, Lee Y, Lee W, Yang T, Lee M, Suh H, Park J. Cationic hyperbranched poly (amino ester): a novel class of DNA condensing molecule with cationic surface, biodegradable three-dimensional structure, and tertiary amine groups in the interior. J. Am. Chem. Soc 2001;123:2460-2461.

[46] Li X, Su Y, Chen Q, Lin Y, Tong Y, Li Y. Synthesis and characterization of biodegradable hyperbranched poly (ester-amide) s based on natural material. Biomacromolecules;6:3181.

[47] Wu D, Liu Y, Jiang X, He C, Goh SH, Leongs KW. Hyperbranched poly (amino ester) s with different terminal amine groups for DNA delivery. Biomacromolecules 2006;7:1879-1883.

[48] Wang J, Mao HQ, Leong KW. A novel biodegradable gene carrier based on polyphosphoester. J. Am. Chem. Soc 2001;123:9480-9481.

[49] Wang J, Zhang PC, Lu HF, Ma N, Wang S, Mao HQ, Leong KW. New polyphosphoramidate with a spermidine side chain as a gene carrier. Journal of Controlled Release 2002;83:157-168.

[50] Wang J, Huang SW, Zhang PC, Mao HQ, Leong KW. Effect of side-chain structures on gene transfer efficiency of biodegradable cationic polyphosphoesters. Int. J. Pharm. 2003;265:75-84.

[51] Zhang J, Lynn DM. Ultrathin multilayered films assembled from “charge-shifting” cationic polymers: extended, long-term release of plasmid DNA from surfaces. Advanced Materials 2007;19:4218-4223.

[52] Jewell CM, Lynn DM. Surface-mediated delivery of DNA: Cationic polymers take charge. Current opinion in colloid & interface science 2008;13:395-402.

[53] Rihova B, Kubackova K. Clinical implications of N-(2-hydroxypropyl) methacrylamide copolymers. Current Pharmaceutical Biotechnology 2003;4:311-322.

[54] Gillies ER, Goodwin AP, Frechet JMJ. Acetals as pH-sensitive linkages for drug delivery. Bioconjugate Chem 2004;15:1254-1263.

[55] Gillies ER, Frechet JMJ. pH-responsive copolymer assemblies for controlled release of doxorubicin. Bioconjugate Chem 2005;16:361-368.

[56] Gillies ER, Frechet JMJ. Dendrimers and dendritic polymers in drug delivery. Drug Discovery Today 2005;10:35-43.

[57] Gillies ER, Fréchet JMJ. Development of acid-sensitive copolymer micelles for drug delivery. Pure and Applied Chemistry 2004;76:1295-1308.

[58] Gingras M, Raimundo JM, Chabre YM. Cleavable dendrimers. Angew. Chem. Int. Ed 2007;46:1010-1017.

[59] Zhang JT, Chua LS, Lynn DM. Multilayered thin films that sustain the release of functional DNA under physiological conditions. Langmuir 2004;20:8015-8021.

[60] Jewell CM, Zhang JT, Fredin NJ, Lynn DM. Multilayered polyelectrolyte films promote the direct and localized delivery of DNA to cells. Journal of Controlled Release 2005;106:214-223.

[61] Luten J, van Nostruin CF, De Smedt SC, Hennink WE. Biodegradable polymers as non-viral carriers for plasmid DNA delivery. Journal of Controlled Release 2008;126:97-110.

[62] Bennet AJ, Wang QP, Slebockatilk H, Somayaji V, Brown RS, Santarsiero BD. Relationship between amidic distortion and ease of hydrolysis in base - if amidic resonance does not exist, then what accounts for the accelerated hydrolysis of distorted amides. Journal of the American Chemical Society 1990;112:6383-6385.

[63] Glusenkamp KH, Mengede C, Drosdziok W, Jahde E, Rajewsky MF. Rapid hydrolysis of amides under physiological conditions: Influence of the microenvironment on the stability of amide bond. Bioorg. Med. Chem. Lett. 1998;8:285-288.

[64] Kahne D, Still WC. Hydrolysis of a peptide-bond in neutral water. Journal of the American Chemical Society 1988;110:7529-7534.

[65] Somayaji V, Keillor J, Brown RS. Model for the aspartate proteinases - hydrolysis of a distorted amide catalyzed by dicarboxylic-acids capable of forming cyclic anhydrides. Journal of the American Chemical Society 1988;110:2625-2629.

[66] Liu Y, Reineke TM. Degradation of Poly(glycoamidoamine) DNA Delivery Vehicles: Polyamide Hydrolysis at Physiological Conditions Promotes DNA Release. Biomacromolecules 2010;11:316-325.

[67] Taori VP, Liu YM, Reineke TM. DNA delivery in vitro via surface release from multilayer assemblies with poly(glycoamidoamine)s. Acta biomaterialia 2009;5:925-933.

[68] Pietersz GA, Tang CK, Apostolopoulos V. Structure and design of polycationic carriers for gene delivery. Mini-Rev. Med. Chem. 2006;6:1285-1298.

[69] Thomas CE, Ehrhardt A, Kay MA. Progress and problems with the use of viral vectors for gene therapy. Nat. Rev. Genet. 2003;4:346-358.

[70] Boulaiz H, Marchal JA, Prados J, Melguizo C, Aranega A. Non-viral and viral vectors for gene therapy. Cell. Mol. Biol. 2005;51:3-22.

[71] Marshall E. Clinical trials - Gene therapy death prompts review of adenovirus vector. Science 1999;286:2244-2245.

[72] Ziebarth JD, Wang Y. Understanding the Protonation Behavior of Linear Polyethylenimine in Solutions through Monte Carlo Simulations. Biomacromolecules 2009:7297-7301.

[73] Liu YM, Wenning L, Lynch M, Reineke TM. Gene delivery with novel poly(1-tartaramidoamine)s. Polymeric Drug Delivery I: Particulate Drug Carriers, vol. 923. 2006. p.217-227.

[74] Borchard G. Chitosans for gene delivery. Advanced Drug Delivery Reviews 2001;52:145-150.

[75] Suh F. Application of chitosan-based polysaccharide biomaterials in cartilage tissue engineering: a review. Biomaterials 2000;21:2589-2598.

[76] Roy K, Mao HQ, Huang SK, Leong KW. Oral gene delivery with chitosan-DNA nanoparticles generates immunologic protection in a murine model of peanut allergy. Nature Medicine 1999;5:387.

[77] Liu Y, Wenning L, Lynch M, Reineke TM. New poly(D-glucaramidoamine)s induce DNA nanoparticle formation and efficient gene delivery into mammalian cells. J. Am. Chem. Soc. 2004;126:7422-7423.

[78] Srinivasachari S, Liu Y, Prevette LE, Reineke TM. Effects of trehalose click polymer length on pDNA complex stability and delivery efficacy. Biomaterials 2007;28:2885-2898.

[79] Arnett EM, Miller JG, Day AR. Effect of structure on reactivity. IV. Aminolysis of esters with secondary amines. J. Am. Chem. Soc 1951;73:5393-5395.

[80] Gordon M, Miller JG, Day AR. Effect of Structure on Reactivity. II. Influence of Solvents on Ammonolysis of Esters. J. Am. Chem. Soc 1949;71:1245-1250.

[81] Hoagland PD. the Formation of Intermediate Lactones during Aminolysis of Diethyl galactarate. Carbohydr. Res 1981;98:203-204.

[82] Kiely DE, Chen L, Lin T. Hydroxylated nylons based on unprotected esterified D-glucaric acid by simple condensation reaction. J. Am. Chem. Soc. 1994;116:571-578.

[83] Kiely DE, Chen L, Lin T. Synthetic polyhydroxypolyamides from galactaric, xylaric, D-glucaric, and D-mannaric acids and alkylenediamine monomers-some comparisons. Journal of Polymer Science: Part A: Polymer Chemistry 2000;38:594-603.

[84] Koch T, Miller JG, Day AR. Effect of Structure on Reactivty. VI Catalysis in the Ammonolysis and Hydrolysis of Methyl Acetate. J. Am. Chem. Soc 1953;75:953-955.

[85] Liu YM, Wenning L, Lynch M, Reineke TM. New poly(D-glucaramidoamine)s induce DNA nanoparticle formation and efficient gene delivery into mammalian cells. Journal of the American Chemical Society 2004;126:7422-7423.

[86] Prevette LE, Kodger TE, Reineke TM, Lynch ML. Deciphering the role of hydrogen bonding in enhancing pDNA-Polycation interactions. Langmuir 2007;23:9773-9784.

[87] Lee CC, Liu Y, Reineke TM. General structure-activity relationship for poly (glycoamidoamine) s: the effect of amine density on cytotoxicity and DNA delivery efficiency. Bioconjugate Chemistry 2008;19:428.

[88] Podestà A, Indrieri M, Brogioli D, Manning GS, Milani P, Guerra R, Finzi L, Dunlap D. Positively charged surfaces increase the flexibility of DNA. Biophys. J. 2005;89:2558-2563.

Chapter 3

Auto Lysing Intramolecular Amide Substrates (ALIAS): A Strong Tool for the Design of New Biomaterials

3.1 - Abstract

Tartaramidoamines, a new class of biomaterials promote hydrolysis of amide bond selectively on one side under physiological conditions. An amine attached to β or γ carbon to the amidic nitrogen is necessary for the hydrolysis of amide bond. Increase in the proximity of tertiary amine from amidic nitrogen decreases the rate of hydrolysis of the amide bond. Methylation or absence of tertiary amines results in no hydrolysis. Rate of the hydrolysis can be controlled by varying the functional groups attached to the carbon α or β to the amide bond.

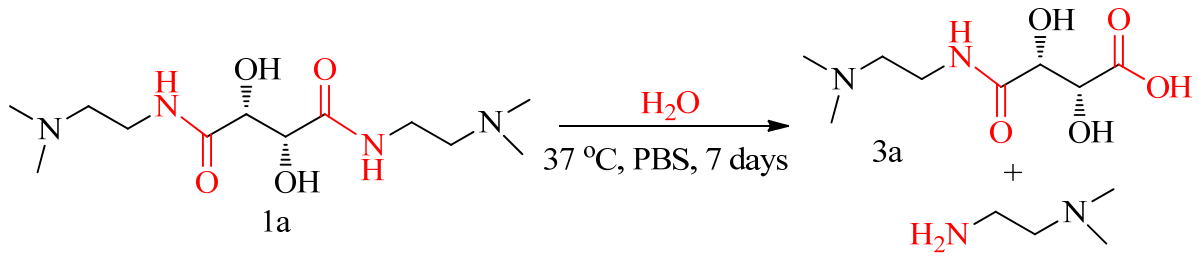

Scheme 3.1 One side observed hydrolysis of the 1a at physiological condition. The hydrolysis begin in one hour following the pseudo first order kinetics and approaches completion in about 7 days.

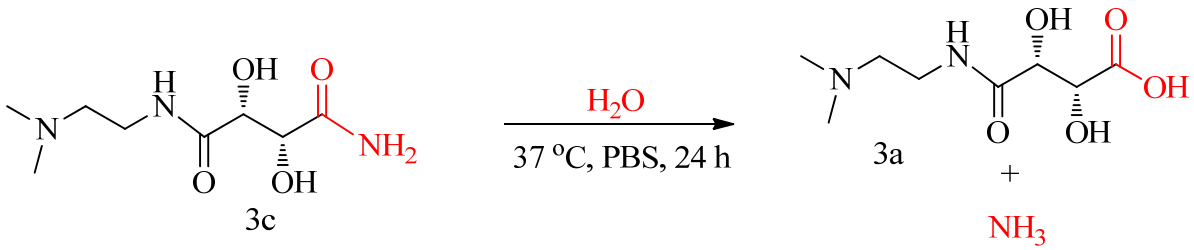

Scheme 3.2 The asymmetric compound reveals the hydrolysis of amide on the opposite side.

In order to understand the reason for the one side hydrolysis of the symmetric compounds, one tartarate based asymmetric compound with a tertiary amine end on one side and the amide end on the opposite side was synthesized and studied for the hydrolysis behavior under

similar conditions. Interestingly, it was discovered that the amine on one side of the asymmetric tartarate based compound assists in the hydrolysis of the amide on the opposite side.

The hydrolysis reaction follows pseudo first order kinetics and is independent on the concentration of the model compounds. Designed experiments in these studied models also reveal that the hydrolysis is a intramolecular phenomenon.

keywords: *Amide hydrolysis, polymer degradation, physiological conditions, controlled release, PGAA*

3.2 - Introduction

A smart design of biomaterials is very critical to achieve high selectivity in the delivery of therapeutics. In the area of drug delivery, a biodegradable linkage can facilitate the controlled release of a targeted drug over a longer period of time [1]. In the area of nucleic acid delivery, degradation of the vehicle complexed to the therapeutic DNA or siRNA could assist in the release of the cargo in the cytoplasm or the nucleus. In the area of tissue engineering, a controlled release of growth factors is preferred to increase the cell proliferation rate [2, 3]. This concept requires the incorporation of a cleavable linkage in a polymer or biomaterial without increasing the cytotoxicity [3, 4]. Also, cleavable linkages can assist in the selective targeting of therapeutics to specific tissue types, resulting in a decreased dosage of the therapeutic.

Biomaterials incorporating ester or acetal functionalities that undergo hydrolysis are often used as biodegradable nucleic acid delivery and/or as controlled release vehicles [5-7]. Ester linkages can hydrolyze very quickly and may not prove sufficient for sustained release over a longer period of time. Hydrolysis of acetal functionality is promoted in lower pH of 4.5 over physiological pH of 7.4, and thus does not offer a good control over degradation rate promoting controlled or sustained release of therapeutics. Therefore, a hydrolyzable linkage under physiological conditions (pH 7.4 and 37 ^{o}C) whose hydrolysis rate can be tailored by altering the chemical structure would be very appealing.

Inspired by previous reports on ammonolysis chemistry [8-13], poly(glycoamidoamine)s (PGAAs), synthesized from oligoamines and “activated” diesters[14-16], show remarkable transfection properties while making them non-toxic over other plasmid DNA (pDNA) delivery vehicles. Even though the oligoamine and carbohydrate moieties are attached via amide bonds in each repeat unit, PGAAs have been studied to be biodegradable under the physiological conditions.[17, 18] The degradation property of PGAAs was also explored to build the layer-by-

layer constructs of poly(L-tartaramidopentaethylenetetramine) (**T4**) (Figure 3.3 a) and pDNA to demonstrate the controlled release of pDNA over the period of 11 days while retaining the integrity of the green fluorescent protein-pDNA (GFP-pDNA) to express GFP in HeLa cells [18].

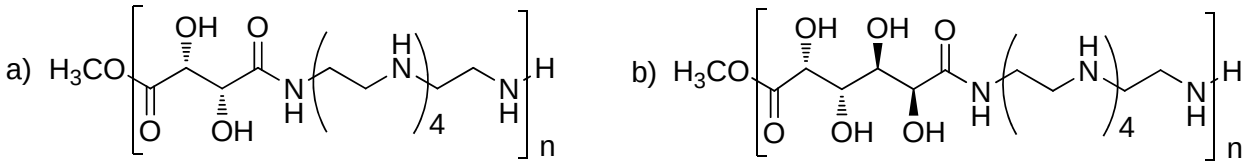

Figure 3.1 Structures of a) poly(L-tartaramidopentaethylenetetraamine) (**T4**) and b) poly(meso-galactaramidopentaethylenetetramine) (**G4**)

The degradation of **T4** was suspected to proceed via the hydrolysis of the amide linkages surrounded by different functional groups, such as amines and hydroxyls present on carbons α and β to the amide. Although enzymatic degradation of the amide bond under physiological conditions is common and under investigation [19-21], the non-enzymatic hydrolysis of amide bonds at physiological conditions has a half-life of over 7 years [22, 23]. A few studies, however, have shown faster hydrolysis of distorted [24, 25] amides, especially amides with sp^3-like nitrogen [25]. It is this curiosity about the hydrolysis of **T4**, which led to the exploration of the hydrolysis chemistry in **T4** utilizing model small molecules. For this purpose, we synthesized a library of molecules (Figure 3.3, 3.4, 3.5) mimicking the **T4** repeat unit structure with varying functionalities on α, β, and γ carbon to the amide bond such as hydroxyl, amine, proximity of the amine to the amidic nitrogen and quaternary ammonium charges. A detailed study of the hydrolysis of these different compounds were done under the physiological conditions understand this chemistry.

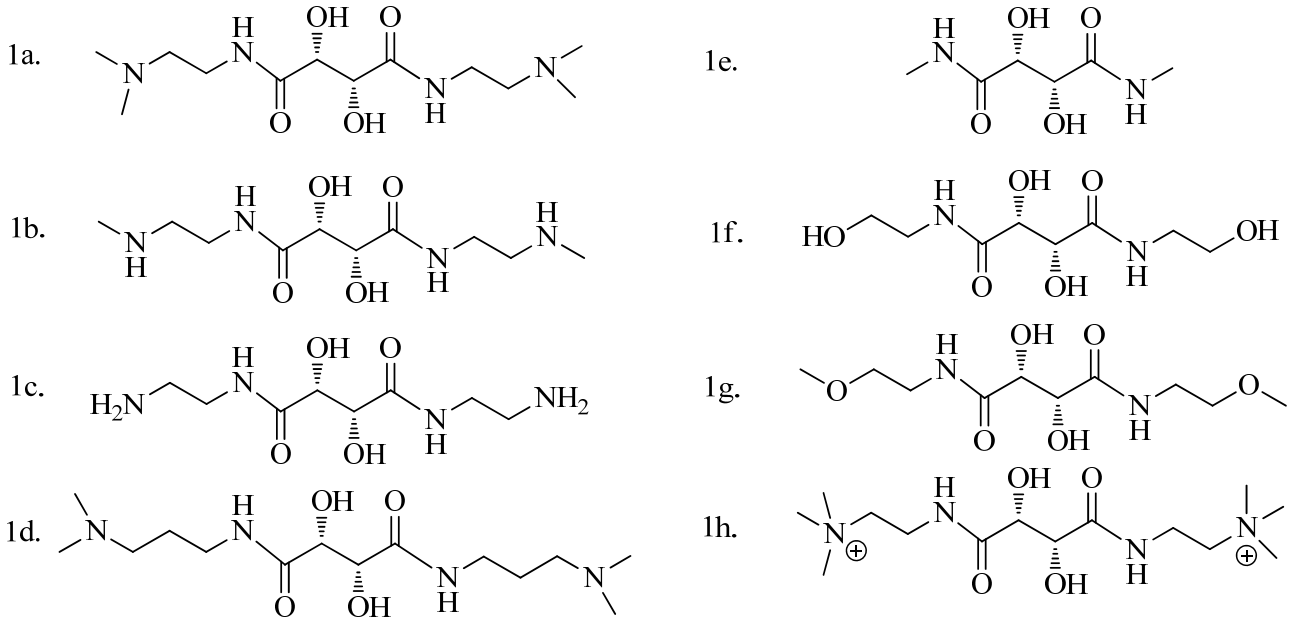

Figure 3.2 Structures of different tartarate based small model compounds.

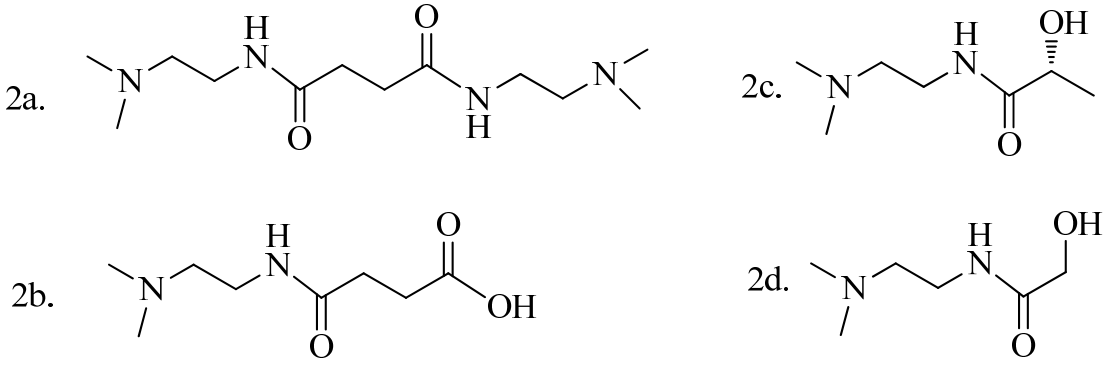

Figure 3.3 Structures of different succinate, lactate, and glycolate based small model compounds.

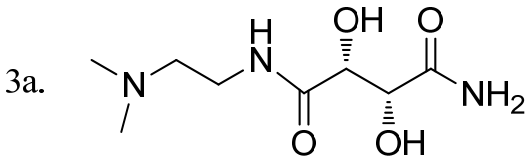

Figure 3.4 Tartarate based asymmetric small model compound with a tertiary amine functional group on one side and amide functional group on the other side.

3.3 - Materials and Methods

3.3.1 General: Unless specified otherwise, all the chemicals were purchased from Sigma Aldrich Chemical Co. and were used without any further purification. NMR spectra were collected on an Inova MR-400MHz spectrometer and mass spectra were obtained on an IonSpec HiResESI mass spectrometer. Phosphate buffered-saline (PBS) was purchased from Invitrogen (Carlsbad, CA). Duetarated phosphate buffered-saline (D_2O_{PBS}) was prepared by freeze drying 20 ml of PBS to obtain white salt mixture, which was then redissolved while stirring slowly in to D_2O to get the final volume of the solution to 20 ml.

3.3.2 Synthesis of small L-tartarate based model compounds

(2R,3R)-N1,N4-bis(2-(dimethylamino)ethyl)-2,3-dihydroxysuccinamide (1a): 3.5 g (19.9 mmol) of dimethyl-L-tartarate (**T**) was weight out in a RBF and 25 ml of methanol was added to this RBF in order to dissolve **T**. Three times molar excess of N^1,N^1-dimethylethane-1,2-diamine (2) (119.4 mmol (10.5 g)) was added to this solution and was stirred at room temperature for 48 hours. Methanol was then evaporated under reduced pressure to obtain yellowish oil. This product was then recrystallized from 50 ml of ethyl acetate to obtain 3.2 g (yield 56%) of white solid. The product obtained was then dried under vacuum and characterized with FT-IR, NMR and exact mass. FT-IR (neat) 3370, 3300, 2941, 2818, 2780, 1644, 1533, 1460 cm^{-1}. ^1H NMR (400 MHz, D_2O) δ = 4.44 (s, 2H), 3.31 (t, 4H), 2.44 (t, 4H), 2.14 (s, 12H). ^{13}C NMR δ = 173.59, 72.19, 56.66, 43.77, 36.46. ESI-MS: calculated for $(M+H)^+$ $C_{12}H_{27}N_4O_4$ 291.2027 found 291.2029.

(2R,3R)-2,3-dihydroxy-N1,N4-bis(2-(methylamino)ethyl)succinamide (1b): 100 mg (0.56 mmol) of dimethyl-L-tartarate was dissolved in 25 ml of ethyl acetate and the solution (solution 1) was brought to 4 ^oC. A solution (solution 2) (of 832 mg (20 x 0.56 mmol) of N^1-methylethane-

1,2-diamine in 25 ml of ethyl acetate was prepared separately and was also brought to 4 ^{o}C. Solution 1 was slowly added to solution 2 and temperature of the reaction was maintained between 4 ^{o}C – 10 ^{o}C for 6 hours. And then reaction was warmed up to room temperature and the reaction mixture was stirred overnight. Ethyl acetate was then evaporated under reduced pressure and to leave yellowish oil behind. The product which was sticky white solid was recrystalized from ethyl acetate. The product obtained was then dried under vacuum and characterized with FT-IR, NMR and exact mass. FT-IR (neat) 3316, 3257, 2906, 1632, 1444 cm^{-1}. ^{1}H NMR (400 MHz, D_2O) δ = ^{1}H NMR (400 MHz, d_2o) δ = 4.49 (s, 2H), 3.33 (dt, 4H), 2.79 (t, 4H).

(2R,3R)-N1,N4-bis(2-aminoethyl)-2,3-dihydroxysuccinamide (1c): 1.0 g (5.61 mmol) of dimethyl-L-tartarate was weighed out in a RBF and 50 ml of ethyl acetate was added to this in order to dissolve the dimethyl-L-tartarate. To this solution 16.86 g (50 x 5.61 mmol) of ethylenediamine was added to this solution. Reaction mixture was stirred 48 hours at room temperature. Methanol and ethylenediamine was evaporated under reduced pressure to leave white solid behind. White solid were dissolved in hot ethyl acetate and the product was recrystallized.

(2R,3R)-N1,N4-bis(3-(dimethylamino)propyl)-2,3-dihydroxysuccinamide(1d): 5.0 g (28.07 mmol) of 2 was weighed out in a RBF and 40 ml methanol was added to this RBF to dissolve 2. To this solution 6.31 g (2.2 x 28.07 mmol) of N^1,N^1-dimethylpropane-1,3-diamine was added while stirring. The reaction mixture was stirred at room temperature for 48 hours. Methanol was then evaporated under reduced pressure to leave viscous oily yellowish liquid behind. About 100 ml of hot ethyl acetate was added slowly while stirring to dissolve the viscous oil. 4.2 g (yield 47%) of 1c was recrystallized from this solution. The product obtained was then dried under vacuum and characterized with FT-IR, NMR and exact mass. FT-IR (neat) 3409, 3350, 2940,

2862, 2768, 1652, 1519, 1433 cm^{-1}. ^{1}H NMR (400 MHz, D_2O) δ = 4.37 (s, 2H), 3.19 – 3.08 (m, 4H), 2.22 (t, 4H), 2.05 (s, 12H), 1.78 – 1.35 (m, 4H). ^{13}C NMR δ = 173.59, 72.18, 55.56, 43.65, 37.21, 26.05. ESI-MS: calculated for $(M+H)^+$ $C_{14}H_{31}N_4O_4$ 319.2340 found 319.2347.

(2R,3R)-2,3-dihydroxy-N1,N4-dimethylsuccinamide (1e): 2.0 g (11.3 mmol) of 2 was weighed out in a dry RBF and 20 ml of Tetrahydrofuran (THF) was added to the RBF to completely dissolve 2. To this solution 20 ml of 4.0 N methylamine in THF was added and stirred for about 5 minutes. White precipitate started to crash out of THF solution immediately after five minutes. About 10 ml of methanol was added to this mixture to redissolve everything back in the THF-methanol mixture and to make sure the reaction goes to completion. After 48 hours of stirring methanol, THF and excess methylamine was evaporated under reduced pressure to leave yellowish sticky solid behind. Product was then washed with THF (2x20 ml) to get 1.9 g (yield 96%) of white powder. The product obtained was then dried under vacuum and characterized with FT-IR, NMR and exact mass. FT-IR (neat) 3451, 3342, 3318, 3193, 1628, 1539, 1413 cm^{-1}. ^{1}H NMR (400 MHz, D_2O) δ = 4.45 (s, 2H), 2.71 (s, 6H). ESI-MS: calculated for $(M+H)^+$ $C_6H_{13}N_2O_4$ 177.087 found 177.0873.

(2R,3R)-2,3-dihydroxy-N1,N4-bis(2-hydroxyethyl)succinamide (1f): 500 mg (2.8 mmol) of **T** was weighed out in a RBF. 40 ml of methanol was added to this RBF to completely dissolve **T**. To this solution 514 mg (3 x 2.8 mmol) of 2-aminoethane was added while stirring. The reaction mixture was stirred at room temperature for 48 hours. Methanol was then evaporated under reduced pressure to leave viscous yellowish oil behind. About 100 ml of hot ethyl acetate was added slowly while stirring to dissolve the viscous oil. 411 mg (yield 62%) of product (1f) was recrystallized from this solution and characterized with FT-IR, NMR and exact mass. FT-IR (neat) 3319, 3139, 2940, 2819, 1645, 1534 cm^{-1}.^{1}H NMR (400 MHz, D_2O) δ = 4.51 (d, 2H), 3.59

(t, 4H), 3.36 (t, 4H). ^{13}C NMR δ = 173.94, 72.33, 59.98, 41.26. ESI-MS: calculated for $(M+H)^+$ $C_8H_{17}N_2O_6$ 237.1087 found 237.1098.

(2R,3R)-2,3-dihydroxy-N1,N4-bis(2-methoxyethyl)succinamide (1g): 500 mg (2.8 mmol) of **T** was weighed out in a RBF. 40 ml of methanol was added to this RBF to completely dissolve **T**. To this solution 632 mg (3 x 2.8 mmol) of 2-methoxyethanamine was added while stirring. The reaction mixture was stirred at room temperature. White precipitate was observed in the reaction mixture after 48 hours. Methanol was then evaporated under reduced pressure to leave off-white powder behind. About 50 ml of hot ethanol was added slowly while stirring to dissolve the off-white powder. 310 mg (yield 42%) of product (1g) was recrystallized from this solution. The product obtained was then dried under vacuum and characterized with FT-IR, NMR and exact mass. FT-IR (neat) 3359, 3284, 2975, 2871, 2808, 1636, 1552 cm^{-1}. ^{1}H NMR (400 MHz, D_2O) δ = 4.58 (s, 2H), 3.65 – 3.58 (m, 4H), 3.53 – 3.46 (m, 4H), 3.43 – 3.38 (m, 6H). ^{13}C NMR δ = 173.85, 72.32, 70.26, 57.98, 38.59. ESI-MS: calculated for $(M+H)^+$ $C_{10}H_{21}N_2O_6$ 265.1400 found 265.1411

2,2'-(((2R,3R)-2,3-dihydroxysuccinyl)bis(azanediyl))bis(N,N,N-trimethylethanaminium) iodide (1h): 1.0 g of 1b was dissolved in acetonitrile. To this 5 ml of methyl iodide was added to quaternize the terminal tertiary amines. The reacting mixture was stirred at 40^{0}C for 3 hrs. The precipitate was observed and which was filtered and washed 10 ml of Acetonitrile and 2 x 10 ml of methanol. The product obtained was then dried under vacuum and characterized with FT-IR, NMR and exact mass. FT-IR (neat) 3287, 1649, 1542, 1516, 1486 cm^{-1}.^{1}H NMR (400 MHz, D_2O) δ = 4.49 (s, 2H), 3.71-3.64 (br m, 4H), 3.45 (t, 4H), 3.10 (s, 18H). ^{13}C NMR δ = 174.15, 72.48, 64.29, 53.65, 33.62. ESI-MS: calculated for M^{+2} (m/z) $C_{14}H_{32}N_4O_4$, 160.1206 found 160.1207.

3.3.3 Synthesis of succinate, glycolate and lactate based small model compounds

N1,N4-bis(2-(dimethylamino)ethyl)succinamide (2a): 1.0 g (6.4 mmol) of succinyl chloride (5) was weighed out and added to a dry RBF under nitrogen containing 20 ml of dry methylene chloride (CH_2Cl_2). A solution of 2.26 g (4x6.45mmol) of 3 in dry CH_2Cl_2 was added drop wise to the earlier prepared solution of 5 under nitrogen at 0^o C over the period of 20 minutes. This reaction mixture was brought to room temperature and was stirred for four hours. CH_2Cl_2 was then evaporated under reduced pressure to leave dark orange oil behind. 20 ml of THF was added to this oily residue. The precipitate formed in this mixture was filtered out. This filtration was repeated (3-4times) until no residue was observed in the mother liquor. THF was then evaporated under reduced pressure and multiple recrystalizations in THF were carried out to obtain 110 mg (yield 7%) pure 1d. The product obtained was then dried under vacuum and characterized with FT-IR, NMR and exact mass. FT-IR (neat) 3249, 2601, 2512, 2485, 1651, 1534, 1483 cm^{-1}. ^1H NMR (400 MHz, D_2O) δ = 3.18 (t, 4H), 2.39 (s, 4H), 2.37 (t, 4H), 2.10 (s, 12H). ^{13}C NMR δ = 173.31, 60.41, 49.82, 37.62, 32.16. ESI-MS: calculated for $(M+H)^+$ $C_{12}H_{27}N_4O_2$ 258.2056 found 258.2051.

4-((2-(dimethylamino)ethyl)amino)-4-oxobutanoic acid (2b): 500 mg (5.0 mmol) of succinic anhydride was dissolved in 50 ml of dry DMF. 0.66 g (1.5 x 5.0 mmol) of N^1,N^1-dimethylethane-1,2-diamine was added to this solution at room temperature and the solution mixture was stirred overnight at room temperature. DMF was then evaporated under reduced pressure to leave white powder behind. The desired product was recrystalized from ethyl acetate then dried under vacumm and characterized with FT-IR, NMR and exact mass. FT-IR (neat) 3303, 2959, 2930, 2873, 1706, 1645, 1598, 1545, 1396 cm^{-1}.^1H NMR (400 MHz, D_2O) δ = 3.53

(t, 2H), 3.23 (t, 2H), 2.85 (s, 6H), 2.41 (m, 4H). ^{13}C NMR δ = 173.81, 173.26, 60.41, 41.82, 37.62, 32.26, 31.73. ESI-MS: calculated for $(M+H)^+$ $C_8H_{17}N_2O_3$ 189.1161 found 189.1171.

(R)-N-(2-(dimethylamino)ethyl)-2-hydroxypropanamide (2c): 300 mg (2.88 mmol) of methyl-D-lactate was dissolved in 50 ml of methanol. To this solution 279 mg (2.88 mmol x 1.1) of N^1,N^1-dimethylethane-1,2-diamine was added and the solution mixture was stirred overnight at room temperature. Methanol was then evaporated under reduced pressure to obtain yellow oil. This oil was dried under vacuum and then product was characterized with NMR and exact mass. ^{1}H NMR (400 MHz, D_2O) δ = 4.11 (q, 1H), 3.29 (td, 2H), 2.57 (t, 2H), 2.25 (s, 6H), 1.21 (d, 3H). ^{13}C NMR δ = 172.71, 67.21, 60.42, 46.76, 39.32, 19.37. ESI-MS: calculated for $(M+H)^+$ $C_8H_{17}N_2O_3$ 161.1290 found 161.1296.

N-(2-(dimethylamino)ethyl)-2-hydroxyacetamide (2d): 300 mg (3.33 mmol) of methyl glycolate was dissolved in 50 ml of methanol. To this solution 323 mg (3.33 mmol x 1.1) of N^1,N^1-dimethylethane-1,2-diamine was added and the solution mixture was stirred overnight at room temperature. Methanol was evaporated under reduced pressure to obtain slight orange oil. Product was dried under vacuum and characterized with NMR and exact mass. ^{1}H NMR (400 MHz, D_2O) δ = 3.91 (s, 2H), 3.26 (t, 2H), 2.44 (m, 2H), 2.13 (s, 6H). ^{13}C NMR δ = 168.61, 61.61, 60.42, 46.76, 39.02. ESI-MS: calculated for $(M+H)^+$ $C_6H_{15}N_2O_3$ 147.1134 found 147.1129.

3.3.4 Synthesis of L-tartarate based small asymmetric model compounds

(2R,3R)-4-((2-(dimethylamino)ethyl)amino)-2,3-dihydroxy-4-oxobutanoic acid (3a): 400 mg of compound 1a was weighed out and was dissolved in 10 ml of PBS. This solution was stirred for 7 days at 37 ^{o}C. The solution was then flash frozen with liquid nitrogen and water was freeze dried to leave white powder behind. This mixture was then slowly dissolved in 10 ml of ethanol

and slowly 5 ml of ethyl acetate was added to this. A cloudy solution was obtained. Further addition of the ethyl acetate resulted in the white precipitate. Then ethanol ethyl acetate mixture was decanted and again this white precipitate was washed with ethanol ethyl acetate mixture. The product obtained was then dried under vacuum and characterized with FT-IR, NMR and exact mass. FT-IR (neat) 3274, 1598, 1533, 1366 cm^{-1}. ^{1}H NMR (400 MHz, D_2O) δ = 3.91 (s, 2H), 3.26 (t, 2H), 2.44 (m, 2H), 2.13 (s, 6H). ^{13}C NMR δ = 168.61, 61.61, 60.42, 46.76, 39.02. ESI-MS: calculated for $(M+H)^+$ $C_8H_{17}N_2O_5$ 221.1137 found 221.1139.

(2R,3R)-methyl 4-((2-(dimethylamino)ethyl)amino)-2,3-dihydroxy-4-oxobutanoate (3b): 300 mg of 3a was weighed out in a RBF and 50 ml of methanol was added to the RBF to partially dissolve the compound 3a. A drop of H_2SO_4 was added to this solution and refluxed overnight after 24 hrs the solution was clear and it was refluxed again for 24 more hours. Methanol was then evaporated under reduced pressure to leave white powder behind. The product obtained was then dried under vacuum and characterized with FT-IR, NMR and exact mass. FT-IR (neat) 3316, 1714, 1647, 1534 cm^{-1}. ^{1}H NMR (400 MHz, D_2O) δ = 4.74 (d, 1H), 4.53 (d, 1H), 3.82 (d, *J* = 1.4 Hz, 21H), 3.77 – 3.40 (m, 2H), 3.47 – 3.28 (m, 2H), 2.94 (s, 6H) ESI-MS: calculated for $(M+H)^+$ $C_9H_{19}N_2O_5$ 235.1294 found 235.1276.

(2R,3R)-N1-(2-(dimethylamino)ethyl)-2,3-dihydroxysuccinamide (3c): 100 mg of 3b was dissolved in 20 ml of methanol. To this solution 4 x 20 ml of 6.0 M ammonia in methanol was added every 4 hours and then reaction was stirred for 48 hours. Methanol was then evaporated under reduced pressure to obtain a off-white powder. Product was characterized with NMR and exact mass. ^{1}H NMR (400 MHz, D_2O) δ = 4.58 (m, 2H), 3.75 (s, 1H), 3.59 (t, 4H), 3.04 (t, 4H), 2.66 (s, 6 H), ESI-MS: calculated for $(M+H)^+$ $C_8H_{17}N_2O_5$ 220.1297 found 220.1304.

3.3.5 Synthesis of galactarate based small model compounds

(2R,3S,4R,5S)-N1,N6-bis(2-(dimethylamino)ethyl)-2,3,4,5-tetrahydroxyhexanediamide (4a): 100 mg (0.56 mmol) of dimethyl *meso*-galactarate (G) was weighed out in a RBF. 40 ml of methanol was added to this RBF to get a suspension. 74 mg (3 x 0.56 mmol) of N^1,N1-dimethylethane-1,2-diamine was added to the RBF and the reaction mixture was stirred at room temperature. The reaction mixture was then filtered and washed with 2 x 20 ml of methanol. The white powder obtained from the filtration was then dried under vacuum. 130 mg (yield 65%) of white powder was then characterized by NMR and ESI-MS. ^{1}H NMR (400 MHz, D_2O) δ = 4.32 (s, 2H), 3.91 (s, 2H), 3.33 (t, 4H), 2.44 (t, 4H), 2.14 (s, 12H). ESI-MS: calculated for $(M+H)^+$ $C_{14}H_{31}N_4O_6$ 351.2244 found 351.2231.

N^1,N^6-bis(2-(dimethylamino)ethyl)adipamide (4b): 1.12 g (5 x 2.73 mmol) of N^1,N^1-dimethylethane-1,2-diamine was weighed out in a round bottom flask. 100 ml of CH_2Cl_2 was added to the RBF in order to dissolve N^1,N^1-dimethylethane-1,2-diamine. The solution was brought to 0 ^oC and slowly 500 mg (2.73 mmol) of adipoyl chloride in 50 ml of CH_2Cl_2 was added to this solution drop wise while stirring over half an hour. The reaction mixture was stirred overnight and then CH2Cl2 was evaporated under reduced pressure to get yellowish powder. It was then dissolved in ethyl acetate and recrystallized to get the product. The product obtained was then dried under vacuum and characterized with NMR and exact mass. ^{1}H NMR (400 MHz, D_2O) δ = 3.22 (t, 4H), 2.50 (t, 4H), 2.21 (s, 12H), 2.12 (m, 1H), 1.43 (t, 4H).

3.3.6 X-ray crystallography: (Characterization was done by Dr. Carla Slebodnick)

A colorless plate (0.02 x 0.14 x 0.33 mm^3) was centered on the goniometer of an Oxford Diffraction Gemini A Ultra diffractometer operating with MoKα radiation. The data collection routine, unit cell refinement, and data processing were carried out with the program CrysAlisPro.

The Laue symmetry and systematic absences were consistent with the monoclinic space groups $P2_1$ and $P2_1/m$. The acentric space group $P2_1$ was chosen based on the E-statistics ($|E^2-1|$ = 0.769). The Friedel pairs were merged during refinement and the absolute configuration assigned arbitrarily. The structure was solved using SHELXS-97[26] and refined using SHELXL-97 [26] via the OLEX2 Program System [27]. The final refinement model involved anisotropic displacement parameters for non-hydrogen atoms. A riding model was used for the alkyl and amide hydrogens. The hydrogen atom positions of the hydroxyl groups were located from the residual electron density map and refined independently.

3.4 - Results and Discussion:

3.4. 1 Synthetic schemes

As shown in scheme 3.3, a small model compound 1a was synthesized to mimic the structure of **T4** repeat unit in order to study the hydrolysis phenomenon. Compound 1d, an analogous structure to 1a, with a propyl spacer (over an ethyl spacer in 1a) between the amidic nitrogen and the tertiary amine, was synthesized in order to examine the effect of the amide bond on the proximity of the tertiary amine to the amide nitrogen on the hydrolysis. Similarly, compound 1e was synthesized to study the effect of absence of amine on the carbon β to the nitrogen of the amide on its hydrolysis. 1f and 1g were synthesized to study the effect of replacing amine (as in compound 1a) functionality by hydroxyl and methoxy functionality respectively. In order to study the effect of hard charge such as quaternary ammonium groups compared to terminal amines on the hydrolysis, compound 1a was methylated to get compound 1h.

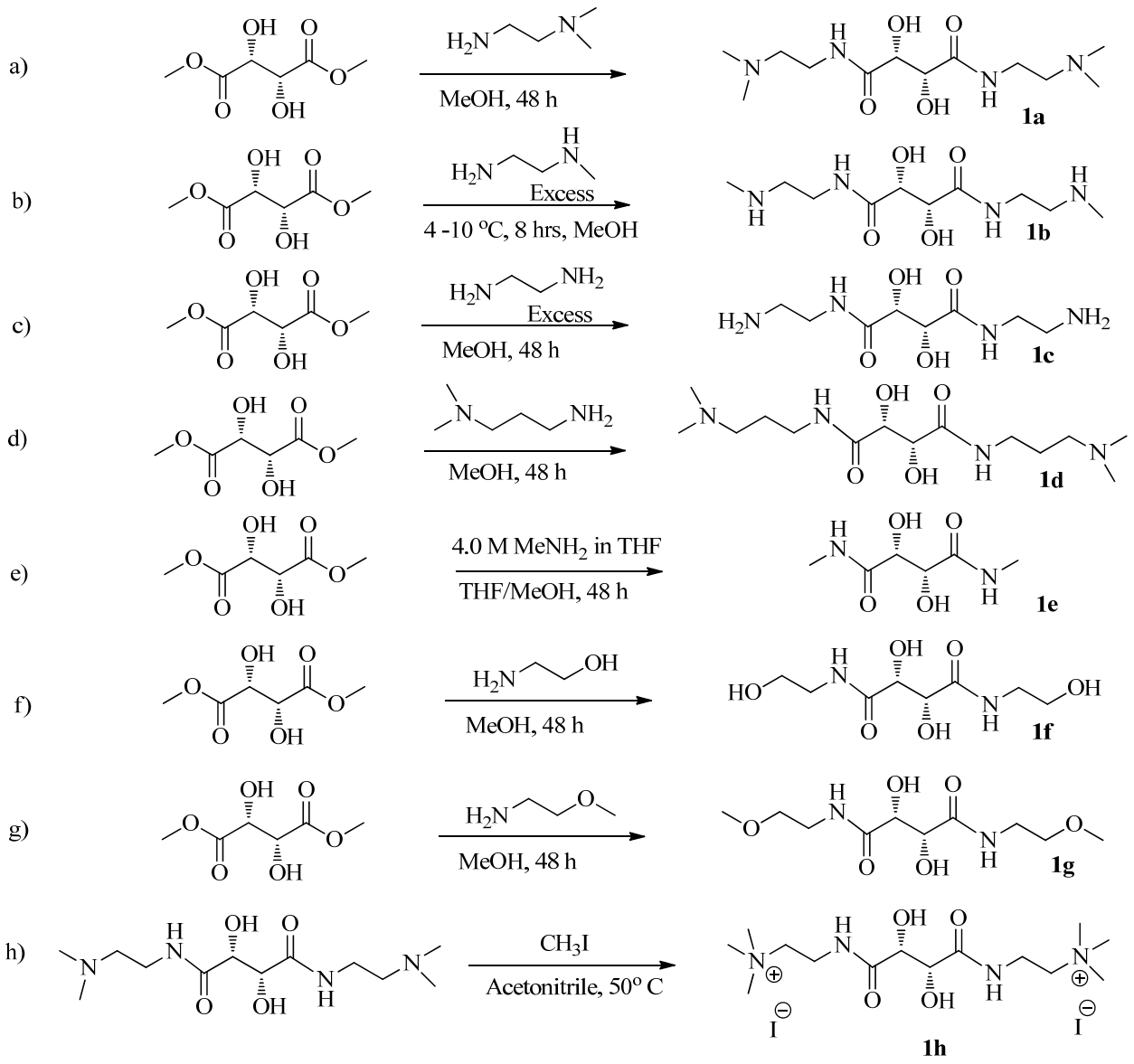

Scheme 3.3. Synthetic scheme for tartarate based model compounds

As shown in the Scheme 3.4, another series of small model compounds was synthesized. Compound 2a was synthesized to examine the effect of the absence of hydroxyls attached to the carbons α and β to the carbonyl of the amide on the amide hydrolysis. Three other small model compounds (2b, 2c, and 2d) were designed and synthesized to see the pattern of hydrolysis in the

compounds with one amide group per molecule as compared to the tartarate based series, which incorporate two amide groups per molecule.

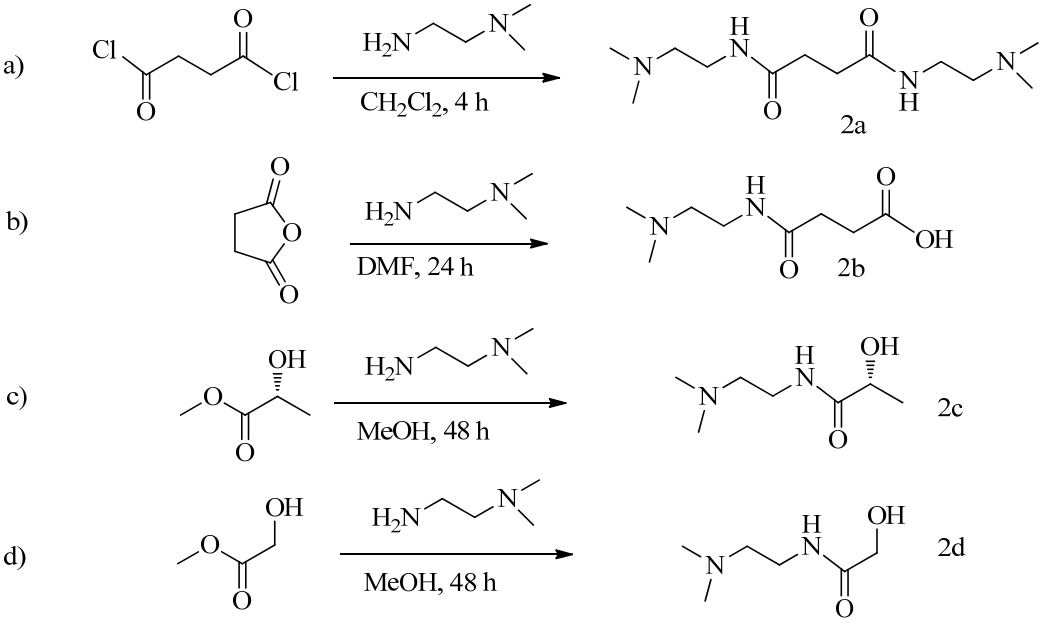

Scheme 3.4. Synthetic scheme for succinate, lactate and glycolate based model compounds

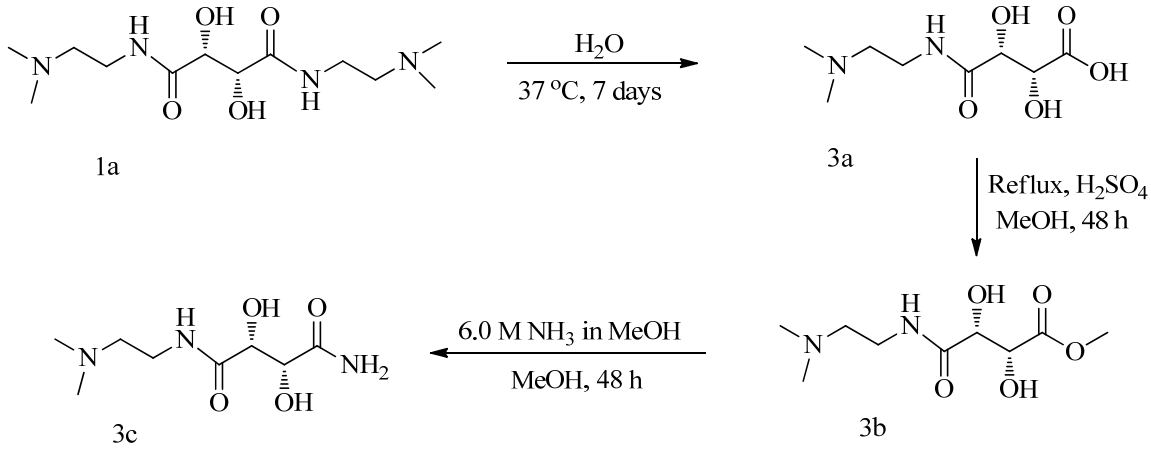

Scheme 3.5 Synthetic scheme for tartarate based asymmetric compound.

This series of compound based on the succinate, lactate and glycolate were designed in order investigate any intermolecular or intra molecular assistance for the hydrolysis

Compound 3c was designed, as all the other compounds with two amides groups per molecule are symmetric compound and might not reveal the important characteristics of the amide

hydrolysis in the molecule due to symmetry. Thus an asymmetric compound upon hydrolysis can provide more information which could be helpful in the design of new biomaterials. Synthesis was done by simple esterfication of the compound 3a to get 3b. Compound 3b was then treated with ammonia to finally get compound 3c.

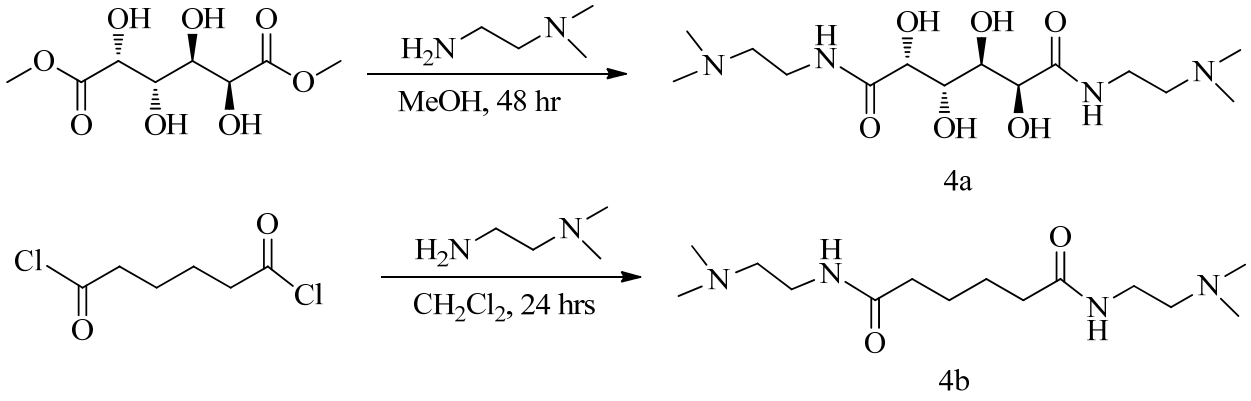

Scheme 3.6 Synthetic scheme for galactarate and adipate based small model compounds.

In order to study the amide hydrolysis of **G4** (Figure 3.1) small model compounds 4a and 4b were synthesized. 4a mimics the repeat unit of **G4** with galactarate moiety incorporated between amide groups which are connected to ethylamine functionality. In order to understand if there is any effect of hydroxyls present in the galactarate moiety α and β to the carboxyl of the amide on the its hydrolysis, compound 4b a non hydroxylated analogue of 4a was studied for hydrolysis

3.4.2 Fast amide hydrolysis: In an effort to examine, degradation behavior of **T4**, compound 1a with terminal tertiary amines (as compared to secondary amines in **T4**) was synthesized. Due to the ease of synthesis and purification, tertiary amine ends were preferred over secondary amine ends. In order to study the amide hydrolysis, 1a was characterized using nuclear magnetic resonance (NMR) spectroscopy under physiological conditions.

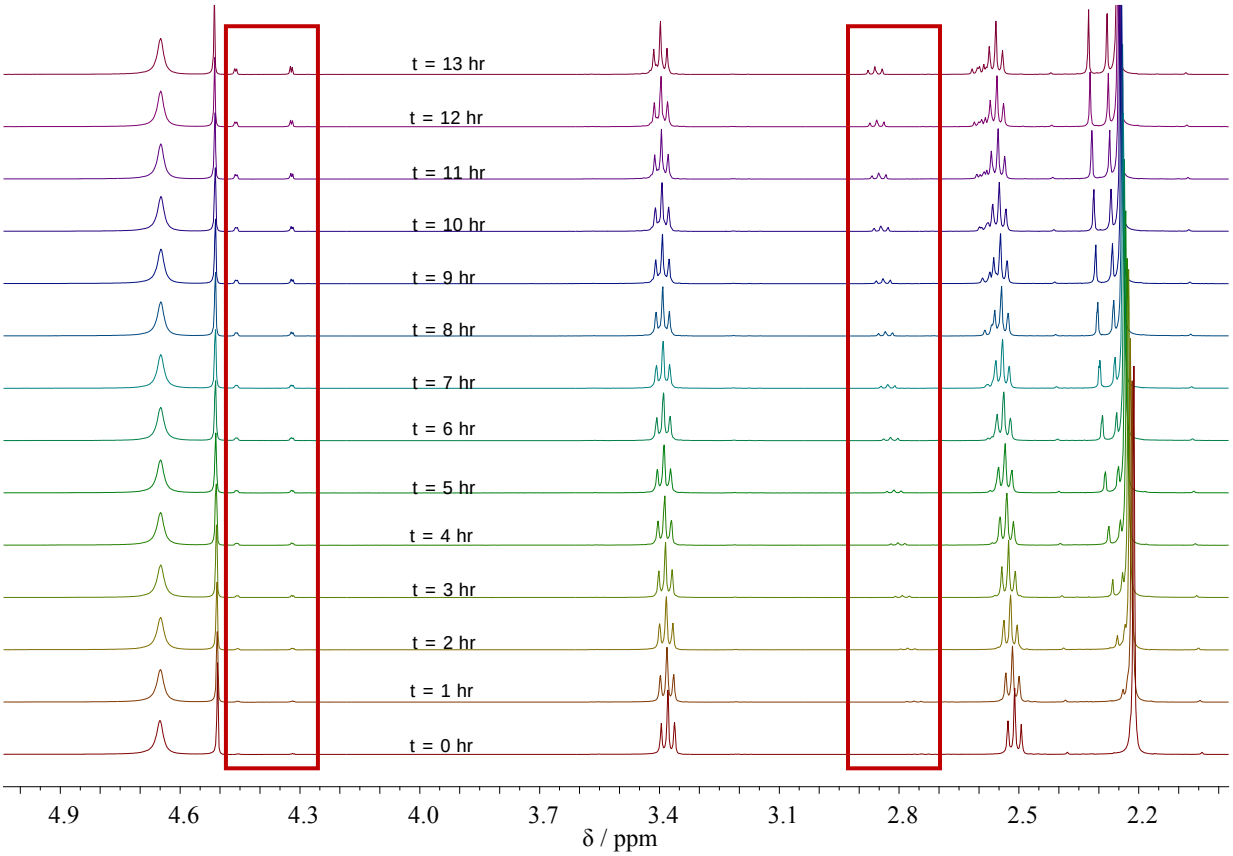

Figure 3.5 An *in-situ* array NMR carried in D_2O_{PBS} at 37 ^oC to take a proton NMR spectra every hour for compound 1a. The spetra shows key new peaks imphasized in red rectangle.

To simulate physiological conditions, deuterated phosphate buffer saline (D_2O_{PBS}) was prepared as described in the methods and materials section, and the NMR spectrometer was regulated at 37^oC. A solution of 100 mg/ml of 1a in D_2O_{PBS} was prepared immediately prior to starting an NMR experiment set to record a spectrum every hour for 13 hours. As shown in Figure 3.5 the

development of new resonances in the amine region from 2.20 to 2.88 ppm, and carbohydrate region from 4.31 to 4.47 ppm were observed. The new resonances in the amine region are indication of an amide hydrolyzing to produce new amine. The appearance of the new resonances in the amine region as early as in the first hour is also an indication of an unusually fast hydrolysis of amide. The similar array experiments were run for two sets of compounds from 1b-1h and 2a-2d and the results are reported in the Table 3.1. It is interesting to note that all the compounds that have amine (tertiary, secondary, primary) functionality at the ends show appearance of new peaks in the amine region indicating the hydrolysis of the starting material. As shown in Table 3.1, replacing the terminal amines, with hydroxyl (1f), methoxy (1g), and quaternary ammonium charge (Figure 3.9, 1h) or absence of terminal amines (Figure 3.8, 1e) do not show any indication of any new products over the longer periods of time implying that for the hydrolysis to occur presence of terminal amines is absolutely necessary.

Table 3.1 Compounds 1a-1h and 2a-2d were characterized with an array experiment to take a spectra every one hour in duetarated PBS at 37 ^{o}C. Plus (+) sign indicates: observed amide hydrolysis and minus (-) sign indicates: no observed amide hydrolysis.

Compound	Hydrolysis of amide observed in an array experiment(±)
1a	+
1b	+
1c	+
1d	+
1e	-
1f	-
1g	-
1h	-
2a	+
2b	-
2c	-
2d	-

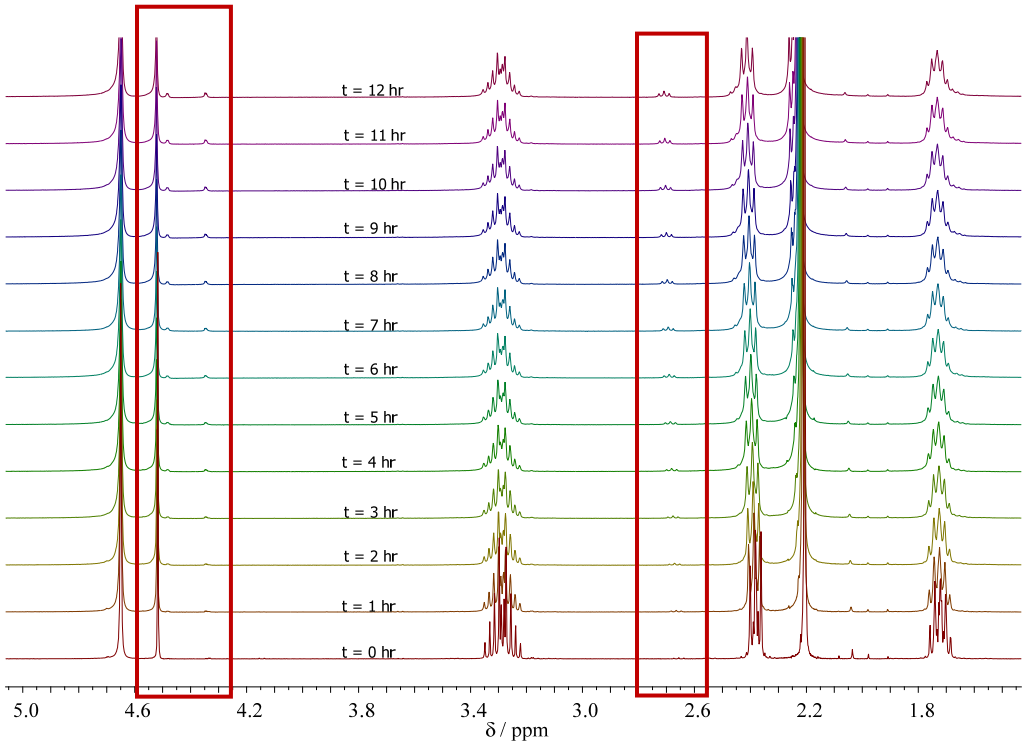

Figure 3.6 An *in-situ* array NMR obtained in D_2O_{PBS} at 37 ^oC to take a proton NMR spectra every hour for compound 1d. The spetra shows key new peaks imphasized in red rectangle.

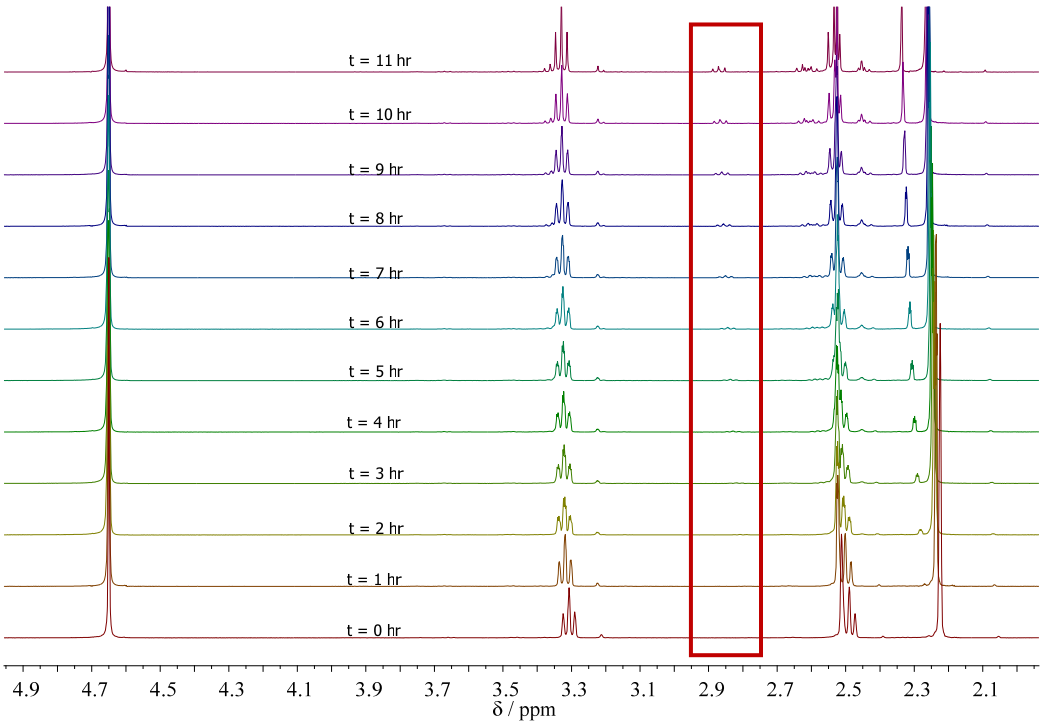

Figure 3.7 An *in-situ* array NMR obtained in D_2O_{PBS} at 37 ^oC to take a proton NMR spectra every hour for compound 2a. The spetra shows key new peaks imphasized in red rectangle.

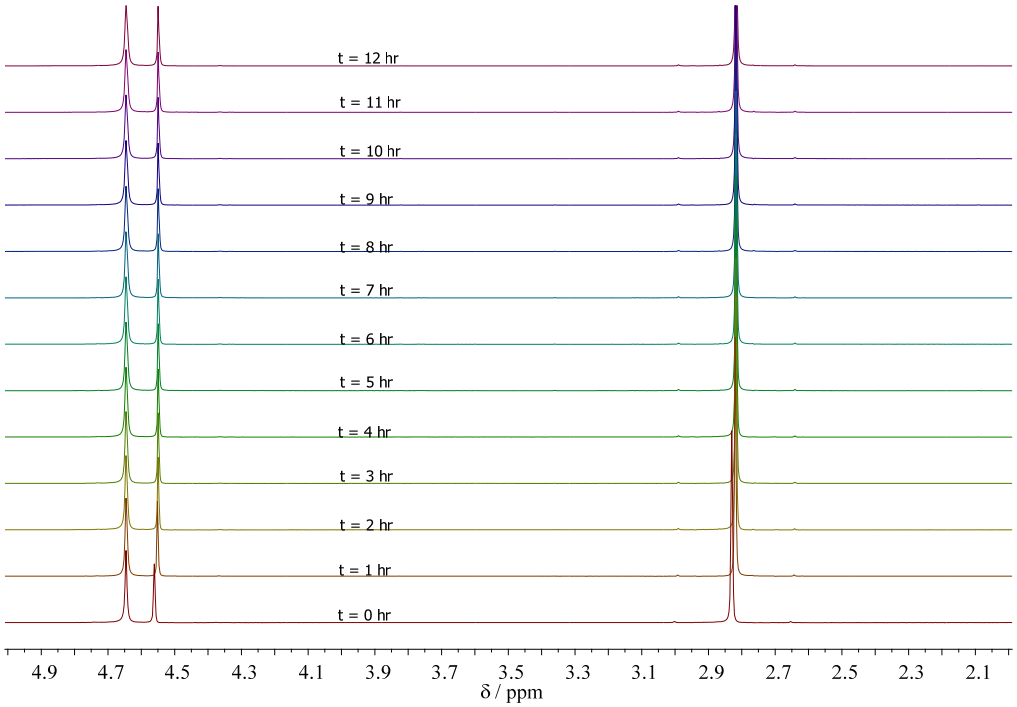

Figure 3.8 An *in-situ* array NMR obtained in D_2O_{PBS} at 37 ^oC to take a proton NMR spectra every hour for compound 1g which lack terminal amines and do not show any change in the NMR over the time, implying no amide hydrolysis

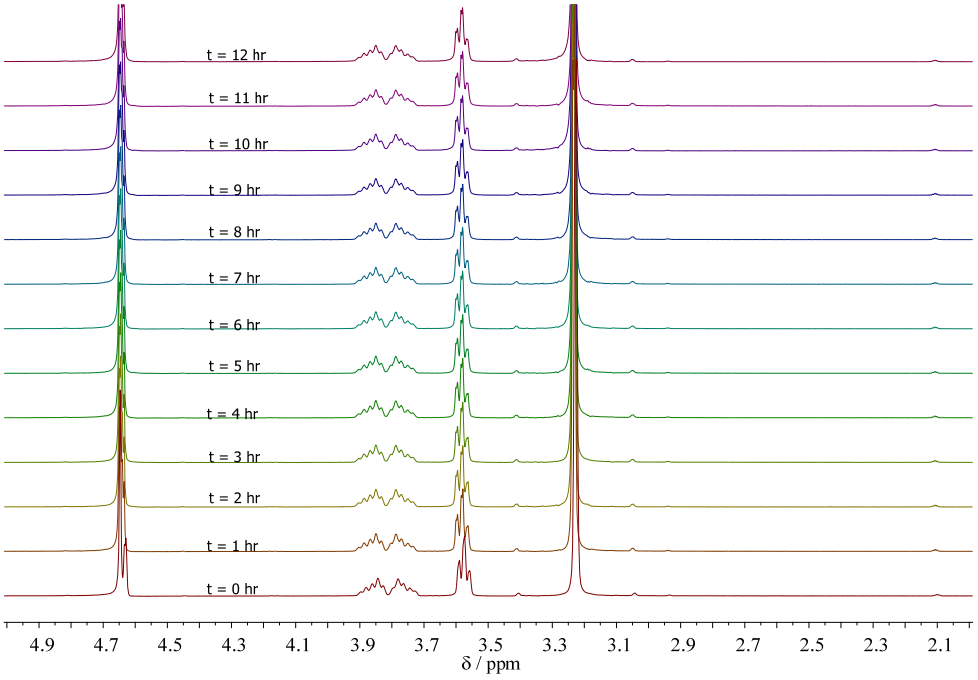

Figure 3.9 An *in-situ* array NMR obtained in D_2O_{PBS} at 37 ^oC to take a proton NMR spectra every hour for compound 1h which contain quateranary ammonium charge as compared to terminal amine in case of 1a. NMR indicates no amide hydrolysis.

3.4.3 X-ray crystallography study to analyze the amide bond length and angles (Characterization was done by Dr. Carla Slebodnick):

As explained in the introduction that few distorted amides reported before show hydrolysis due to the increased bond length or torsion angles. As studied before compound 1d shows the hydrolysis under physiological conditions while 1e does not show any hydrolysis in similar conditions. Therefore 1d and 1e were chosen for x-ray crystallography in order to analyze any available difference in the amide bond angle and bond length. The detailed results for these two compounds for bond angles and bond length are listed in the Tables 3.2 to 3.8. In summary, for compound 1d and 1e the amide bond angle (N-C-O) is around 123^{o} and amide bond length (N-C) is around 1.338 Å (see Table 3.2 below) (Please note that for compound 1d, there are two molecules per unit cell resulting four amide bond values.)

Table 3.2. Summary of Amide bond length and angle for compound 1d and 1e obtained by X-ray crystallography. Note that for compound 1d, there are two molecules in one unit cell resulting four amide bond values.

Compound 1d(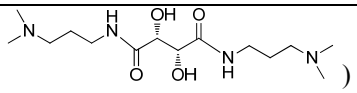)				Compound 1e (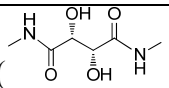)			
Bond length(Å)		Bond angle (^{o})		Bond length(Å)		Bond angle (^{o})	
N(2)-C(6)	1.3296(19)	O(1)-C(6)-N(2)	122.88(13)	N(1)-C(2)	1.331(3)	O(1)-C(2)-N(1)	122.4(2)
N(3)-C(9)	1.338(2)	O(4)-C(9)-N(3)	124.67(14)	N(2)-C(5)	1.328(3)	O(4)-C(5)-N(2)	123.8(2)
N(6)-C(20)	1.342(2)	O(5)-C(20)-N(6)	122.94(15)	-	-	-	-
N(7)-C(23)	1.339(2)	O(8)-C(23)-N(7)	123.84(15)	-	-	-	-

Characterization of compound 1d with X-ray crystallography:

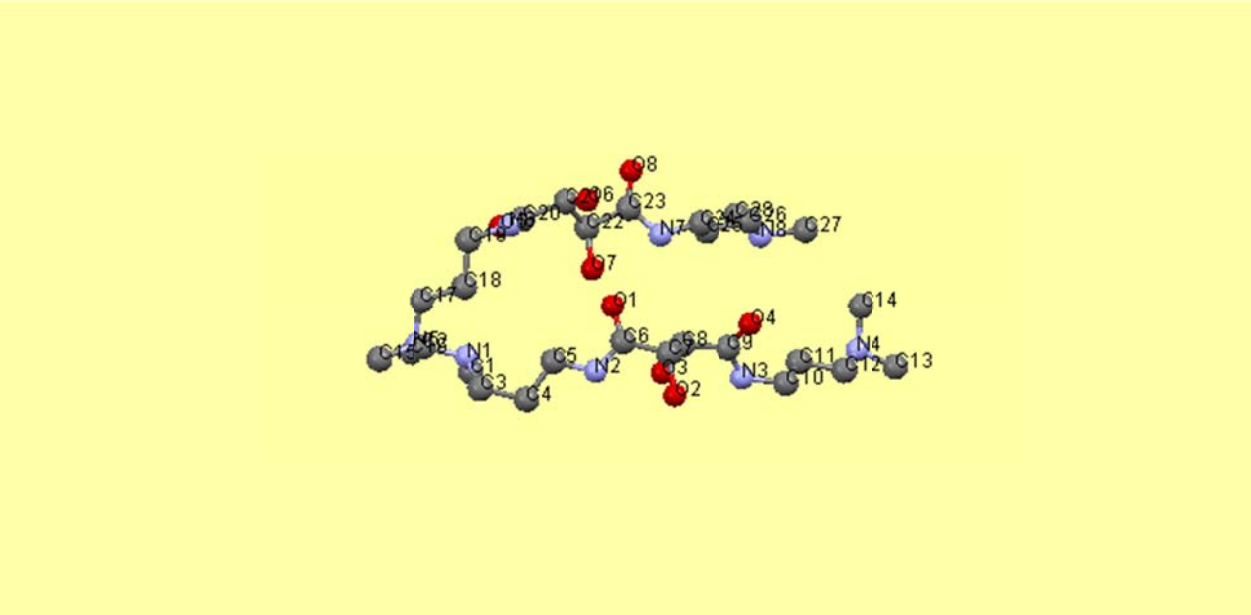

Figure 3.10. Representation of compound 1d from X-ray crystallography

Table 3.3 Crystal data and structure refinement for compound 1d

Identification code	1d
Empirical formula	$C_{14}H_{30}N_4O_4$
Formula weight	318.42
Temperature	100(2) K
Wavelength	0.71073 Å
Crystal system	Monoclinic
Space group	$P2_1$
Unit cell dimensions	a = 12.4836(2) Å α= 90°.
	b = 9.85868(12) Å β= 111.7617(19)°.
	c = 15.6124(3) Å γ = 90°.
Volume	1784.52(5) $Å^3$
Z	4
Density (calculated)	1.185 Mg/m^3
Absorption coefficient	0.087 mm^{-1}
F(000)	696
Crystal size	0.49 x 0.41 x 0.15 mm^3

Theta range for data collection	3.34 to 30.03°.
Index ranges	-17<=h<=17, -13<=k<=13, -21<=l<=21
Reflections collected	41477
Independent reflections	5487 [R(int) = 0.0416]
Completeness to theta = 30.03°	99.8 %
Absorption correction	None
Refinement method	Full-matrix least-squares on F^2
Data / restraints / parameters	5487 / 1 / 417
Goodness-of-fit on F^2	0.974
Final R indices [I>2sigma(I)]	R1 = 0.0337, wR2 = 0.0784
R indices (all data)	R1 = 0.0408, wR2 = 0.0802
Largest diff. peak and hole	0.367 and -0.190 e.$Å^{-3}$

Table 3.4 Bond lengths [Å] and angles [°] for 1d. Values highlighed in yellow represents the bond lengths and values hilighed in red represents the bond anlges for the amides in 1d 1d

O(1)-C(6)	1.2435(18)	N(3)-C(10)	1.4514(19)	C(3)-C(4)	1.522(2)
O(2)-C(7)	1.4137(17)	N(4)-C(14)	1.457(2)	C(4)-C(5)	1.515(2)
O(3)-C(8)	1.4119(17)	N(4)-C(13)	1.472(2)	C(6)-C(7)	1.5265(19)
O(4)-C(9)	1.2314(18)	N(4)-C(12)	1.474(2)	C(7)-C(8)	1.5353(19)
O(5)-C(20)	1.2293(19)	N(5)-C(16)	1.459(2)	C(8)-C(9)	1.526(2)
O(6)-C(21)	1.4213(18)	N(5)-C(15)	1.463(2)	C(10)-C(11)	1.526(2)
O(7)-C(22)	1.4199(19)	N(5)-C(17)	1.467(2)	C(11)-C(12)	1.524(2)
O(8)-C(23)	1.2374(19)	N(6)-C(20)	1.342(2)	C(17)-C(18)	1.526(2)
N(1)-C(1)	1.466(2)	N(6)-C(19)	1.458(2)	C(18)-C(19)	1.519(2)
N(1)-C(2)	1.476(2)	N(7)-C(23)	1.339(2)	C(20)-C(21)	1.526(2)
N(1)-C(3)	1.477(2)	N(7)-C(24)	1.449(2)	C(21)-C(22)	1.528(2)
N(2)-C(6)	1.3296(19)	N(8)-C(26)	1.467(2)	C(22)-C(23)	1.531(2)
N(2)-C(5)	1.4627(18)	N(8)-C(28)	1.467(3)	C(24)-C(25)	1.524(2)
N(3)-C(9)	1.338(2)	N(8)-C(27)	1.471(2)	C(25)-C(26)	1.521(2)

C(1)-N(1)-C(2)	109.51(12)	C(5)-C(4)-C(3)	111.23(12)	N(5)-C(17)-C(18)	112.93(13)
C(1)-N(1)-C(3)	110.29(13)	N(2)-C(5)-C(4)	112.34(12)	C(19)-C(18)-C(17)	111.73(14)
C(2)-N(1)-C(3)	108.28(12)	O(1)-C(6)-N(2)	122.88(13)	N(6)-C(19)-C(18)	113.05(13)
C(6)-N(2)-C(5)	118.41(12)	O(1)-C(6)-C(7)	118.97(13)	O(5)-C(20)-N(6)	122.94(15)
C(9)-N(3)-C(10)	122.20(12)	N(2)-C(6)-C(7)	118.09(12)	O(5)-C(20)-C(21)	120.31(14)
C(14)-N(4)-C(13)	109.02(15)	O(2)-C(7)-C(6)	111.34(11)	N(6)-C(20)-C(21)	116.74(13)
C(14)-N(4)-C(12)	111.33(13)	O(2)-C(7)-C(8)	110.07(11)	O(6)-C(21)-C(20)	112.52(12)
C(13)-N(4)-C(12)	110.44(13)	C(6)-C(7)-C(8)	106.22(11)	O(6)-C(21)-C(22)	110.83(13)
C(16)-N(5)-C(15)	108.98(15)	O(3)-C(8)-C(9)	112.03(11)	C(20)-C(21)-C(22)	108.56(12)
C(16)-N(5)-C(17)	110.84(15)	O(3)-C(8)-C(7)	108.18(11)	O(7)-C(22)-C(21)	111.40(13)
C(15)-N(5)-C(17)	110.66(13)	C(9)-C(8)-C(7)	110.14(11)	O(7)-C(22)-C(23)	111.18(13)
C(20)-N(6)-C(19)	122.02(13)	O(4)-C(9)-N(3)	124.67(14)	C(21)-C(22)-C(23)	111.47(12)
C(23)-N(7)-C(24)	123.33(14)	O(4)-C(9)-C(8)	120.08(13)	O(8)-C(23)-N(7)	123.84(15)
C(26)-N(8)-C(28)	112.01(14)	N(3)-C(9)-C(8)	115.25(12)	O(8)-C(23)-C(22)	121.36(15)
C(26)-N(8)-C(27)	110.01(14)	N(3)-C(10)-C(11)	111.71(12)	N(7)-C(23)-C(22)	114.72(14)
C(28)-N(8)-C(27)	110.16(17)	C(12)-C(11)-C(10)	111.54(12)	N(7)-C(24)-C(25)	113.31(13)
N(1)-C(3)-C(4)	114.29(12)	N(4)-C(12)-C(11)	111.89(12)	C(26)-C(25)-C(24)	109.93(13)

Table 3.5 Torsion angles [°] for 1d

C(1)-N(1)-C(3)-C(4)	65.29(16)	O(2)-C(7)-C(8)-C(9)	-69.93(14)
C(2)-N(1)-C(3)-C(4)	-174.90(13)	C(6)-C(7)-C(8)-C(9)	169.42(11)
N(1)-C(3)-C(4)-C(5)	55.36(18)	C(10)-N(3)-C(9)-O(4)	-3.5(2)
C(6)-N(2)-C(5)-C(4)	159.97(13)	C(10)-N(3)-C(9)-C(8)	176.60(13)
C(3)-C(4)-C(5)-N(2)	173.24(12)	O(3)-C(8)-C(9)-O(4)	176.46(13)
C(5)-N(2)-C(6)-O(1)	4.5(2)	C(7)-C(8)-C(9)-O(4)	-63.09(17)
C(5)-N(2)-C(6)-C(7)	-172.78(12)	O(3)-C(8)-C(9)-N(3)	-3.63(17)
O(1)-C(6)-C(7)-O(2)	179.13(12)	C(7)-C(8)-C(9)-N(3)	116.83(13)
N(2)-C(6)-C(7)-O(2)	-3.50(17)	C(9)-N(3)-C(10)-C(11)	-95.73(17)
O(1)-C(6)-C(7)-C(8)	-61.04(16)	N(3)-C(10)-C(11)-C(12)	-175.95(13)
N(2)-C(6)-C(7)-C(8)	116.33(13)	C(14)-N(4)-C(12)-C(11)	72.83(17)
O(2)-C(7)-C(8)-O(3)	52.82(15)	C(13)-N(4)-C(12)-C(11)	-165.91(14)
C(6)-C(7)-C(8)-O(3)	-67.83(14)	C(10)-C(11)-C(12)-N(4)	179.97(13)

C(16)-N(5)-C(17)-C(18)	-73.90(18)	O(6)-C(21)-C(22)-C(23)	-64.01(17)
C(15)-N(5)-C(17)-C(18)	165.07(14)	C(20)-C(21)-C(22)-C(23)	171.94(12)
N(5)-C(17)-C(18)-C(19)	170.97(13)	C(24)-N(7)-C(23)-O(8)	-3.4(2)
C(20)-N(6)-C(19)-C(18)	83.73(18)	C(24)-N(7)-C(23)-C(22)	173.40(13)
C(17)-C(18)-C(19)-N(6)	178.59(13)	O(7)-C(22)-C(23)-O(8)	-174.01(14)
C(19)-N(6)-C(20)-O(5)	-1.6(2)	C(21)-C(22)-C(23)-O(8)	-49.06(19)
C(19)-N(6)-C(20)-C(21)	177.07(14)	O(7)-C(22)-C(23)-N(7)	9.09(18)
O(5)-C(20)-C(21)-O(6)	-172.01(14)	C(21)-C(22)-C(23)-N(7)	134.04(14)
N(6)-C(20)-C(21)-O(6)	9.3(2)	C(23)-N(7)-C(24)-C(25)	-91.08(18)
O(5)-C(20)-C(21)-C(22)	-49.0(2)	N(7)-C(24)-C(25)-C(26)	-176.84(14)
N(6)-C(20)-C(21)-C(22)	132.30(14)	C(28)-N(8)-C(26)-C(25)	65.00(19)
O(6)-C(21)-C(22)-O(7)	60.82(16)	C(27)-N(8)-C(26)-C(25)	-172.12(17)
C(20)-C(21)-C(22)-O(7)	-63.23(16)	C(24)-C(25)-C(26)-N(8)	166.68(14)

Characterization of coumpound 1e with X-ray crystallography:

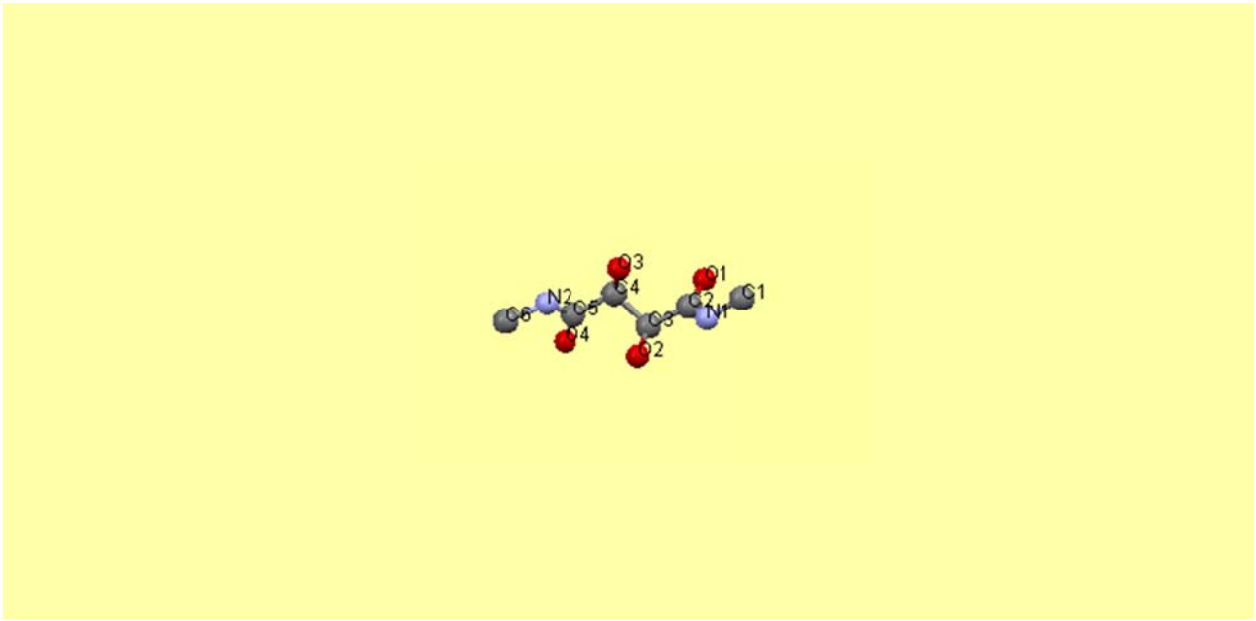

Figure 3.11. Representation of compound 1e from X-ray crystallography

Table 3.6 Crystal data and structure refinement for compound 1e

Identification code	1e
Empirical formula	$C_6H_{12}N_2O_4$
Formula weight	176.18
Temperature	100(2) K
Wavelength	0.71073 Å
Crystal system	Monoclinic
Space group	$P2_1$
Unit cell dimensions	a = 8.6070(4) Å α= 90°
	b = 5.09176(17) Å β= 112.097(6)°
	c = 10.5404(5) Å γ = 90°
Volume	428.00(3) $Å^3$
Z	2
Density (calculated)	1.367 Mg/m^3
Absorption coefficient	0.115 mm^{-1}
F(000)	188
Crystal size	0.33 x 0.14 x 0.02 mm^3
Theta range for data collection	3.86 to 28.28°.
Index ranges	-11<=h<=11, -6<=k<=6, -14<=l<=14
Reflections collected	8603
Independent reflections	1176 [R(int) = 0.0559]
Completeness to theta = 28.28°	99.7 %
Absorption correction	None
Refinement method	Full-matrix least-squares on F^2
Data / restraints / parameters	1176 / 1 / 117
Goodness-of-fit on F^2	0.964
Final R indices [I>2sigma(I)]	R1 = 0.0373, wR2 = 0.0758
R indices (all data)	R1 = 0.0512, wR2 = 0.0786
Largest diff. peak and hole	0.263 and -0.181 $e.Å^{-3}$

Table 3.7 Bond lengths [Å] and angles [°] for 1e. Values highlighed in yellow represents the bond lengths and values hilighed in red represents the bond anlges for the amides in 1d 1e

O(1)-C(2)	1.236(2)	N(1)-C(2)	1.331(3)	C(2)-C(3)	1.517(3)
O(2)-C(3)	1.431(2)	N(1)-C(1)	1.450(3)	C(3)-C(4)	1.533(3)
O(3)-C(4)	1.414(3)	N(2)-C(5)	1.328(3)	C(4)-C(5)	1.531(3)
O(4)-C(5)	1.239(3)	N(2)-C(6)	1.455(3)		

C(2)-N(1)-C(1)	121.69(19)	O(2)-C(3)-C(2)	109.96(17)	C(5)-C(4)-C(3)	108.63(17)
C(5)-N(2)-C(6)	122.47(19)	O(2)-C(3)-C(4)	109.00(17)	O(4)-C(5)-N(2)	123.8(2)
O(1)-C(2)-N(1)	122.4(2)	C(2)-C(3)-C(4)	109.12(18)	O(4)-C(5)-C(4)	121.0(2)
O(1)-C(2)-C(3)	121.12(19)	O(3)-C(4)-C(5)	112.07(18)	N(2)-C(5)-C(4)	115.2(2)
N(1)-C(2)-C(3)	116.48(18)	O(3)-C(4)-C(3)	107.96(17)		

Table 3.8 Torsion angles [°] for 1e

C(1)-N(1)-C(2)-O(1)	5.8(4)	O(2)-C(3)-C(4)-C(5)	-47.0(2)
C(1)-N(1)-C(2)-C(3)	-173.2(2)	C(2)-C(3)-C(4)-C(5)	-167.13(17)
O(1)-C(2)-C(3)-O(2)	179.3(2)	C(6)-N(2)-C(5)-O(4)	2.3(3)
N(1)-C(2)-C(3)-O(2)	-1.7(3)	C(6)-N(2)-C(5)-C(4)	-178.12(18)
O(1)-C(2)-C(3)-C(4)	-61.2(3)	O(3)-C(4)-C(5)-O(4)	-172.81(19)
N(1)-C(2)-C(3)-C(4)	117.8(2)	C(3)-C(4)-C(5)-O(4)	-53.6(3)
O(2)-C(3)-C(4)-O(3)	74.7(2)	O(3)-C(4)-C(5)-N(2)	7.6(2)
C(2)-C(3)-C(4)-O(3)	-45.4(2)	C(3)-C(4)-C(5)-N(2)	126.84(19)

3.4.4 One side amide hydrolysis

An *in-situ* array NMR for compounds 1a-1d and 2a indicate the initial hydrolysis., In case of compounds 1a-1d, evolution of two new peaks in the carbohydrate region (4.2 to 4.5 ppm) indicates breaking the symmetry of the starting molecules. To further understand this phenomenon, analysis of the hydrolyzed product was necessary. In order to analyze the hydrolyzed products, 400 mg of compound 1a was dissolved in 10 ml of PBS and stirred at 37 ^{o}C. The hydrolysis was monitored via NMR to observe the disappearance of the carbohydrate proton resonance (singlet) at 4.5 ppm and appearance of two new resonances (doublets) in the same region (4.2 to 4.5 ppm).

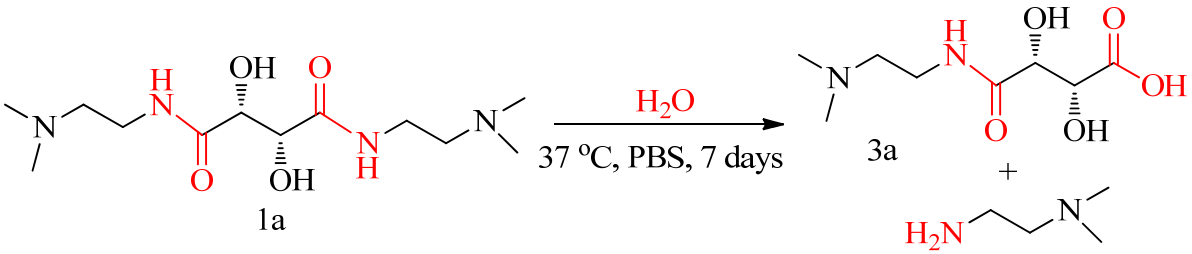

Figure 3.12 Compound 1a shows one side hydrolysis to produce compound 3a.

The hydrolysis product was isolated from the reaction mixture as explained in the materials and methods section. The NMR characterization of the hydrolyzed product shows two different resonances (H_A and H_B, Figure 3.13) in the carbohydrate region indicating loss of symmetry. Also the exact mass of the compound was found $(M+H)^{+1}$ = 221.1139 and the calculated exact mass for the compound 3a (one side hydrolyzed 1a) is 221.1137. Characterization strongly suggests the hydrolysis of 1a on one side. This is intriguing chemistry as the selectivity on one side hydrolysis can trigger new designs of biomaterials for very specific application involving selectivity. Compounds 1b-1d and 2a were characterized for the similar chemistry and the positive results for all above metioned compounds were found for the one side hydrolysis.

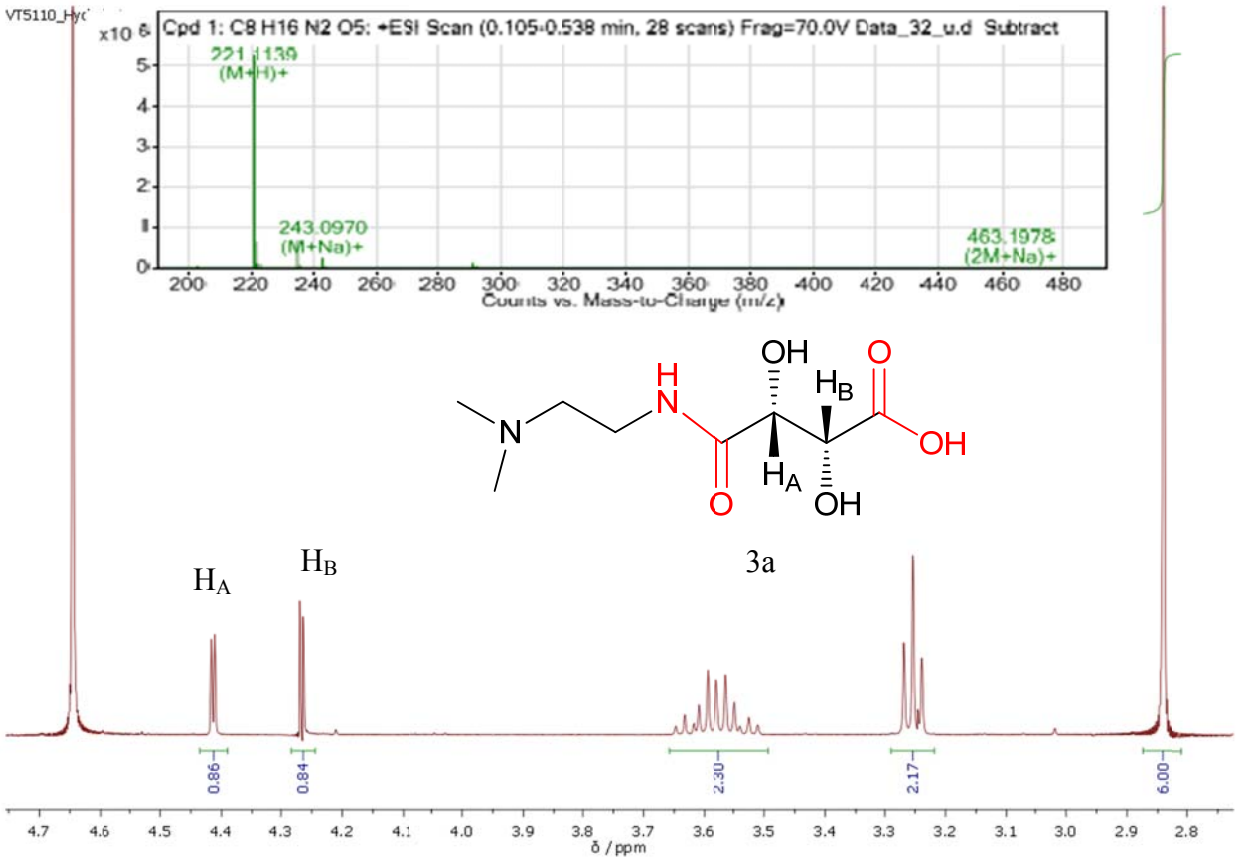

Figure 3.13 The ^{1}H NMR and exact mass spectrum for the isolated product (3a) of hydrolyzed 1a

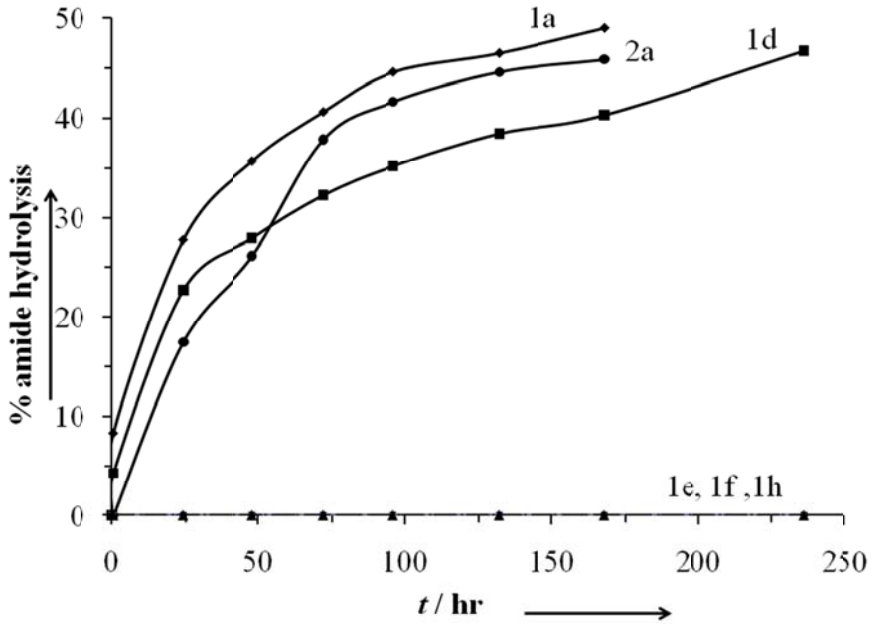

Figure 3.14 Compounds 1a, 1d, 2a show one side amide hydrolysis and attains maximum of 50% amide hydrolysis at different time points. Compounds 1e, 1f and 1h do not show any hydrolysis.

In order to further investigate the rate of hydrolysis of the amide bonds, compounds 1a, 1d, 1e, 1f, 1h and 2a were incubated under physiological conditions and were monitored over 7 days with NMR. It was noted that 1a starts to undergo amide hydrolysis as early as 30 minutes but 1d and 2a did not undergo hydrolysis in first 30 minutes of incubation. As shown in Figure 3.14, the rate of hydrolysis of 1a was faster, with about 70% of 1a undergoing hydrolysis in 48 hours. It is interesting to note that in Figure 3, only about 35% of the amide bonds were shown to be hydrolyzed as each molecule have two amide bonds and there is selective amide hydrolysis on one side of the compounds 1a, 1d, and 2a. Compounds 1d and 2a show slower hydrolysis and up to 50% of the molecules show hydrolysis in 48 hours. The hydrolysis of 1d is approximately 94% after ~ 14 days. These experiments reveal that as the distance between terminal tertiary amine and the nitrogen of the amide increases from an ethyl spacer to propyl spacer, the hydrolysis rate decreases dramatically. This discovery can be very important in tailoring the controlled and selective cleavage of amide linkages over an extended period.

In case of 2a, the rate of hydrolysis is slower in the first 48 hrs as compared to 1a and 1d and achieves about 50% amide hydrolysis of molecules (25% of total amides present) but it was observed that the rate of hydrolysis increases after 50% hydrolysis of molecules and the rate increases and hydrolysis becomes faster after than hydrolysis rate of 1d and achieves about 90% of in about 7 days as compared to about 98% hydrolysis of 1a in 7 days and about 80% of hydrolysis of 1d. This study reveals that the presence of hydroxyls attached to the carbons α and β to the carboxyl of the amide has an effect on the rate of hydrolysis and the rate is slower for 2a over 1a. This study also indicates that in case of compounds 1f, and 1g where the terminal amines are replaced by the hydroxyls and methoxy groups respectively did not show any hydrolysis of the amides. In case of compound 1e that lacks the terminal amines as compared to

the compound 1a, the compound 1e did not show any hydrolysis. The presence of quaternary ammonium charges replacing the terminal amines in case of 1h did not result in any hydrolysis of amides either. We further investigated this phenomenon by taking 0.66 mg of 1a in 660 µl of D_2O (not D_2O_{PBS}) and adding a drop of DCl to this mixture (pH 1.0 or less). This compound, when studied for the amide hydrolysis for 14 days, did not show any significant development of new resonances (Figure 3.23, appendix section). Hence the studies show that protonating the terminal tertiary amines can either stop or significantly reduce the hydrolysis of the amides.

The analysis was also useful to determine kinetics of amide hydrolysis. More specifically, the rate constants, order of the reaction and half-life of the amide hydrolysis can be determined from the NMR data for the amide hydrolysis. From the NMR studies, the ratio of concentration of the starting material and the hydrolyzed product was calculated for different time points and were fit to the different kinetic equations. As shown in Figure 3.16 the reaction coordinates fit for the pseudo first order reaction for the amide hydrolysis. Higher slope of the plot is an indication for the faster amide hydrolysis.

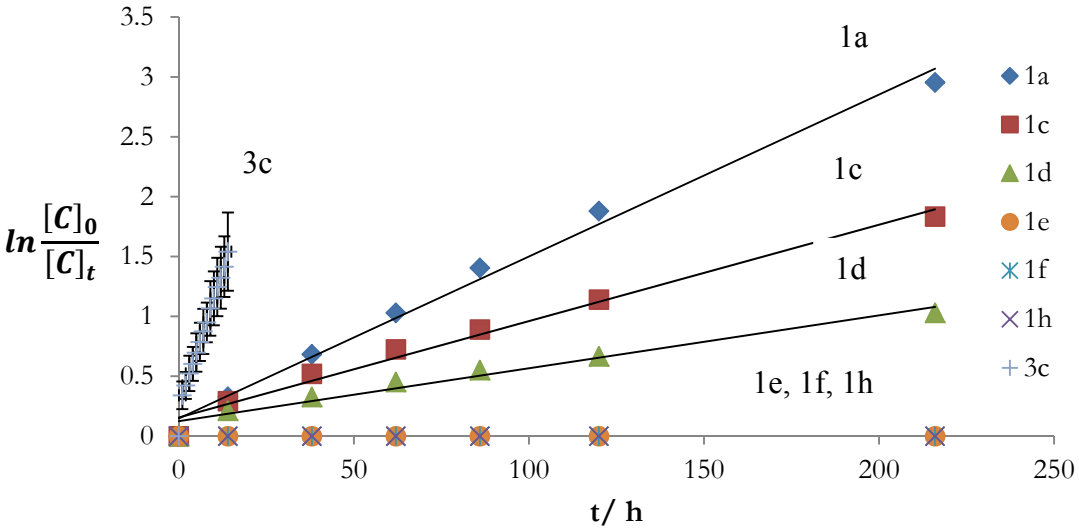

3.15 Kinetic study show the reaction of one side amide hydrolysis follows the pseudo first order kinetics.

Table 3.9 Rate constants and half life of the amide hydrolysis values for different small model compounds.

Compound	k x 10^3 (h^{-1})	$t_{1/2}$ (h)	Selective amide hydrolysis on one side (±)
1a	13.5	51	+
1c	8.3	83	+
1d	5.5	126	+
1e	0	-	-
1f	0	-	-
1h	0	-	-
3c	97	7	+

From the half-life ($t_{1/2}$) and the rate constant (k) data (Table 3.9) calculated from the kinetic study plot in the Figure 3.15, it can be extrapolated that the rate of hydrolysis for compound 1a is ~2.5 times faster than 1d due to the proximity of amine from the amidic nitrogen. In addition, the rate of hydrolysis of the compound with the terminal primary ends was slower over the terminal tertiary ends and the detailed studies to understand this phenomenon are underway. Similar results of no hydrolysis for the compounds 1e, 1f, 1g, and 1h as conclude from the *in-situ* array NMR experiment were observed for longer period. These studies confirm that the presence of the terminal amines in these compounds is of utmost importance for the amide hydrolysis to occur.

One side hydrolysis of the compounds is evident from these studies and it is very interesting, that such high selectivity without the use of specific enzymes is possible. It is this reason an asymmetric compound 3c (Figure 3.16) was also characterized for the amide hydrolysis to find out if the amide which have the ethylamine attached (Amide 1) hydrolyzes or the other side amide (amide B) which does not have any substituent show the hydrolysis. As shown in Figure 3.16 and 3.17, the *in-situ* array NMR study for 3c show the hydrolysis for the amide B. The hydrolysis rate as shown in Table 3.9 is very fast as compared to the other studied compounds as this is verified from the Figure 3.15 and 3.17.

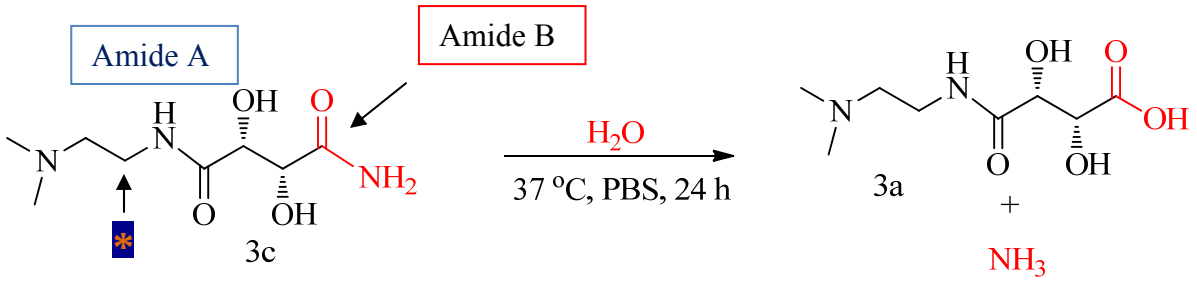

Figure 3.16 Asymmetric compound with a twodifferent amides to analyze which amide undergoes the hydrolysis

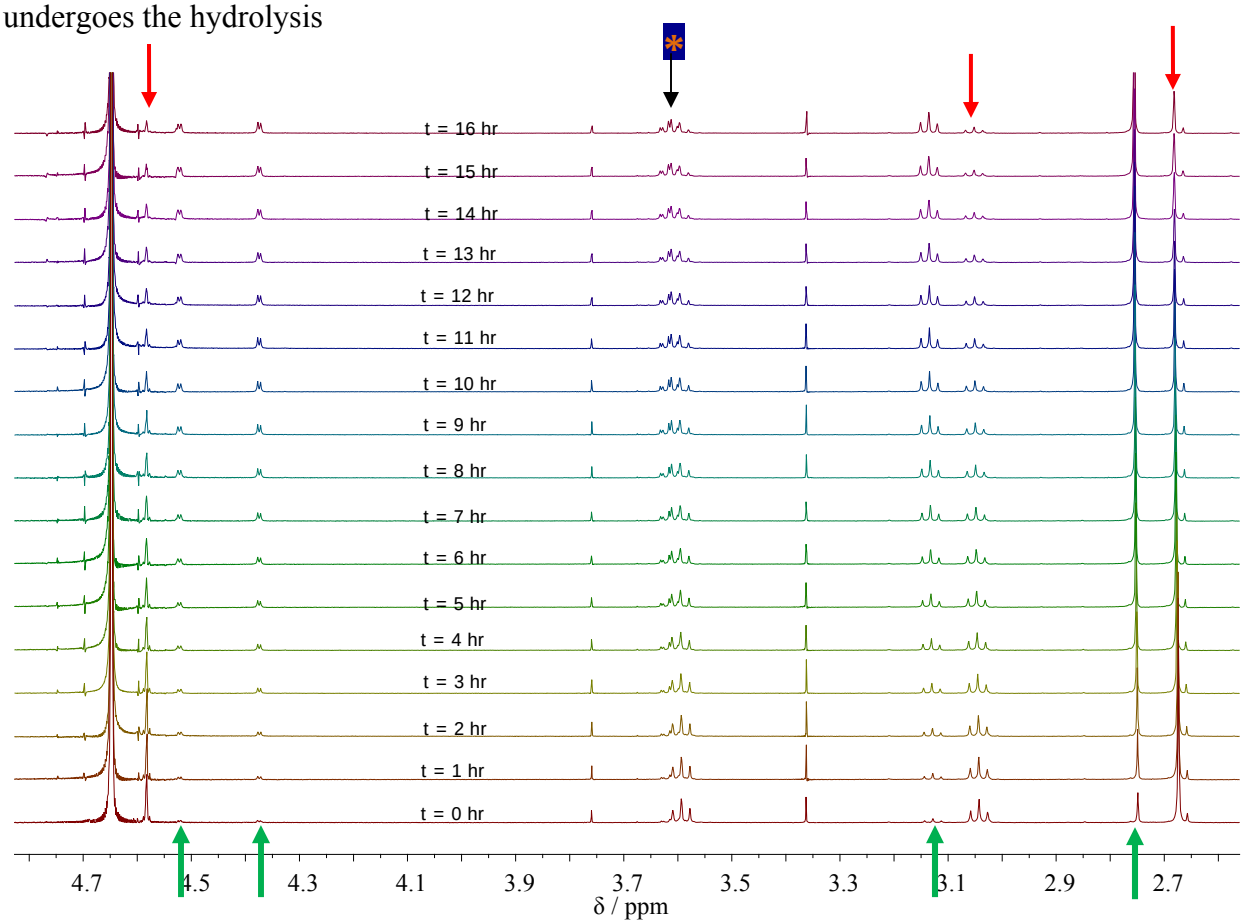

Figure 3.17 An *in-situ* array NMR of compound 3c obtained in D_2O_{PBS} at 37 °C. One NMR spectum was taken every hour for 16 hours. The red arrows indicate the disappearnce of the peaks for the 3c and green arrows indicate the appearance of the new peaks for the hydrolyzed product.

As shown in Figure 3.17 the evolution of two new peaks in the carbohydrate region is a classic one side hydrolysis as studied earlier in this chapter. The peaks in the amine and amide region show a shift indicating formation of new molecule although resonance the amide region (3.6 ppm) which comes from the methylene protons adjacent to amide A (indicated by * in Figure

3.16 and 3.17) does not subside. This implies that there is no hydrolysis of the amide A. The hydrolyzed product when characterized by the ESI-MS for exact mass shows resonance for the hydrolyzed compound 3a and does not show any resonace for starting material (compound 3c). ESI-MS calculated for $C_8H_{17}N_2O_5$ 221.1137. Found 221.1122 (Mass spec shown in Figure 3.22 in the Appendix section)

3.4.5 Intramolecular versus intermolecular hydrolysis

The one side hydrolysis of 1a raises the question, if the reaction is an intermolecular hydrolysis or an intramolecular hydrolysis phenomenon. To investigate this raised concern two different experiments were designed.

Effect of concentration on the hydrolysis rate of 1a: The kinetics of the reaction were investigated and it was found that the rate of the reaction fits the pseudo first order kinetics and from the first order kinetics law the rate constant (k) should be independent of the concentration of the starting material. In addition, if the rate of the reaction or rate constant is dependent on the concentration of the reaction then it can indicate the intermolecular hydrolysis phenomenon. In order to investigate the effect of concentration on the rate of the reaction four different samples with varying concentration of the compound 1a were prepared as shown in the Table 3.10. The concentrations under investigation were 5 mg/700 μl, 10 mg/700 μl, 20 mg/700 μl and 40 mg/700 μl. Four different NMR tube were loaded with the samples and then incubated at 37 ^{o}C. Samples were characterized with NMR at different time points and then analysis was done in order to investigate the ratio of concentration of 1a to concentration of hydrolyzed 1a for each time point and plot as shown in the Figure 3.18 was obtained. The rate constant (k) was derived for each sample and is reported in the Table 3.10. It was found that there is no significant difference in the k and the plots for all the samples are similar indicating no effect of

concetration on the rate of the reaction. This result indicates that the amide hydrolysis in case of 1a is not a intermolecular phenomenon.

Table 3.10 Compound 1a characterized for the effect of concentration on the rate constant of the reaction.

Sample name for the compound 1a 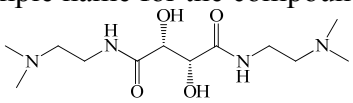	Concentration (mg/700 µl)	Rate constant (k x10^3 h^{-1})
VT6019A	5	16.5
VT6019B	10	15.9
VT6019C	20	15.3
VT6019D	40	14.5

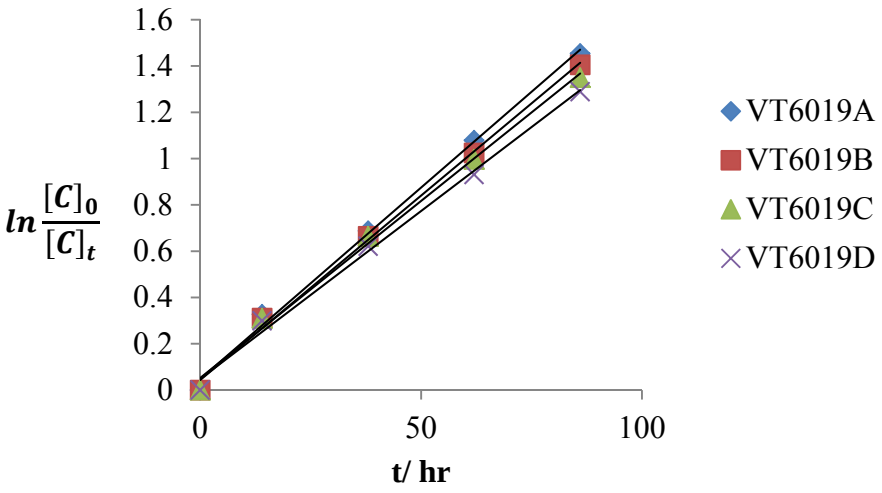

Figure 3.18 Four different sample of the compound 1a with different concentration analyzed for the effect of concentration on the rate constant (k).

An investigation of the hydrolysis pattern of the lactate and glycolate based compounds.

After the one side hydrolysis of the 1a, the hydrolyzed product was again characterized for the hydrolysis under physiological conditions. Although the product did not show any further hydrolysis on the other side, it could be a stretch to conclude that the amide hydrolysis is a intramolecular phenomenon as the compound (3a) has a carboxyl functionality and an amine functionality in the chemical structure, which can potentially form a zwitorionic complex. Although the pH of the reaction can be changed to disrupt the zwitterionic complex but the investigation in different pH is not comparable as the rate of amide hydrolysis decreases as the pH is lowered. For this purpose we investigated the lactate (2c) and glycolate (2d) based models which has only one functionality of each amide, amine and hydroxyl groups in its chemical structure. Upon the studies for amide hydrolysis of compounds 2c, and 2d under the similar conditions as 1a, compounds 2c, and 2d did not show any amide hydrolysis up to the 14 days. This result indicates that the amide hydrolysis of series of compounds (1a-1d, 2a) studied earlier is an intramolecular phenomenon.

3.4.6 Investigation of the hydrolysis mechanism in the galactarate based models.

As described earlier, the tartarate based models show a different hydrolysis pattern for the amides as compared to the regular amide functionality.

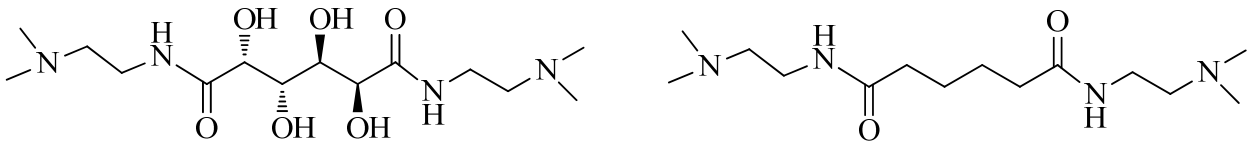

4a 4b

Figure 3.19 Galactarate based model (4a) and adipate based model (4b) to understand the hydrolysis pattern in the galactarate based polymers **G4**

The degradation of **G4** was an inspiration to follow the similar study in the galactarate-based model (4a) and another model (4b) which is a non-hydroxylated analogue of 4a. This study was undertaken to find if there is any effect of the hydroxyl groups attached to the carbon α and β to the carbonyl of the amide group. Compound 4a was characterized for the hydrolysis of amide with earlier described *in-situ* NMR Figure 3.19. The evolution of new peaks in the amine region and carbohydrate region were observed indicating the hydrolysis of amides. On the other hand the compound 4b which lack hydroxyl groups as compared to compound 4a do not show evolution of new peaks (Figure 3.21) any region for when incubated for 14 days under physiological conditions

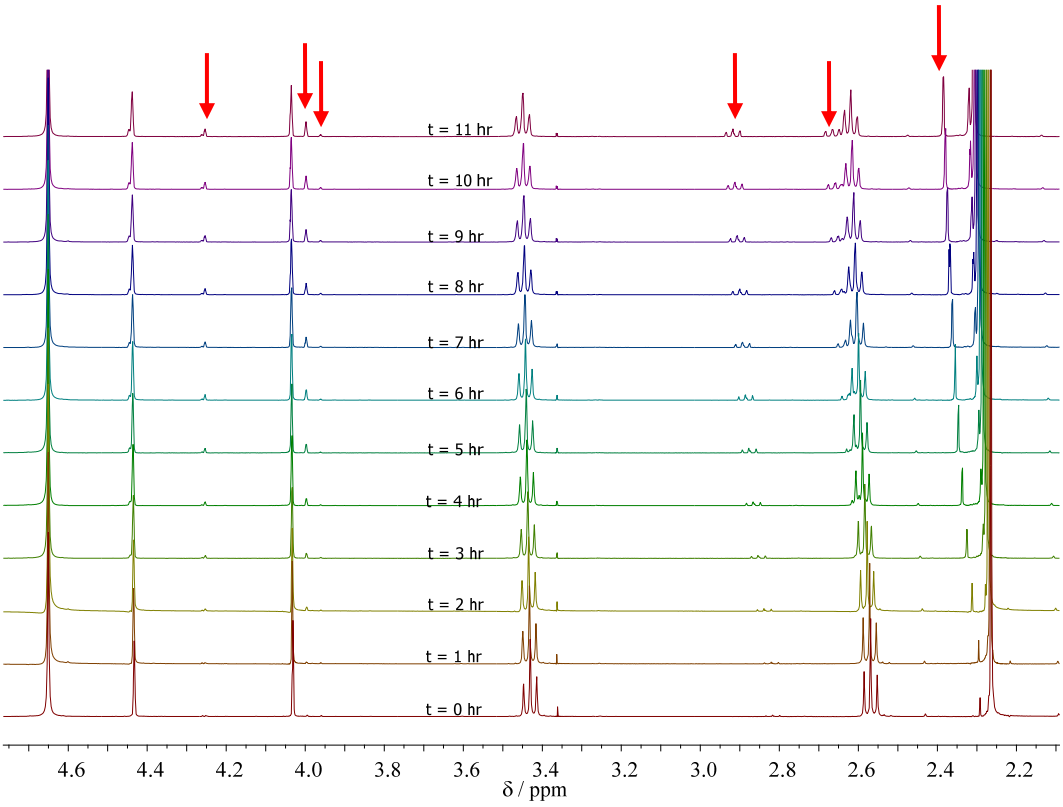

Figure 3.20 An *in-situ* array NMR of compound 4a obtained in D_2O_{PBS} at 37 ^oC. One NMR spectum was taken every hour for 16 hours. The evolution of new peaks are highlighted by the red arrows

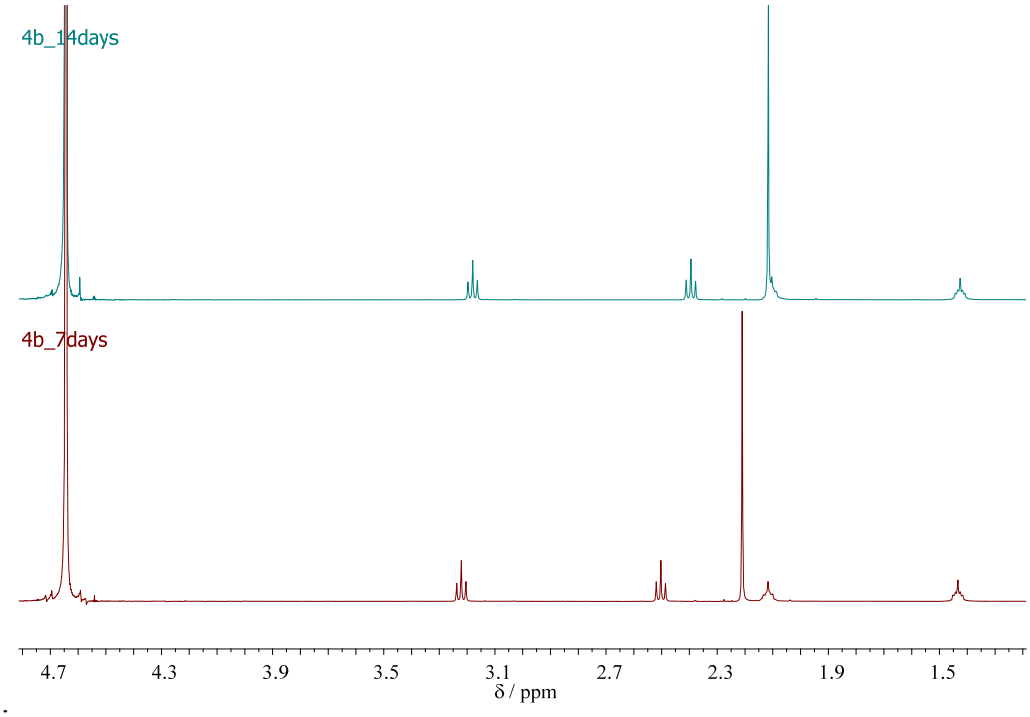

Figure 3.21 NMR spectra of 4b obtained in D_2O_{PBS} at 37 ^oC. The bottom spectrum taken after 7 days incubation and the top spectrum taken after 14 days of incubation and do not show evolution of any new peaks indicating that compound 4b does not go under hydrolysis

This implies that there could be an electron withdrawing effect due to the hydroxyl groups attached to the carbon α and β to the carbonyl of the amide group but in order to confirm this hypothesis more detailed studies are needed

3.5 - Conclusion

In conclusion, the degradation of **T4** and **G4** has led to very interesting studies revealing that the tartarate based small model compounds with terminal amine ends show hydrolysis of the amide selectively on one side. The asymmetric small model compound reveals that the amine on one side of the tartarate moiety assists the hydrolysis of the amide on the other side of the tartarate moiety. Replacing amine with hydroxyl, methoxy, and quaternary ammonium charges do not result in the hydrolysis of the compounds. In addition, removing the amine group from the small

model compounds result in no hydrolysis as well. These studies show that the presence of the terminal amine in these compounds is of utmost importance. The hydrolysis rate can be controlled by varying the functionalities on α, β and γ carbon attached to the amide bond. The small model compounds in case of galactarate based compounds also show hydrolysis but the non hydroxylated analogue indicates that it is essential to have hydroxyl groups attached to the carbon α and β to the carbonyl of the amide functional group.

Synthesis of biomaterials incorporating amide linkage is versatile due to ease of synthesis. Although its hydrolysis (non-enzymatic) under physiological conditions is uncommon but would be very useful for controlled/sustained release of therapeutics. Here we have explored useful chemistry in this direction and have shown that such a hydrolysis is possible with articulate but easy synthesis.

3.6 - Appendix: Useful NMRs and Mass spectrum

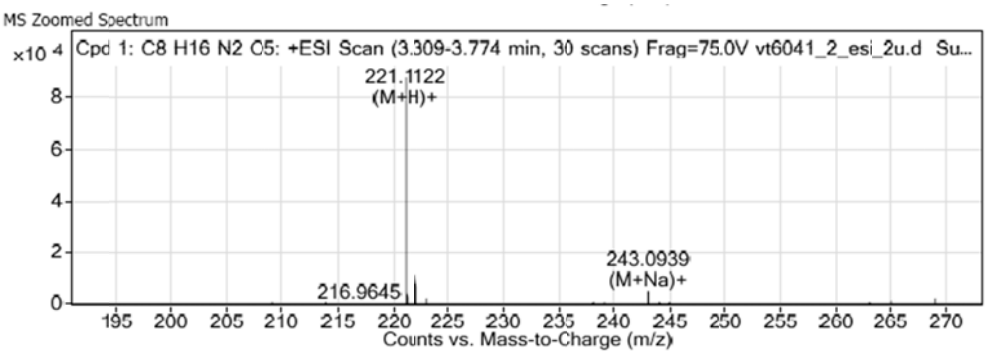

MS Spectrum Peak List

m/z	*Calc m/z*	Diff(ppm)	z	Abund	Formula	Ion
221.1122	221.1132	-4.37		88346	C8 H17 N2 O5	(M+H)+
221.2493				690		
221.3029				194		
221.9718				162		
222.1161	222.1162	-0.36		11164	C8 H17 N2 O5	(M+H)+
223.1177	223.1179	-0.95		1797	C8 H17 N2 O5	(M+H)+
224.1185	224.1205	-8.99		197	C8 H17 N2 O5	(M+H)+
243.0939	243.0951	-5.24	1	4808	C8 H16 N2 Na O5	(M+Na)+
244.0982	244.0981	0.24	1	530	C8 H16 N2 Na O5	(M+Na)+
245.0808	245.0999	-77.62	1	177	C8 H16 N2 Na O5	(M+Na)+

Figure 3.22 ESI-MS for the hydrolyzed product (3a) of the asymmetric compound 3c.

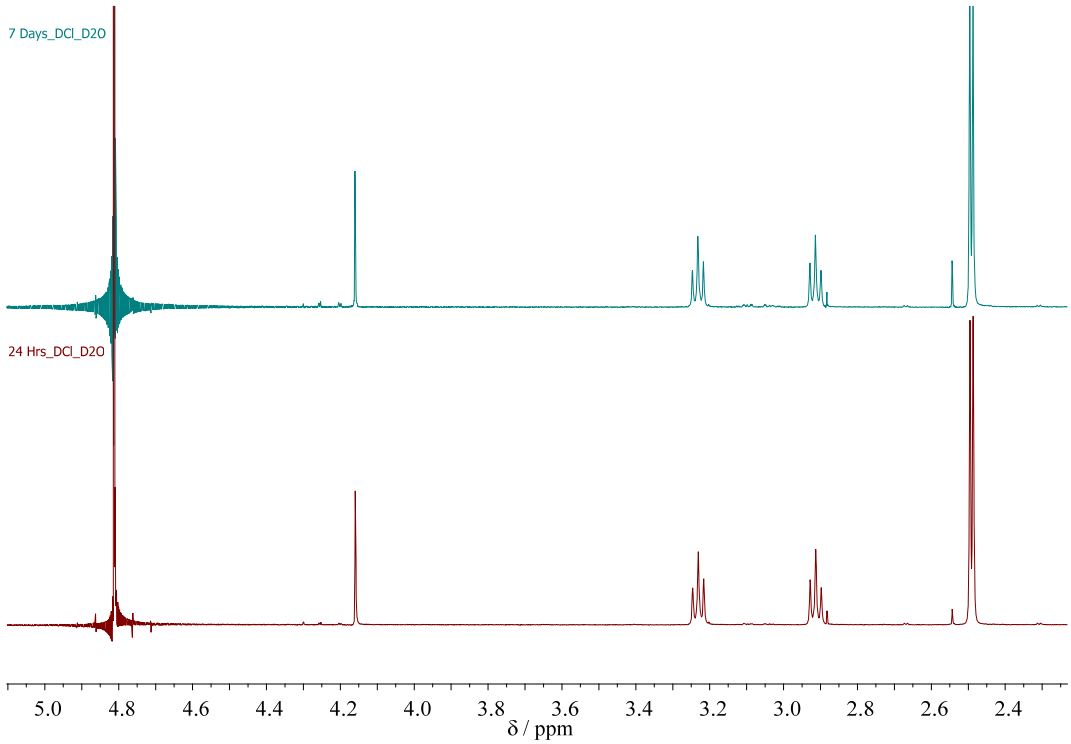

3.23 NMR spectra of 1a obtained in D_2O (one drop of DCl). The bottom spectrum was taken after 24 hours of incubation and top spectrum was taken after 7 days of incubation for protonated 1b. In presence of DCl compound 1b do not show any amide hydrolysis.

3.7 - References

[1] Neffe AT, Hanh BD, Steuer S, Lendlein A. Polymer Networks Combining Controlled Drug Release, Biodegradation, and Shape Memory Capability. Advanced Materials 2009;21:3394-3398.

[2] Murphy WL, Peters MC, Kohn DH, Mooney DJ. Sustained release of vascular endothelial growth factor from mineralized poly(lactide-co-glycolide) scaffolds for tissue engineering. Biomaterials 2000;21:2521-2527.

[3] Kanczler JA, Ginty PJ, Barry JJA, Clarke NMP, Howdle SM, Shakesheff KM, Oreffo ROC. The effect of mesenchymal populations and vascular endothelial growth factor delivered from biodegradable polymer scaffolds on bone formation. Biomaterials 2008;29:1892-1900.

[4] Cassell OCS, Hofer SOP, Morrison WA, Knight KR. Vascularisation of tissue-engineered grafts: the regulation of angiogenesis in reconstructive surgery and in disease states. Br. J. Plast. Surg. 2002;55:603-610.

[5] Jewell CM, Zhang JT, Fredin NJ, Lynn DM. Multilayered polyelectrolyte films promote the direct and localized delivery of DNA to cells. Journal of Controlled Release 2005;106:214-223.

[6] Zhang JT, Chua LS, Lynn DM. Multilayered thin films that sustain the release of functional DNA under physiological conditions. Langmuir 2004;20:8015-8021.

[7] Tomlinson R, Klee M, Garrett S, Heller J, Duncan R, Brocchini S. Pendent chain functionalized polyacetals that display pH-dependent degradation: a platform for the development of novel polymer therapeutics. Macromolecules 2002;35:473-480.

[8] Arnett EM, Miller JG, Day AR. Effect of structure on reactivity. IV. Aminolysis of esters with secondary amines. J. Am. Chem. Soc 1951;73:5393-5395.

[9] Gordon M, Miller JG, Day AR. Effect of Structure on Reactivity. II. Influence of Solvents on Ammonolysis of Esters. J. Am. Chem. Soc 1949;71:1245-1250.

[10] Hoagland PD. the Formation of Intermediate Lactones during Aminolysis of Diethyl galactarate. Carbohydr. Res 1981;98:203-204.

[11] Kiely DE, Chen L, Lin T. Hydroxylated nylons based on unprotected esterified D-glucaric acid by simple condensation reaction. J. Am. Chem. Soc. 1994;116:571-578.

[12] Kiely DE, Chen L, Lin T. Synthetic polyhydroxypolyamides from galactaric, xylaric, D-glucaric, and D-mannaric acids and alkylenediamine monomers-some comparisons. Journal of Polymer Science: Part A: Polymer Chemistry 2000;38:594-603.

[13] Koch T, Miller JG, Day AR. Effect of Structure on Reactivty. VI Catalysis in the Ammonolysis and Hydrolysis of Methyl Acetate. J. Am. Chem. Soc 1953;75:953-955.

[14] Liu Y, Reineke TM. Hydroxyl stereochemistry and amine number within poly(glycoamidoamine)s affect intracellular DNA delivery. J. Am. Chem. Soc. 2005;127:3004-3015.

[15] Liu Y, Wenning L, Lynch M, Reineke TM. New poly(D-glucaramidoamine)s induce DNA nanoparticle formation and efficient gene delivery into mammalian cells. J. Am. Chem. Soc. 2004;126:7422-7423.

[16] Liu Y, Wenning L, Lynch M, Reineke TM. Gene delivery with novel poly(L-tartaramidoamine)s. In: Svenson S, editor. Polymeric Drug Delivery Volume I - Particulate Drug Carriers, vol. 923. Washington DC: American Chemical Society, 2006.

[17] Liu Y, Reineke TM. Degradation of Poly(glycoamidoamine) DNA Delivery Vehicles: Polyamide Hydrolysis at Physiological Conditions Promotes DNA Release. Biomacromolecules 2010;11:316-325.

[18] Taori VP, Liu YM, Reineke TM. DNA delivery in vitro via surface release from multilayer assemblies with poly(glycoamidoamine)s. Acta biomaterialia 2009;5:925-933.

[19] Chebrou H, Bigey F, Arnaud A, Galzy P. Study of the amidase signature group. Biochimica Et Biophysica Acta-Protein Structure and Molecular Enzymology 1996;1298:285-293.

[20] Kobayashi M, Fujiwara Y, Goda M, Komeda H, Shimizu S. Identification of active sites in amidase: Evolutionary relationship between amide bond- and peptide bond-cleaving enzymes. Proceedings of the National Academy of Sciences of the United States of America 1997;94:11986-11991.

[21] Sharma M, Sharma NN, Bhalla TC. Amidases: versatile enzymes in nature. Reviews in Environmental Science and Biotechnology 2009;8:343-366.

[22] Glusenkamp KH, Mengede C, Drosdziok W, Jahde E, Rajewsky MF. Rapid hydrolysis of amides under physiological conditions: Influence of the microenvironment on the stability of amide bond. Bioorg. Med. Chem. Lett. 1998;8:285-288.

[23] Kahne D, Still WC. Hydrolysis of a peptide-bond in neutral water. Journal of the American Chemical Society 1988;110:7529-7534.

[24] Bennet AJ, Wang QP, Slebockatilk H, Somayaji V, Brown RS, Santarsiero BD. Relationship between amidic distortion and ease of hydrolysis in base - if amidic resonance does not exist, then what accounts for the accelerated hydrolysis of distorted amides. Journal of the American Chemical Society 1990;112:6383-6385.

[25] Somayaji V, Keillor J, Brown RS. Model for the aspartate proteinases - hydrolysis of a distorted amide catalyzed by dicarboxylic-acids capable of forming cyclic anhydrides. Journal of the American Chemical Society 1988;110:2625-2629.

[26] Sheldrick GM. A short history of SHELX. Acta Crystallographica Section A 2008;64:112-122.

[27] Dolomanov OV, Bourhis LJ, Gildea RJ, Howard JAK, Puschmann H. OLEX2: a complete structure solution, refinement and analysis program. Journal of Applied Crystallography 2009;42:339-341.

Chapter 4

DNA Delivery In-vitro via Surface Release from Multilayer Assemblies with Poly(glycoamidoamine)s*

*Chapter adapted from: Taori VP, Liu Y, Reineke TM. DNA Delivery *In-vitro* via Surface Release from Multilayer Assemblies with Poly(glycoamidoamine)s. Acta Biomaterialia 2009;5:925-933.

4.1 - Abstract

Localized controlled-release of nucleic acid therapeutics could be an effective way to reduce the extracellular barriers associated with systemic delivery. Herein, we have used the layer-by-layer film deposition approach to construct ultra thin multilayer assemblies for *in-vitro* controlled-release of plasmid DNA (pDNA). Layer-by-layer assemblies containing alternate layers of cationic poly(L-tartaramidopentaethylenetetramine) (**T4**), and anionic pDNA were fabricated. The film thickness and the absorbance at 260 nm for different **T4**/pDNA multilayer assemblies were characterized by ellipsometry and UV-visible spectrophotometry respectively. The results indicated an increased loading capacity of pDNA with respect to an increase in the number of **T4**/pDNA bilayers deposited. For the controlled-release studies we incubated the bilayers coated on quartz slides in phosphate buffered saline (PBS) at 37 ºC and collected the media at different incubation time points. The collected PBS samples were characterized for pDNA release by complexing solutions containing the released pDNA with Lipofectamine 2000 and following cellular pDNA uptake via flow cytometry and GFP gene expression assays with HeLa cells. The study showed that the multilayer films started to release pDNA after 1 day of incubation and increased after 7 days of incubation. Assays monitoring green fluorescent protein (GFP) expression in HeLa cells indicated that about 20% of the cells were positive for GFP expression at all sample time points up to 11 days. Although an increase in cells positive for Cy5-pDNA was found as the incubation time increased, the number of cells positive for GFP expression remained constant over the same time frame.

Keywords: Multilayer assembly; glycopolymer; gene delivery; controlled release; polymer degradation.

4.2 - Introduction

Research in the fields of nucleic acid therapeutics [1, 2] and tissue engineering [3, 4] has rapidly developed over the last three decades [5-8] and yielded many promising results [9, 10]. Although approximately 75% of clinical trials in the area of gene therapy utilize viral vectors for the delivery of nucleic acids [6, 11], disadvantages such as immunogenicity [2], random genome integration, and systemic inflammatory response [12] have caused serious health concerns [11] and increased the use of non-viral delivery techniques [13]. Cationic polymers, an important class of non-viral delivery vehicles, are being widely studied in this area [14] and have shown an outstanding capacity to bind and compact nucleic acids into nanoparticles with similar sizes and morphologies to viral vectors. Cationic polymers have also shown to exhibit low toxic and immunogenic effects [15], are biodegradable, and can help nucleic acid therapeutics survive the different extracellular and intracellular pathways during cellular uptake and intracellular trafficking [16, 17]. For this purpose, many studies have been completed with a variety of polymer structures such as polyethylenimine (PEI), poly-L-lysine (PLL), and chitosan to gain an understanding of the different extracellular and intracellular mechanisms involved in the delivery with non-viral vehicles [18, 19].

Our group has developed and explored a new and promising class of polymeric delivery vehicles, termed poly(glycoamidoamine)s or PGAAs [20-22]. This polymer class was designed to have both oligoethyleneamine (for binding and compacting DNA) and carbohydrate moieties (for reducing toxicity) within the repeat unit. The extensive previous work conducted by our group on these PGAA vehicles have revealed that the structures with four secondary amines in the oligoethyleneamine moiety yield the highest transfection efficiency (comparable to PEI)

within the group of structures (that contained between 1-4 ethyleneamines) without the cytotoxicity associated with PEI-like structures [20, 21].

A major issue with systemic delivery of nucleic acids with polymeric vehicles is that the polymer-DNA complexes (termed polyplexes) spend a considerable amount of time in the extracellular environment prior to cellular internalization and uptake. During this time, the polyplexes can bind to different plasma proteins, cause erythrocyte aggregation in the blood, and be cleared by the reticuloendothelial system (RES) [6, 7, 23, 24]. For this reason, these complexes typically have a short circulation half-life and after only 10 minutes, typically less than 2% of the therapeutic complexes remain in circulation [7]. Coating polyplexes with polyethylene glycol (PEG) groups has been used to overcome this problem, shield the therapeutic complexes from non-specific binding, and avoid RES clearance [23, 24]. Cell-specific targeting groups such as antibodies [25] and carbohydrates have also been added to the ends of PEG chains to help increase specificity and efficacy of tissue-specific delivery [16, 26, 27].

Localized and controlled-release of therapeutics from devices and/or surfaces also has the potential to innovate DNA delivery [28, 29]. For example, implanting devices coated with therapeutic DNA adjacent to specific tissues can provide a direct means of targeting and controlled-release of the therapeutic to avoid unwanted toxicity. This method also avoids the issues related to systemic injection of DNA therapeutics *in-vivo*. Drug delivery with controlled-release systems are indeed quite useful for engineering the drug/gene release rate adjacent to the targeted tissue [28, 30]. For example, the approach of layer-by-layer (LBL) deposition of films containing therapeutics onto devices has been utilized for the localized delivery of heparin for the repair of blood vessels *in vivo* [31]. Also, related techniques have been used to create tissue

engineering scaffolds from poly(lactide-co-glycolide) and plasmid DNA encoding tissue-inductive proteins; elution of pDNA from these scaffolds were shown to enhance matrix deposition and tissue growth around the materials as compared to direct pDNA injection, which did not enhance tissue formation [32].

Previous work in the field of gene delivery from LBL assemblies show successful transfection of cells both with and without secondary transfection agents [33, 34]. Here, we have examined the LBL method to coat substrates with pDNA and a successful transfection reagent developed in our laboratory, **T4** (Figure 1a). In this study, we have utilized this polymer for another purpose, to form LBL assemblies with pDNA on substrates as we reveal that this polymer is degradable and has the ability to release naked pDNA from the LBL assemblies into solution. As shown in Figure 1b, degradation studies reveal that **T4** degrades and hydrolyzes faster at physiological pH (pH = 7.4) as compared to a lower pH environment (pH = 5.0). This property is advantageous for preparing the multilayer assemblies with the cationic polyelectrolyte at lower pH, which improves its ionic strength (cationic character) at pH 5.0 and enhances the electrostatic interaction with the polyanion (pDNA) without degrading polymer **T4**. It should be noted that the pH in early endosome rapidly reaches to 6.0 and can go as low as 4.6 [35, 36]. Thus, forming the LBL assemblies at a pH = 5.0 should not have an effect on the pDNA on the substrate. Among the many different PGAA structures created in our laboratory with various carbohydrates, polycation **T4** was selected for this study because it has the easiest synthetic route (can obtain multi-gram quantities easily) and strongly binds to pDNA when compared to the other PGAA structures we have created. These features are desirable for device fabrication and the creation of stable and compact bilayer assemblies. Herein, silicon or quartz slides were dip-coated via LBL methods with polycation **T4** and polyanionic pDNA. The

thickness of these LBL models was found to be between 3-8 nm depending on the number of layers coated on the slides. Some of the models were built with Cy5-labled pDNA to monitor the cellular uptake of pDNA released into solution (after complexation with Lipofectamine 2000), by measuring the average cellular fluorescence increase. Another LBL model was built by using pDNA that expresses green fluorescent protein (GFP), to monitor gene expression. The results represent our first examination of using our degradable PGAA polymers for controlled-release of pDNA from solid substrates and demonstrate that **T4** has potential to be further studied and engineered for localized delivery of nucleic acids.

a

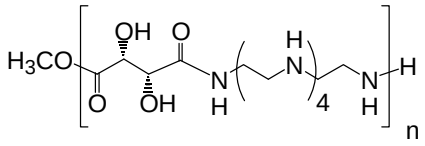

Poly(L-tartaramidopentaethylenetetramine)s
T4

b

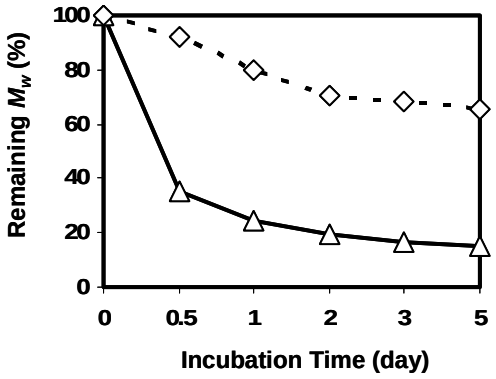

4.1 (a) Structure of poly(L-tartaramidopentaethylenetetramine). (b) The changes in Mw of polymer T4 incubated at 37 °C in PBS (solid line) and pH 5 (dotted line) buffers between 0-5 days.

4.3 - Experimental

Polymer **T4** was synthesized by copolymerization of dimethyl L-tartarate (**T**) with pentaethylenehexamine in methanol, as previously described [21]. Sodium acetate buffer (100 mM) was made by dissolving sodium acetate in 18MΩ Millipore water and titrating the solution to pH 5.0 with glacial acetic acid. Plasmid DNA (pDNA) [gWiz-GFP and pCMVβ] were purchased from Aldevron (Fargo, ND) and PlasmidFactory (Bielefeld, Germany), respectively. pCMVβ was labeled with a LabelIT-Cy5 nucleic acid labeling kit (Mirus, Madison, WI), and purified with a QIAquick PCR purification kit (QIAGEN, Valencia, CA). Heparin was purchased from Sigma (St. Louis, MO) in the form of heparin ammonium salt from porcine intestinal mucosa. Dulbecco's Modified Eagle Medium (DMEM), reduced serum medium (OPTI-MEM), supplements, nuclease-free water, and phosphate-buffered saline (PBS) were purchased from Invitrogen (Carlsbad, CA). HeLa cells were purchased from ATCC (Rockville, MD) and cultured according to ATCC specifications in DMEM (supplemented with 10% FBS, 100 units/mg penicillin, 100 μg/mL streptomycin, and 0.25 μg/mL amphotericin) in 5% CO_2 at 37 ºC.

The quartz slides (1.5 cm in diameter) and silicon slides (2.0 cm × 1.0 cm), used as the substrates in the LBL formation, were purchased from Fisher (Pittsburgh, PA). It should be noted here that both of these materials have a SiO_2 surface (after treatment with NaOH) and should have similar LBL deposition properties. These two different model substrates were used due to their differing properties for characterization of the multilayer films. The silicon substrate was used for the characterization of the thickness of the deposited multilayer films using ellipsometry and for uniformity measurements with AFM. For all other experiments and characterization, the fabrication of the multilayer films was completed on the quartz substrate.

4.3.1 Gel Permeation Chromatography (GPC) of Hydrolyzed T4. Polymer **T4** was incubated in pH 5.0 and pH 7.4 buffers at 37 °C in a number of vials. At the desired time points (0, 0.5, 1, 2, 3, and 5 days), a vial containing each incubated mixture (at both pH=5 and pH=7) was flash frozen with liquid N_2 and stored at -80 °C until further analysis. The change in polymer molecular weight as a function of incubation time and pH was analyzed with a ViscoGel PC-MBLMW-3078 column at a flow rate of 0.8 mL/min. The mobile phase used for the analysis was a solution of water/methanol/acetic acid (55/40/5, v/v/v) .

4.3.2 Preparation of the Polyelectrolytes. Solutions of the polyelectrolytes were prepared at two different concentrations. To fabricate the multilayer models on the quartz substrates, a 0.5 mM solution of **T4** (based on the molecular weight of the repeat unit) was prepared in fresh 100 mM (pH adjusted to 5.0) sodium acetate solution. The anionic polyelectrolyte was prepared by diluting pDNA or heparin to 0.2 mg/mL with DNAse and RNAse-free water. Similarly, to fabricate the multilayer models on the silicon substrates, a 5 mM solution of **T4** and a 1 mg/mL solution of pDNA was prepared and used to fabricate the multilayer films. When the same concentration of polyelectrolytes were used to fabricate films on the silicon substrate, the resulting multilayer thin films were difficult to characterize due to limitations in the instruments utilized. For these experiments the concentrations were slightly increased for this characterization technique (*vide infra*).

4.3.3 Fabrication of the Multilayered Films. Two different models were fabricated based on the substrates of quartz and silicon, again, for characterization purposes. To prepare the substrates, the slides were first rinsed and washed in methylene chloride, methanol, and finally ultrapure water to remove any organic or water soluble impurities from the surface of the substrates. The substrates were then dipped in a 1 M sodium hydroxide solution for 15 min to

treat the surface of the substrate to form a uniform surface layer of SiO_2. The substrates were then thoroughly rinsed with ultra pure water and dried overnight (in a laminar flow biosafety cabinet). To form the multilayer films, the substrates were then dipped in the cationic (**T4**) polyelectrolyte solution for 3 minutes and rinsed with 2 washes of ultrapure water. To then deposit one bilayer on the substrates, the slides were then dipped in the pDNA polyelectrolyte (or heparin) for 3 minutes and then rinsed with 2 washes of ultrapure water to remove the excess anionic polyelectrolyte. This procedure of dip coating was repeated until the desired number of **T4**/pDNA bilayers was deposited on the substrate.

4.3.4 Thickness Measurements by Ellipsometry. The silicon substrate-based models were used to measure the correlation between the number of **T4**/pDNA bilayers and the thickness of the multilayer films. The thickness of the film was determined using a variable angle spectroscopic ellipsometer (VASE, J. A. Woolam Co.). Optical parameters (Δ and Ψ) were collected from 300 to 1000 nm at 10 nm intervals and for the angles of incidence between 60-75 degrees, at 5 degree intervals. The computer program WVASE32 was used to fit a mathematical model to the experimental data. The data was reported as the average and standard of deviation of triplicate measurements recorded at three different locations on the substrates. Each reading taken was corrected for the thickness of the oxide layer formed due to the treatment of the silicon substrate with the 1 M NaOH solution.

4.3.5 Absorbance Measurements. An Agilent 8453 (Model G1103A) UV-visible spectrophotometer was used to measure the UV absorbance of the multilayer films deposited on the quartz substrate due to the UV transparency. The absorbance at 260 nm, which is the characteristic absorbance for double stranded DNA, showed the deposition of the pDNA in the deposited multilayer films and the absorbance increased as a function of bilayer thickness.

4.3.6 Ethidium Bromide Intercalation for LBL Film Imaging. Quartz slides containing eight bilayers of **T4**/pDNA or **T4**/heparin were dipped in an aqueous ethidium bromide solution (100 μg/mL) for 15 min. The slides were then each rinsed by dipping the slide in ultra pure water and photographed under an excitation wavelength of 254 nm.

4.3.7 AFM Imaging of LBL Film Uniformity. A Vecco MultiMode Atomic Force Microscope was used to analyze the topology of a 8 bilayer (**T4**/pDNA) film fabricated on a microscope slide. The image of the 5 μm X 5 μm area was obtained in a tapping mode using a silicon cantilever.

4.3.8 Incubation of LBL Films and Release of pDNA. The quartz slide coated with eight bilayers of **T4**/pDNA were incubated in 5 mL of PBS buffer at 37 ºC. Due to the hydrolysis/degradation of polymer **T4**, naked pDNA is released from the slides (two different LBL film models were created with Cy5-pDNA and gWiz-GFP for a range of analysis techniques). At certain time points (0, 1, 3, 5, 7, 9, and 11 days), 200 μL of the slide incubation solution was aliquotted and frozen at -80 ºC until experimental completion, when all of the solutions could be analyzed together for transfection efficiency (procedure described below).

4.3.9 Cell Transfection Assays. In 12-well plates, HeLa cells were seeded with a density of 100,000 cells/well in 2 mL of DMEM and cultured for 24 h in 5% CO_2 at 37 ºC. Then, 200 μL of the final transfection solution (described below) was added directly to each well with 400 μL of Opti-MEM. The final transfection solution was prepared by mixing 100 μL of the slide incubation solution containing the released pDNA (Cy5-labeled pDNA or gWiz-GFP) from the coated quartz slides (removed after each incubation time point of 0, 1, 3, 5, 7, 9, and 11 days) with 100 μL of a diluted Lipofectamine 2000 solution (Invitrogen, Carlsbad, CA, 5 μL stock

diluted into 95 μL of water). The solutions were mixed and allowed to sit for 30 minutes before adding the mixture to the HeLa cells for transfection efficiency analysis [34].

Four hours after initial transfection, the cells exposed to the Cy5-pDNA/Lipofectamine 2000 mixtures were rinsed with PBS buffer three times, trypsinized, pelleted, and resuspended in PBS containing 2% FBS. The cells were then analyzed via flow cytometry analysis. A FACSCanto II (Becton Dickenson, San Jose, CA) equipped with an helium-neon laser used to excite Cy5 (633 nm) was utilized in the analysis. Ten thousand events were collected in duplicate for each sample.

Forty-eight hours after initial transfection, the cells exposed to the gWiz-GFP-Lipofectamine 2000 mixtures were imaged and photographed using a Nikon inverted microscope TE2000-U with the software MetaMorph. These cells were then rinsed with PBS buffer three times, trypsinized, and the amount of expressed GFP was quantified via flow cytometry with an argon ion laser (488 nm). The number of cells positive for GFP was established by first removing autofluorescence (by gating a negative control of untransfected cells such that less than 1% of cells was defined as positive) so these parameters could be more accurately quantified via flow cytometry.

4.4 - Results and Discussion

4.4.1 Multilayer Film Fabrication. In our previous studies we have demonstrated that the PGAAs (**T4**, **G4**, **D4**, **M4**) developed in our laboratory have the ability to condense pDNA into nanoparticles and deliver pDNA into a variety of cell types with high efficacy and low toxicity [20, 21]. In particular, polycation **T4**, consistently yields high efficiency and is the easiest model to synthesize. Also, **T4** has been shown to yield higher binding affinity with DNA as compared to the **M4** and **D4** analogs [37]. Also, it has been shown in our earlier studies that almost 50%

of amines along the backbone of **T4** are protonated at pH 5.0 [38], which may assist in the adsorption of multilayers by electrostatic interactions for LBL deposition. For these reasons we hypothesized that **T4** was an excellent candidate to create stable and ultrathin multilayer films via LBL deposition of polyanions and polycations on various substrates.

Fabrication of the multilayer thin film models by the LBL method takes about 1 to 3 hours depending upon the number of **T4**/pDNA bilayers. Hence, it is important that during the fabrication process of these multilayer films, the polymer structure is not altered and/or the polymer does not start to degrade during this process [39]. As shown in Figure 1b, degradation studies of **T4** reveal that this polymer degrades faster at physiological pH (7.4) than at a lower pH of 5.0 (*vide infra*). This property of **T4** is potentially very useful and may offer unique release properties for the multilayer models when compared to polyester-based polycations previously used in similar studies [34, 39].

For the fabrication of the LBL films, two different types of substrates, silicon and quartz, were used. These two different models were used to increase the degree of characterization of the deposited multilayer films on the substrates. As previously stated, both the silicon and quartz substrates have a SiO_2 surface after treatment and the physical and chemical properties of the deposited films by the LBL method on both the substrates should be quite similar. The silicon substrate was used for the characterization of thickness of the deposited multilayer films using ellipsometry. For all other experiments and characterization, the fabrication of the multilayer thin films was completed on the quartz substrate.

Ellipsometry was used to characterize the thickness of the multilayer films deposited on the silicon substrate. Multilayer films up to 8 nm thick could be deposited with the concentrations utilized in this experiment. Figure 2 shows the thicknesses of the multilayer films

on the silicon substrate for 2, 4, 6 and 8 **T4**/pDNA bilayers. As the number of **T4**/pDNA bilayers increased from 2 to 8, the thickness of the multilayer thin film increased from about 3 nm to about 8 nm. The data shows a linear correlation between the number of **T4**/pDNA bilayers and the thickness of the multilayer films indicating that the amount of pDNA incorporation increases with the bilayer thickness.

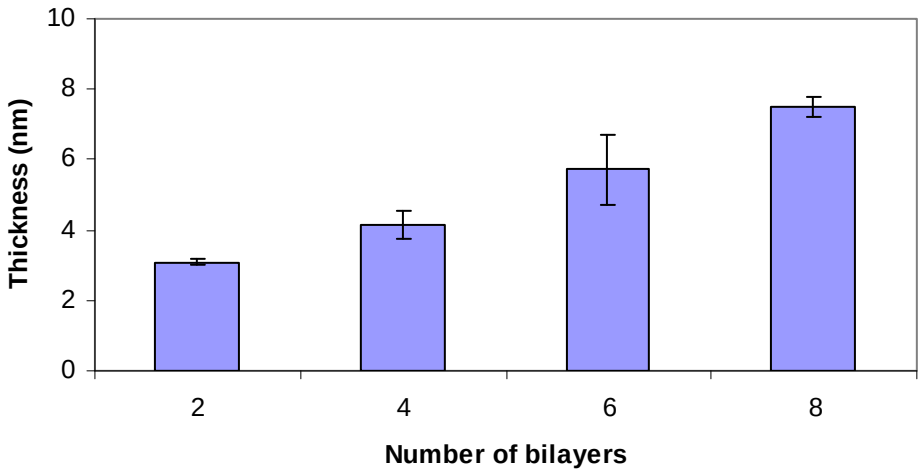

Figure 4.2 The thickness of the multilayer thin films on the silicon substrate measured via ellipsometry for 2, 4, 6, and 8 T4/pDNA bilayers. Each measurement represents the average and standard of deviation of 3 measurements taken on three different locations of the substrate (the measurements have been corrected for the oxide layer formed initially to make the silicon substrate surface anionic).

UV-Vis spectrophotometry was used to support the above data of that the amount of pDNA incorporated into the films increases as a function of multilayer (Figure 3). The characteristic absorbance of double stranded DNA at 260nm was used for this analysis. Although the absorbance increased with the increase in the **T4**/pDNA bilayer, a linear correlation was not observed. It should be noted that this UV-Vis characterization technique on these multilayer films deposited on the quartz substrates is semiquantitative [40] due to change in orientation of

the molecules with every layer adsorbed [41], which likely plays a role in the orientation of the next layer of adsorbed macromolecules (and can affect the absorbance profile).

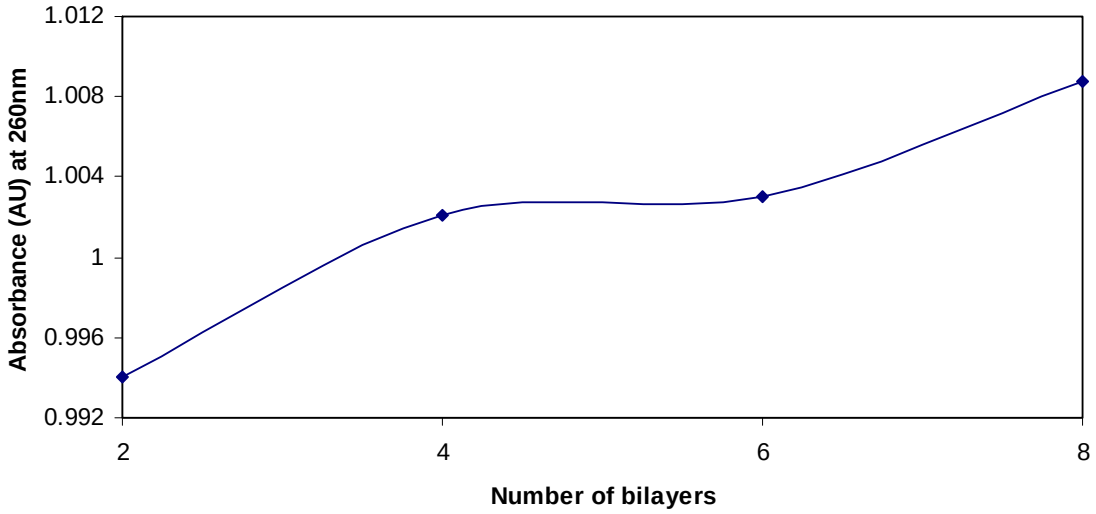

Figure 4.3 Plot of the absorbance of pDNA at 260 nm verses the number of T4/pDNA bilayers adsorbed on the quartz substrates.

To support the coating of the pDNA multilayers on the slides, we used ethidium bromide (intercalates into DNA) to detect the presence of pDNA on the slides. The observed fluorescence of the ethidium bromide on the **T4**/pDNA coated slide with 8 bilayers (Figure 4 (a)) demonstrates that pDNA has been coated on the slide. As a negative control, we also imaged a slide coated with 8 bilayers of **T4**/Heparin (Figure 4(b)). As shown in Figure 4a, the films do not appear to be uniform, which can occur with the LBL coating method. To observe the surface topology of these films, we performed AFM analysis to further observe the surface roughness (Figures 4c and 4d). This technique revealed that the films do not have a uniform surface topology, which also can affect the degradation profiles of the LBL assemblies and release of pDNA into solution.

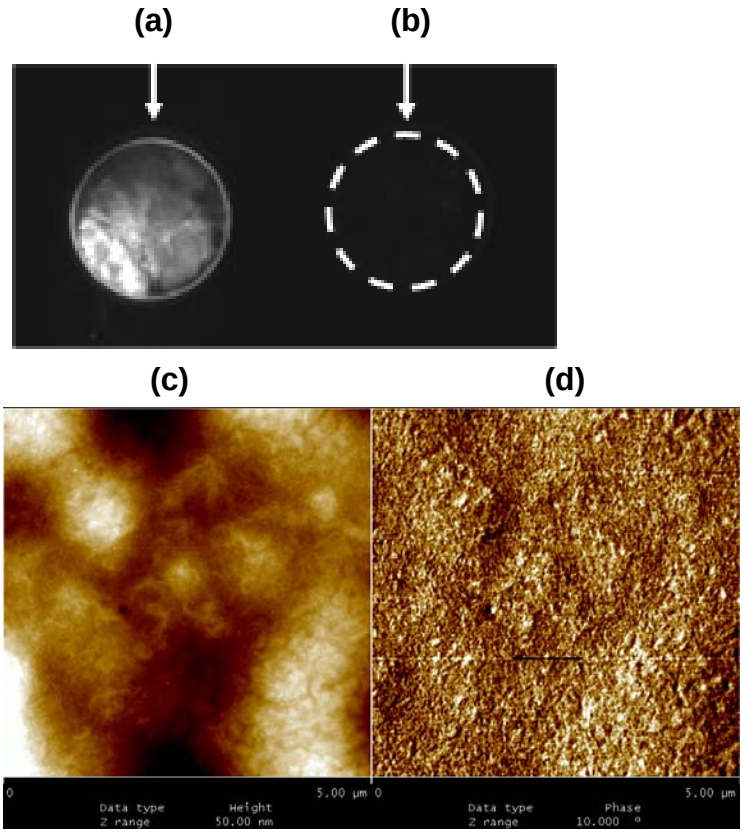

Figure 4.4 (a) Fluorescence images of a quartz slide coated with 8 bilayers of T4/pDNA(b) Fluorescence images of a quartz slide coated with 8 bilayers of T4/heparin as a negative control. (c) Tapping mode atomic force microscopy image of a 5 µm X 5 µm area of a microscope slide coated with a film consisting of 8 T4/pDNA bilayers.

4.4.2 Analysis of the Released pDNA by Transfection in HeLa cells. To evaluate the release of pDNA from the multilayers deposited on the quartz slides, the slides were incubated in aqueous PBS buffer. At various time points between 0 to 11 days, 200 μL aliquots of the PBS solution were removed and stored until all of the solutions could be analyzed together in the cells. After the degradation experiments were completed, Lipofectamine 2000 was added to complex the released pDNA in each solution before adding the final transfection solutions into the HeLa cells. It should be noted that in this experiment, Lipofectamine 2000 was used as a

transfection vector to complex the naked pDNA released from the multilayers and aid cellular internalization. It should also be highlighted here that **T4,** used to form the multilayer assemblies only with pDNA and is being hydrolyzed during the incubation in PBS (for pDNA release). Due to this degradation (Figure 1b), **T4** will not act as a transfection vehicle (only as a material to promote the controlled-release of pDNA, see Figure 5 time point 11*) [16]. Also, it should be mentioned that we tried to grow the cells directly on the multilayered substrates, however, the cells would not attach to the coated slides. This result could be beneficial for applications that require implantation of devices for controlled release of nucleic acid drugs to avoid scar tissue formation on the device, inflammation, and other problems such as immune response.

Flow cytometry was used to evaluate the cellular internalization of the multilayers formed with **T4** and Cy5-pDNA. Four hours after transfection, the number of cells that take up the pDNA, as well as the average intensity of fluorescence (relative amount of pDNA) in the cells were detected by flow cytometry. The flow histograms of HeLa cells and the quantified number of cells positive for Cy5 are shown in Figure 5. After 1 day of incubation in PBS at 37 ºC, the quartz slide coated with 8 bilayers released some pDNA into solution as shown by the increased cellular Cy5 intensity compare to the control sample (at incubation time = 0 days) (Figure 5a). As shown in Figure 5b, the amount of pDNA taken up into the HeLa cells did not change significantly between 1-7 days (percentage of positive cells about 18-25%). However, with further incubation, the Cy5 peak in the histograms shifted to the right (higher intensity). These data indicate that, after 9 days of incubation, the **T4**/pDNA coated quartz slide released more pDNA into solution (43% of HeLa cells were positive for Cy5) than during the initial 7 day incubation period. A further increase (to 70%) in the amount of HeLa cells positive

a.

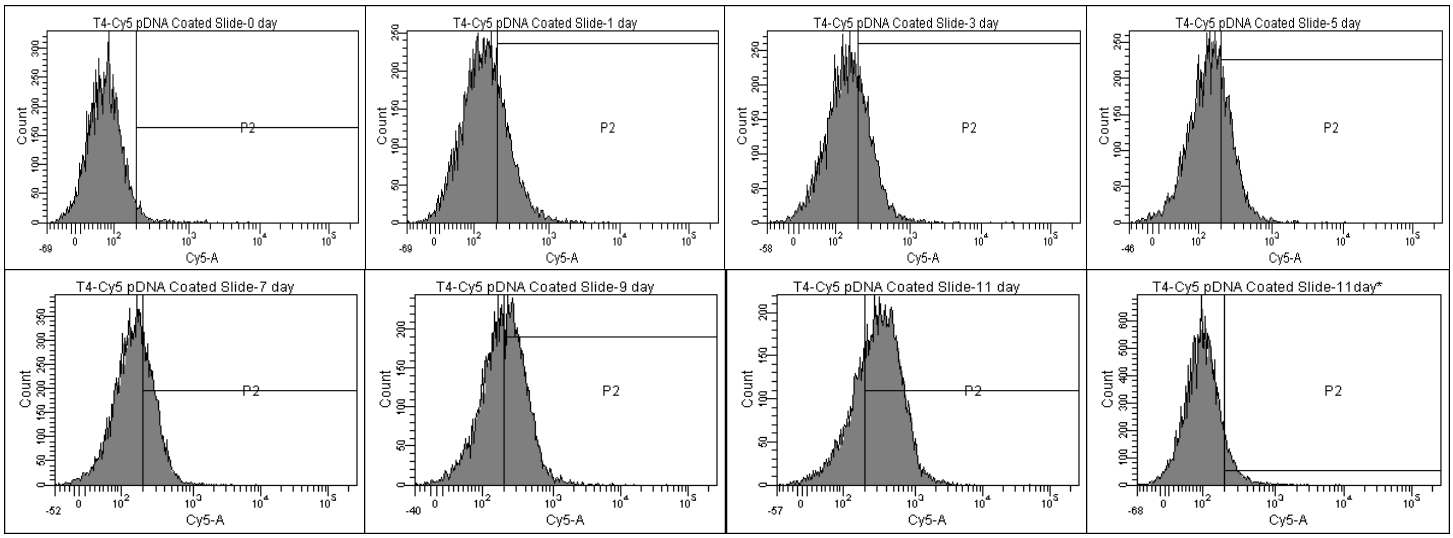

b.

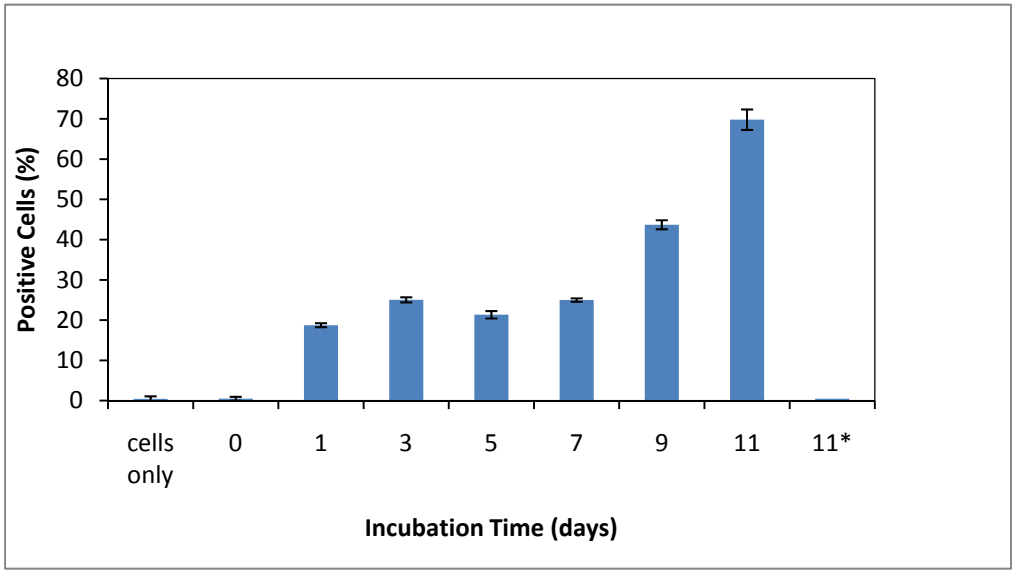

Figure 4.5 (a) Flow histograms of transfected HeLa cells after exposure to each solutions of Cy5-pDNA aliquotted during the bilayer release of the quartz slides at time points of 0-11 days. Lipofectamine 2000 was added to each solution to aid cell internalization, except for 11*. The 11* control signifies incubation for 11 days and transfection as previously described, however, Lipofectamine was not added to the solution prior to transfection. (b) The percentage of cells positive for Cy5 fluorescence. The positive fluorescence level was established by visual inspection of the histogram of cells transfected with non-incubated solution such that less than 1% appeared in the positive region.

for Cy5 fluorescence (Figure 5b) after 11 days was also noted.

One drawback of the analysis on the cellular uptake of released Cy5-pDNA (via flow cytometry), is that this method directly measures the cellular uptake of Cy5 into cells but does not indicate whether the pDNA is degrading. We attempted to evaluate the integrity of the released pDNA into solution via gel electrophoresis, however, due to the very low concentrations of released pDNA, we were not able to detect pDNA within the gel experiment. Thus, to evaluate the integrity of the pDNA that is released upon **T4** hydrolysis within the multilayers, we also performed transfection experiments in HeLa cells with a similar procedure as the previous cellular uptake experiment. The HeLa cells were similarly transfected with the slide incubation solutions (after mixing with Lipofectamine 2000) and the expression of pDNA containing a GFP reporter gene was monitored via flow cytometry and fluorescence microscopy. In this experiment, if the pDNA was damaged during the incubation and release from the multilayers, GFP will not be expressed properly. As shown in Figure 6a-f, all the samples revealed a significant amount of GFP expression. Flow cytometry assays of the isolated cells showed that about 20% of the HeLa cells were positive for GFP expression at all sample time points (Figure 6g). These data were consistent to the Cy5-pDNA uptake experiments, which showed that about 18 - 25% of HeLa cells were positive for Cy5 fluorescence between 1 - 7 days. These data combined indicate that the pDNA released from the slides during this time period is mostly constant and the pDNA is also in tact and competent for expression. It should be noted here that for sample time points at 9 and 11 days, we observed an increase in release of pDNA from the coated slides as indicated by the increased Cy5-labeled pDNA uptake (Figure 5b), however, in the GFP expression experiment, we did not observe an increase in GFP expression level at these two time points. At this point, we do not understand this discrepancy but it could be related to

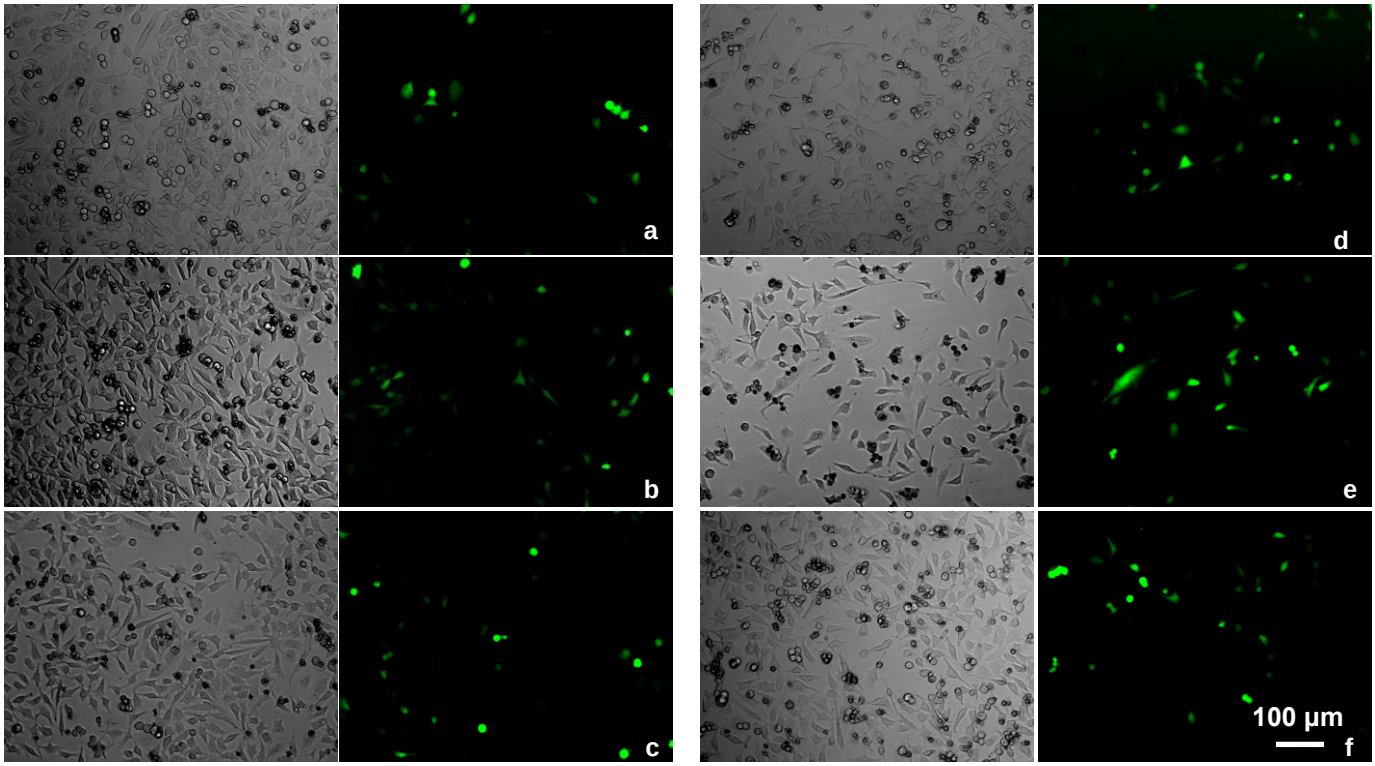

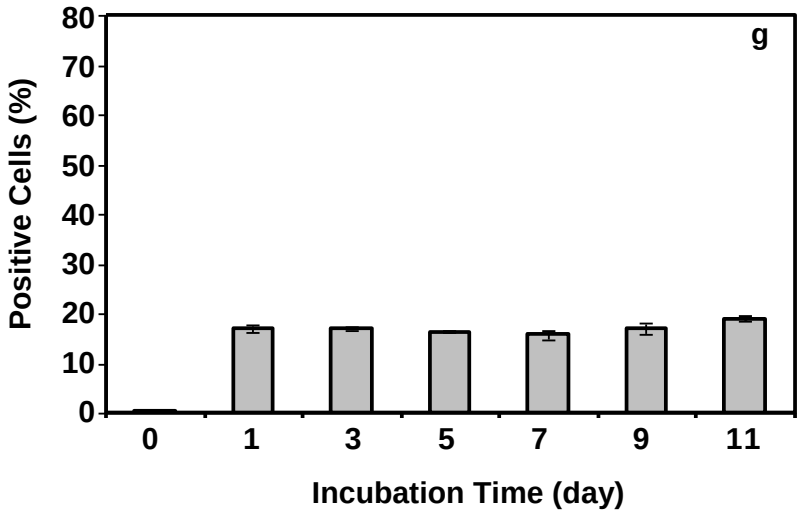

Figure 4.6 (a) – (f) Fluorescence microscopy images showing relative levels of green fluorescent protein (GFP) expression in HeLa cells. Cells were transfected with gWiz-GFP released from the coated quartz slide, using lipofectamine 2000 as the delivery vector. The collection time points for the pDNA released solutions are (a) 1, (b) 3, (c) 5, (d) 7, (e) 9, (f) 11 days. (g) The quantified percentages of HeLa cells positive for GFP in the samples analyzed by flow cytometry. Please note that without Lipofectamine 2000, GFP gene expression was not observed via microscopy and was not observed in the flow cytometry experiments.

to the intracellular barriers for gene trafficking to the nucleus and other intracellular barriers that are directly related to pDNA release from our LBL assemblies.

4.5 - Summary

Layer-by-layer deposition (LBL) of poly(L-tartaramidopentaethylenetetramine) (**T4**) and pDNA was carried out to fabricate ultrathin polycation and polyanion multilayer models on silicon and quartz substrates. Different models that contain an increasing number of **T4**/pDNA bilayers were constructed and the layer thickness was measured with ellipsometry. Stable multilayer models with 8 **T4**/pDNA bilayers showed a thickness of about 8nm and the thickness of theses models increased linearly with increase in number of **T4**/pDNA bilayers (between 2 - 8 bilayers). To support the incorporation of pDNA in the multilayer deposited films, an assay was performed which showed the direct intercalation of ethidium bromide in the pDNA as compared to models coated with **T4**/Heparin bilayers. Incorporation of pDNA was also monitored by characterizing the multilayer models built on the quartz substrates by UV-Vis spectrophotometry. An increase in the characteristic absorbance at 260nm for double stranded pDNA implied the increased incorporation of pDNA with the increase in the number of **T4**/pDNA bilayers.

Slides containing the multilayer models (8 bilayers) fabricated with a low concentration of pDNA (0.2 mg/ml) and **T4** were incubated in PBS at physiological conditions and aliquots of the media were collected at regular time intervals. This media containing the released pDNA was complexed with Lipofectamine 2000 and was then used to carry out the cellular uptake and transfection studies in HeLa cells. The flow cytometry analysis showed that between 18-25% of HeLa cells were consistently positive for Cy5-pDNA between time points of 1-7 days. The number of cells positive for Cy5-pDNA increased up to 70% on day 11. Similar multilayer models incorporating pDNA encoding GFP were used to evaluate the integrity of pDNA for gene

expression. The transfection studies show that about 20% cells were positive for GFP expression between 1-7 days. These results are consistent with the transfection studies completed with the Cy5-labeled pDNA for the first 7 days. However, after day 7, the results were inconsistent with the Cy5-pDNA uptake where only about 20% of cells were positive for GFP expression.

Here, the **T4**-pDNA multilayer films studied herein have shown to be a promising model for the controlled-release of pDNA from surfaces. Because the degradation of **T4** yields different kinetics than polyesters (particularly at lower pH), **T4** offers an alternative material with unique characteristics for controlled drug release from various surfaces. Current studies are aimed at further examining this material and our other PGAA structures for release kinetics, integrity, degradation mechanism, and for coating on more medically-relevant surfaces for drug elution.

4.6 - Acknowledgements.

We sincerely thank Giovanna Grandinetti for helping with a negative control experiment in Figure 6.4. We also sincerely thank the National Science Foundation CAREER Award program for funding of this project.

4.7 - References

[1] Russell DW, Hirata RK. Human gene targeting by viral vectors. Nature Genetics 1998;18:325-330.

[2] Boulaiz H, Marchal JA, Prados J, Melguizo C, Aranega A. Non-viral and viral vectors for gene therapy. Cellular and Molecular Biology 2005;51:3-22.

[3] Barrilleaux B, Phinney DG, Prockop DJ, O'Connor KC. Review: Ex vivo engineering of living tissues with adult stem cells. Tissue Engineering 2006;12:3007-3019.

[4] Frimberger D, Lin HK, Kropp BP. The use of tissue engineering and stem cells in bladder regeneration. Regenerative Medicine 2006;1:425-435.

[5] Luo D, Saltzman WM. Synthetic DNA delivery systems. Nature Biotechnology 2000;18:33-37.

[6] Pietersz GA, Tang CK, Apostolopoulos V. Structure and design of polycationic carriers for gene delivery. Mini-Reviews in Medicinal Chemistry 2006;6:1285-1298.

[7] Li WJ, Szoka FC. Lipid-based nanoparticles for nucleic acid delivery. Pharmaceutical Research 2007;24:438-449.

[8] Heller LC, Heller R. In vivo electroporation for gene therapy. Human Gene Therapy 2006;17:890-897.

[9] Dufes C, Keith WN, Bilsland A, Proutski I, Uchegbu JF, Schatzlein AG. Synthetic anticancer gene medicine exploits intrinsic antitumor activity of cationic vector to cure established tumors. Cancer Research 2005;65:8079-8084.

[10] Cavazzana-Calvo M, Hacein-Bey S, Basile CD, Gross F, Yvon E, Nusbaum P, Selz F, Hue C, Certain S, Casanova JL, Bousso P, Le Deist F, Fischer A. Gene therapy of human severe combined immunodeficiency (SCID)-X1 disease. Science 2000;288:669-672.

[11] Thomas CE, Ehrhardt A, Kay MA. Progress and problems with the use of viral vectors for gene therapy. Nature Reviews Genetics 2003;4:346-358.

[12] Marshall E. Clinical trials - Gene therapy death prompts review of adenovirus vector. Science 1999;286:2244-2245.

[13] Hynynen K. Ultrasound for drug and gene delivery to the brain. Advanced Drug Delivery Reviews 2008;60:1209-1217.

[14] Morille M, Passirani C, Vonarbourg A, Clavreul A, Benoit JP. Progress in developing cationic vectors for non-viral systemic gene therapy against cancer. Biomaterials 2008;29:3477-3496.

[15] Wagner E, Kloeckner J. Gene delivery using polymer therapeutics. Polymer Therapeutics I: Polymers as Drugs, Conjugates and Gene Delivery Systems, vol. 192. 2006. p.135-173.

[16] Anwer K, Rhee BG, Mendiratta SK. Recent progress in polymeric gene delivery systems. Critical Reviews in Therapeutic Drug Carrier Systems 2003;20:249-293.

[17] Akhtar S. Beyond delivery. Gene Therapy 2006;13:739-740.

[18] Godbey WT, Wu KK, Mikos AG. Tracking the intracellular path of poly(ethylenimine)/DNA complexes for gene delivery. Proceedings of the National Academy of Sciences of the United States of America 1999;96:5177-5181.

[19] Pollard H, Remy JS, Loussouarn G, Demolombe S, Behr JP, Escande D. Polyethylenimine but not cationic lipids promotes transgene delivery to the nucleus in mammalian cells. Journal of Biological Chemistry 1998;273:7507-7511.

[20] Liu YM, Reineke TM. Hydroxyl stereochemistry and amine number within poly(glycoamidoamine)s affect intracellular DNA delivery. Journal of the American Chemical Society 2005;127:3004-3015.

[21] Liu YM, Wenning L, Lynch M, Reineke TM. Gene delivery with novel poly(1-tartaramidoamine)s. Polymeric Drug Delivery I: Particulate Drug Carriers, vol. 923. 2006. p.217-227.

[22] Srinivasachari S, Liu YM, Zhang GD, Prevette L, Reineke TM. Trehalose click polymers inhibit nanoparticle aggregation and promote pDNA delivery in serum. Journal of the American Chemical Society 2006;128:8176-8184.

[23] Ogris M, Brunner S, Schuller S, Kircheis R, Wagner E. PEGylated DNA/transferrin-PEI complexes: reduced interaction with blood components, extended circulation in blood and potential for systemic gene delivery. Gene Therapy 1999;6:595-605.

[24] Senior J, Delgado C, Fisher D, Tilcock C, Gregoriadis G. Influence of surface hydrophilicity of liposome on their interaction with plasma-protein and clearance from the circulation-Studies with Poly(ethylene glycol)-coated vesicles. Biochimica Et Biophysica Acta 1991;1062:77-82.

[25] Chiu SH, Ueno NT, Lee RJ. Tumor-targeted gene delivery via anti-HER2 antibody (trastuzumab, Herceptin (R)) conjugated polyethylemmine. Journal of Controlled Release 2004;97:357-369.

[26] Bartlett DW, Davis ME. Physicochemical and biological characterization of targeted, nucleic acid-containing nanoparticles. Bioconjugate Chemistry 2007;18:456-468.

[27] Chen CP, Kim JS, Liu DJ, Rettig GR, McAnuff MA, Martin ME, Rice KG. Synthetic PEGylated glycoproteins and their utility in gene delivery. Bioconjugate Chemistry 2007;18:371-378.

[28] Dorta MJ, Santovena A, Llabres M, Farina JB. Potential applications of PLGA film-implants in modulating in vitro drugs release. Int. J. Pharm. 2002;248:149-156.

[29] Klugherz BD, Jones PL, Cui XM, Chen WL, Meneveau NF, DeFelice S, Connolly J, Wilensky RL, Levy RJ. Gene delivery from a DNA controlled-release stent in porcine coronary arteries. Nature Biotechnology 2000;18:1181-1184.

[30] Langer R. Biomaterials and biomedical engineering. Chemical Engineering Science 1995;50:4109-4121.

[31] Groth T, Lendlein A. Layer-by-layer deposition of polyelectrolytes - A versatile tool for the in vivo repair of blood vessels. Angewandte Chemie-International Edition 2004;43:926-928.

[32] Shea LD, Smiley E, Bonadio J, Mooney DJ. DNA delivery from polymer matrices for tissue engineering. Nature Biotechnology 1999;17:551-554.

[33] Jewell CM, Zhang JT, Fredin NJ, Lynn DM. Multilayered polyelectrolyte films promote the direct and localized delivery of DNA to cells. Journal of Controlled Release 2005;106:214-223.

[34] Zhang JT, Chua LS, Lynn DM. Multilayered thin films that sustain the release of functional DNA under physiological conditions. Langmuir 2004;20:8015-8021.

[35] Murphy RF, Powers S, Cantor CR. Endosome pH Measured in Single Cells by Dual Fluorescence Flow-Cytometry- Rapid Acidification of Insulin to pH-6. Journal of Cell Biology 1984;98:1757-1762.

[36] Rybak SL, Lanni F, Murphy RF. Theoretical considerations on the role of membrane potential in the regulation of endosomal pH. Biophys. J. 1997;73:674-687.

[37] Liu YM, Reineke TM. Poly(glycoamidoamine)s for gene delivery: Stability of polyplexes and efficacy with cardiomyoblast cells. Bioconjugate Chemistry 2006;17:101-108.

[38] Liu YM, Reineke TM. Poly(glycoamidoamine)s for gene delivery. Structural effects on cellular internalization, buffering capacity, and gene expression. Bioconjugate Chemistry 2007;18:19-30.

[39] Chen J, Huang SW, Lin WH, Zhuo RX. Tunable film degradation and sustained release of plasmid DNA from cleavable polycation/plasmid DNA multilayers under reductive conditions. Small 2007;3:636-643.

[40] Shi XY, Sanedrin RJ, Zhou FM. Structural characterization of multilayered DNA and polylysine composite films: Influence of ionic strength of DNA solutions on the extent of DNA incorporation. Journal of Physical Chemistry B 2002;106:1173-1180.

[41] McAloney RA, Sinyor M, Dudnik V, Goh MC. Atomic force microscopy studies of salt effects on polyelectrolyte multilayer film morphology. Langmuir 2001;17:6655-6663.

Chapter 5

Poly(glycoamidoguanine)s: Novel guanidine containing polymers show pDNA delivery efficiency in non-toxic manner

5.1 - Abstract

In this study we have synthesized a new polymer series, poly(glycoamidoguanidine)s (PGAGs), in which each repeat unit contains a guanidine moiety attached to a carbohydrate moiety via amide bond on the backbone. PGAGs were also strategically designed to study the effects of the guanidine charge type on the biological performance as compared to the previously studied DNA delivery vehicles, poly(glycoamidoamine)s (PGAAs) which contain secondary amine (protonatable site) as charge type on the polymer backbone. The guanidine moiety on the polymer backbone facilitates the binding of PGAGs with the negatively charged plasmid DNA (pDNA) at low polymer/pDNA charge (*N/P*) ratio 1.5 to 2.5 and form stable polymer-pDNA complexes (polyplexes) around 100 nm at *N/P* ratio 5 and above. PGAGs when complexed with *Cy5* labeled pDNA (*Cy5*-pDNA) at *N/P* ratio 10 and 25 show 80% to 95% cells positive for *Cy5* fluorescence in HeLa cell line. Only 75% cells positive for *Cy5* fluorescence were noted for PGAA complexes in the same experiment. Toxicity of both PGAA and PGAG polyplexes was studied with MTT assay and over 95% cell survival was observed at *N/P* ratios 5, 10,15, 20, 25 and 30 in HeLa cell line exhibiting non-toxic behavior. The transgene expression was studied with lucifarase assay at different *N/P* ratio and PGAGs show similar transgene expression as compared to the PGAAs. This series of guanidine containing polymers show non-toxic behavior in HeLa cell line as compared to earlier reported guanidine containing DNA delivery vehicles, and they also, show a high cellular uptake and high transfection efficiency. Despite the fact that PGAGs lack in the buffering capacity due to the guanidine hard charge in the

chemical structure in the endosomal environment, the transgene expression in the lucifarase assay in case of PGAGs refutes the proton sponge hypothesis.

KEYWORDS

Charge type, guanidine, buffering capacity, cellular internalization and proton sponge hypothesis

5.2 - Introduction

Nucleic acid delivery has gained enormous attention by scientists due to promising results in the field of medicine [1]. However, in order to overcome various cellular barriers so that therapeutic DNA can be transported to targeted cells or tissues, researchers have typically used viruses as DNA delivery vehicles. Although viral vehicles are the current clinically used candidates as the DNA delivery vehicles but it also show severe immunogenicity, discouraging its use in the clinical trials. Different cationically charged macromolecules are under investigation as non-viral DNA delivery vehicles—principally because they can bind with the DNA and assist its cellular uptake and transport to the nucleus where the DNA can express the protein for which it was encoded. In addition to the low immunogenic response of these new compounds, non-viral DNA delivery vehicles are also easy to synthesize and can be designed to carry a high therapeutic load. Amongst various cationically charged macromolecules that have been proposed as non-viral delivery vehicles thus far, polyethyleneimine (PEI) shows high transfection efficiency; however, it also exhibits high toxicity. Conversely, chitosan, which is a naturally occurring polymer that incorporates a carbohydrate unit in the repeat unit, shows low transfection efficiency and low toxicity as a DNA delivery vehicle. Therefore, a novel series of polymers, poly(glycoamidoamine)s (PGAAs), were strategically designed and synthesized to incorporate oligoamine and carbohydrate moieties in their repeat unit. Several comprehensive studies using different mammalian cell lines have shown that PGAAs exhibit similar transfection efficiency as PEI, but has also displayed significantly reduced toxicity [2-5]. Moreover, earlier studies have shown that the carbohydrate group in PGAAs provides biocompatibily to the polymer and also facilitates the degradation of the polymer through hydrolysis of the amide bond [6, 7]. Among the PGAAs we studied, the compounds with four secondary amines in the oligoamine unit exhibited the best biological results amongst this wide library of glycopolymers. In PGAAs at a

physiological pH, about 20% (**T1**) of the amines were found to be protonated, which facilitates binding with pDNA to afford polymer/pDNA complexes. The interaction of these complexes with the glycosaminoglycans (GAGs) on the cell surface has been shown to be essential for the internalization of these polyplexes. After internalization, the polyplexes must escape from the endosomes before they are recycled out to the cell membrane or are degraded via the lysosomes.

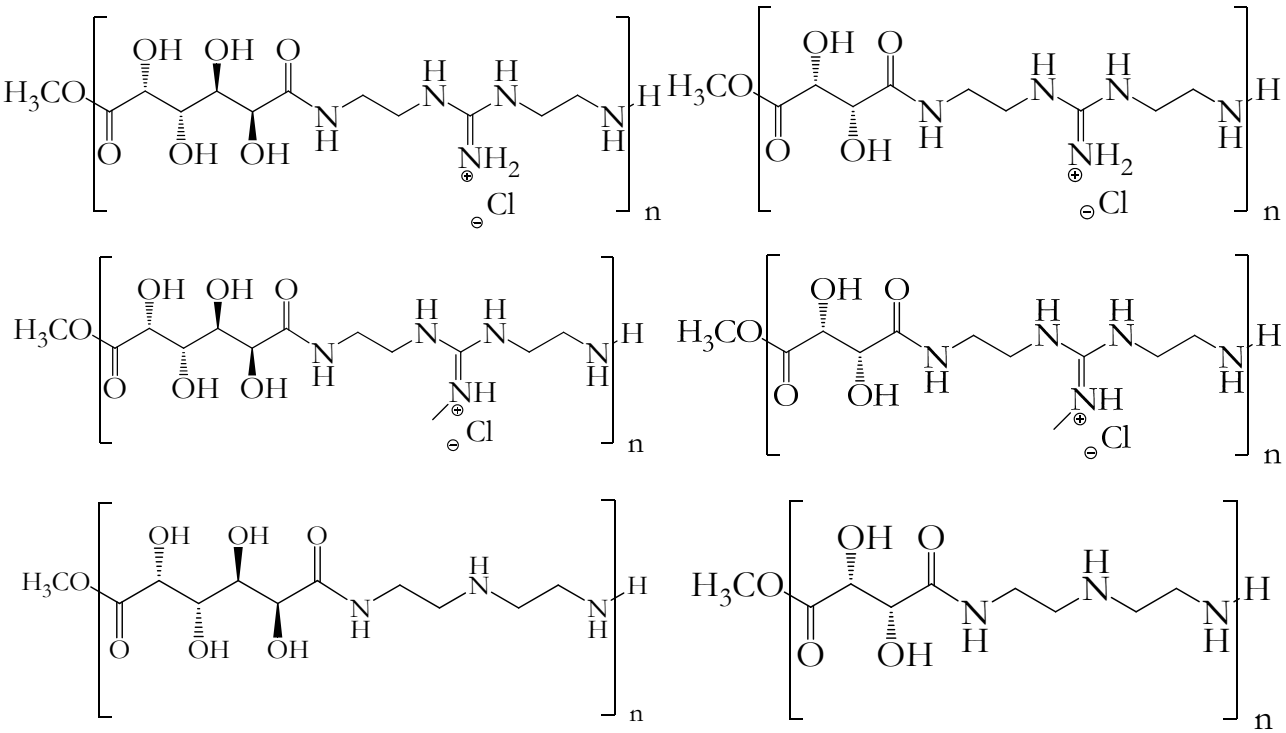

Figure 5.1 Structures of different guanidine containing polymers and amine containing polymers studied in this chapter. The polymers also incorporate the galactarate or tartarate moiety in the structure.

Although PGAAs show high transfection efficiency and non-toxic behavior, a thorough understanding of the complex factors needed to design better DNA delivery vehicles is essential. The processes/parameters that must be investigated include how polymer-DNA complexation results in nanoparticles (termed polyplexes), the internalization and cellular uptake of the polyplexes, the release of polyplexes in the cytoplasm, the transport of these polyplexes to the

nucleus, and the release of DNA from the polyplexes into the nucleus. In addition to the various advantages discussed earlier, non-viral vehicles can also be chemically altered for studying the effects of different functional group on delivery mechanisms [2]. In summary, a systematic investigation of structure-bioactivity relationships is critical for the design of more efficient delivery vehicles for therapeutic compounds.

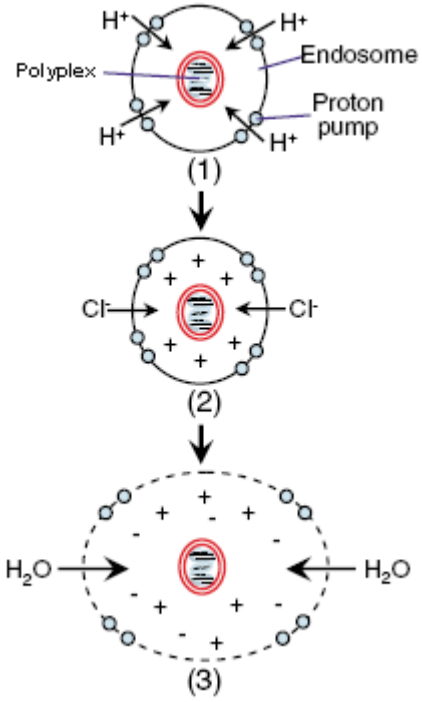

Figure 5.2 Schematic representation of proton sponge theory which explains the release of the polyplexes from the endosomes into the cytoplasm. Figure adapted from Medina-Kauwe *et al*.

One of the essential biological processes in DNA delivery involves the release of the polyplexes from the endosome to the cytoplasm. Endosomolysis, which can be a critical barrier to efficient delivery of macromolecules such as nucleic acids, is involved in the release of different bioconjugates from the endosomes. A variety of theories have been proposed for this process, including pore formation [8, 9], the fusion and/or flip-flop [10] mechanism and the proton sponge hypothesis [11], which is associated with the endosomal escape of the polyplexes so that

they can release their cargo into the cytoplasm. Different polymers and dendrimers based on amino functionality have protonatable amines on the polyplexes. During the acidification of the early endosomes, the protonation of these amines can provide high buffering capacity. The subsequent influx of H^+ ions from proton pumps on the endosomes to reduce the pH of these vesicles also causes high influx of Cl^- ions in the endocytic vesicles. As a result of this osmotic imbalance across the endosomal membrane, water rushes in and swells the endosomes, which eventually rupture and release their cargo into the cytoplasm. Although this theory has been widely studied, it is nonetheless debated in the scientific community [12-14]. Guanidine group is cationically charged at physiological pH and can electrostatically bind to the negatively charged pDNA. Although some polymers have been reported in the past with guanidine functionality, these polymers contain either guanidine groups hanging as the pendant of the backbone, or guanidine groups grafted at the ends of the polymer or the dendrimers. These polymers are capable of forming small particles with pDNA—thereby facilitating its internalization but have also been shown to be very toxic.

In this study, we have synthesized novel group of polymers, poly(glycoamidoguanine) (PGAGs) with guanidine functionality in the backbone and each repeat unit along with a sugar moiety, which to our knowledge is a unique materials based upon its functionality. These polymers with guanidine groups were strategically designed as the analogues of intensively studied PGAAs [2-7, 15-19] replacing the secondary amines in the polymer backbone. These polymers were developed in order to study structure-property relationships and on the different mechanisms involved in nucleic acid delivery—particularly with respect to the effects of changes in amine (PGAAs) versus guanidine (PGAGs) charge type present on the polymer backbone. As discussed earlier, subtle changes in the chemical structures of a delivery vehicle can affect its complexation with DNA, and thus the biological activity of the complex.

As we determined, the low molecular weight PGAGs completely retard the migration of pDNA at *N/P* 4 or less as verified by gel electrophoresis. In addition, at *N/P* 5 or higher, PGAGs could form stable complexes with pDNA (polyplexes) in the range of 60 to 200 nm. Biological assays in HeLa cells revealed that the polyplexes formed with PGAGs displayed higher cellular uptake over PGAA polyplexes. The presence of guanidine groups in the polymer backbone of the PGAGs may provide an artificial transduction domain (ATD) [20] to the PGAG polyplexes, which could promote cellular internalization. The guanidine group has high pKa and is protonated at the physiological pH, and thus provides no buffering capacity to the PGAG polyplexes in endosomes or lysosomes. Despite this lack of buffering capacity, studies have shown that these polymers have good transfection efficiency in HeLa cells. Moreover, research has indicated that PGAG polyplexes exhibit non-toxic behavior studied at all the different polymer to DNA ratio and are the only guanidine containing polymers reported to show such non toxic behavior.

5.3 - Materials and Methods

5.3.1 General: Unless specified otherwise, all the chemicals were purchased from Sigma Aldrich Chemical Co. and were used without any further purification. NMR spectra were collected on an Inova MR-400MHz spectrometer and mass spectra were obtained on an IonSpec HiResESI mass spectrometer. Cell culture media and supplements were purchased from Gibro/Invitrogen (Carlsbad,CA). pCMV*β* was labeled with a Cy5 nucleic acid labeling kit (Mirus, Madison, WI), and purified by QIAquick PCR purification kit (QIAGEN, Valencia, CA). HeLa cells were purchased from ATCC (Rockville, MD). The luciferase assays were completed with a Promega Luciferase Assay Kit (Madison, WI). The toxicity assays were performed with a Bio-Rad DC Protein Assay Kit (Hercules, CA).

5.3.2 Synthesis of small compounds

Tert-butyl 2,2'-thiocarbonylbis(azanediyl)bis(ethane-2,1-diyl)dicarbamate (2): 200 ml of dry methylene chloride was added to a 3 neck flask and was brought to -78^{o}C. 1.665 ml (21.84 mmol) of thiophosgene was added carefully to this flask under nitrogen. A mixture of monobocprotected ethylenediamine (**1**) (7g, 43.68 mmol) and diisopropylethylamine (DIPEA) (5.6 g, 43.68 mmol) in 200 ml of methylene chloride was added slowly and very carefully to the dark orange thiophosgene in methylene chloride over a period of two hrs. This reaction was carried out for two hrs and brought to room temperature. It was stirred for two hrs at room temperature and then was refluxed for two hrs. This reaction mixture was washed with water and the organic layer was dried over Na_2SO_4. Methylene chloride was evaporated under reduced pressure to leave sticky yellow soild. 100 ml of ethyl acetate was added to this residue and was sonicated for half an hour. A white precipitate was filtered out. This product was washed with cold ethylacetate, dried and characterized. Yield (64%). ^{1}H NMR (400 MHz, $CDCl_3$, TMS): δ = 1.44 (s, 18H, C(C$\underline{H}_3$)$_3$), 3.33 (m, 4H, C$\underline{H}_2$NHCO), 3.54 (m, 4H, C$\underline{H}_2$NHCS), 5.14 (br, 2H,

N<u>H</u>CO), 6.70-7.06 (br, 2H, N<u>H</u>CS). ^{13}C NMR ($CDCl_3$): δ = 28.26, 39.73, 44.78, 79.88, 157.18, 181.99. ESI-MS $[C_{15}H_{31}N_4O_4S]^+$: *m/z* observed 363.2065, calcd 363.2061.

1,3-bis(2-(tert-butoxycarbonylamino)ethyl)-2-methylisothiouronium iodide (3): **2** was dissolved in acetonitrile in a RBF and then methyl iodide was added in excess to this reaction mixture. This reaction mixture was stirred at 50^{o}C for 8 hrs. Acetonitrile and excess methyl iodide were evaporated under reduced pressure and pure product was dried and characterized. Yield (92%). ^{1}H NMR (400 MHz, $CDCl_3$, TMS): δ = 1.42 (s, 18H, C(C<u>H</u>$_3$)$_3$), 2.75(s, 3H, C<u>H</u>$_3$S), 3.43-3.56 (m, 6H, C<u>H</u>$_2$C<u>H</u>$_2$NHCO), 3.54 (m, 2H, C<u>H</u>$_2^+$NH=CS), 5.58, 5.72 (2 x s, 2H, N<u>H</u>CO), 8.74, 8.98 (2 x s, 2H, $^+$N<u>H</u>=CS(CH$_3$)N<u>H</u>). ^{13}C NMR ($CDCl_3$): δ = 15.27, 28.33, 38.25, 39.30, 45.94, 79.74, 80.59, 156.65, 158.28, 168.28. ESI-MS $[C_{16}H_{34}N_5O_4 - I]^+$: *m/z* observed 377.2216, calculated 377.2222.

1,3-bis(2-(tert-butoxycarbonylamino)ethyl)-2-methylguanidinium iodide (4): **3** was dissolved in chloroform and was stirred at 50 C. To this 2 ml of 2 M methylamine in tetrahydrofuran (THF) was added every 4 hrs. After 20 hrs low boiling compounds were evaporated under reduced pressure to leave very viscous colorless oil. ^{1}H NMR (400 MHz, $CDCl_3$, TMS): δ = 1.43 (s, 18H, C(C<u>H</u>$_3$)$_3$), 2.99 (s, 3H, C<u>H</u>$_3^+$NH=C), 3.39 (q, 4H, C<u>H</u>$_2$NHCO), 3.51 (m, 4H, C<u>H</u>$_2$NHCS), 5.78 (t, 2H, N<u>H</u>CO), 7.30 (s, 2H, N<u>H</u>CS), 7.32 (s, 1H, $^+$N<u>H</u>=CS). ^{13}C NMR ($CDCl_3$): δ = 28.32, 28.67, 39.24, 43.27, 80.31, 155.00, 157.95. ESI-MS $[C_{16}H_{34}N_5O_4 - I]^+$: *m/z* observed 360.2615, calculated 360.2610.

1,3-bis(2-(tert-butoxycarbonylamino)ethyl)-2-guanidinium iodide (5): **3** was dissolved in chloroform and was stirred at 40C. To this 2 ml of 7 N ammonia in methanol was added every four hrs. After 20 hrs low boiling compounds were evaporated under reduced pressure to leave very viscous colorless oil. ^{1}H NMR (400 MHz, $CDCl_3$, TMS): δ = 1.44 (s, 18H, C(C<u>H</u>$_3$)$_3$), 3.33 (m, 4H, C<u>H</u>$_2$NHCO), 3.40 (m, 4H, C<u>H</u>$_2$NHCS), 5.44 (s, 2H, N<u>H</u>CO), 7.02 (s, 2H, N<u>H</u>CS), 7.68

(s, 2H, $^{+}N\underline{H}_2$=CS). ^{13}C NMR ($CDCl_3$): δ = 28.36, 39.37, 41.92, 80.21, 156.38, 157.19. ESI-MS $[C_{15}H_{32}N_5O_4 - I]^+$: *m/z* observed 346.1934, calcd 346.2449.

1,3-bis(2-aminoethyl)-2-methylguanidine trihydrochloride (6): **4** was dissolved in 10 ml of trifluroacetic acid (TFA) and stirred at room temperature. After two hours the TFA was evaporated under reduced pressure. The dark brown oil was obtained. This oil was dissolved in 20 ml of ethanol and to this 2 ml of concentrated hydrochloride was added. The white precipitate crashed out of the mixture which was then filtered and washed with cold ethanol. This white precipitate was then dried and characterized. Yield 59%. ^{1}H NMR (400 MHz, D_2O): δ = 2.82 (s, 3H, $C\underline{H}_3N$), 3.19 ($C\underline{H}_2NHC$), 3.53 ($C\underline{H}_2NH_2$). ^{13}C NMR ($CDCl_3$): δ = 27.81, 38.07, 38.66, 155.52. ESI-MS $[C_6H_{18}N_5 - Cl]^+$: *m/z* observed 160.1554, calculated 160.1562.

1,3-bis(2-aminoethyl)-2-guanidine trihydrochloride (7): 5 was dissolved in 10 ml of trifluroacetic acid (TFA) and stirred at room temperature. After two hours the TFA was evaporated under reduced pressure. The dark brown oil was obtained. This oil was dissolved in 20 ml of ethanol and to this 2 ml of concentrated hydrochloride was added. The white precipitate crashed out of the mixture which was then filtered and washed with cold ethanol. This white precipitate was then dried and characterized. Yield 63%. ^{1}H NMR (400 MHz, D_2O): δ = 3.19 ($C\underline{H}_2NHC$), 3.53 ($C\underline{H}_2NH_2$). ^{13}C NMR ($CDCl_3$): δ = 38.06, 38.74, 156.26. ESI-MS $[C_5H_{16}N_5 - Cl]^+$: *m/z* observed 146.1402, calcd 146.1406.

5.3.3 Polymer synthesis

*Poly(L-tartaramidodiethyleneamine) T1 (control)***:** 0.1 g (0.9698 mmol) of diethylenetriamine was weighed out in a round bottom flask. To this 0.96 ml (2.0 M) of methanol was added to dissolve diethylenetriamine. 0.1727 g (0.9698 mmol) of dimethyl L-tartarate was weighed out carefully and was added to the roundbottom flask. This mixture was stirred for 24 hrs at room temperature and 5 ml of water was added to this reaction mixture after 24 hrs. The reaction

mixture was completely dissolved in the 5 ml of water. This reaction mixture was then dialyzed in 1000 Da molecular weight membrane against the ultrapure water to get rid of relatively smaller molecular weight compounds. The reaction mixture in water was then lyophilized to dryness. Polymer was then characterized with GPC

*Poly(galactaramidodiethyleneamine) G1 (control)***:** 0.3 g (2.909 mmol) of diethylenetriamine was weight out and was dissolved in 58.1 ml (0.1 M) methanol. 0.693 g (2.909 mmol) of dimethyl *meso*-galactarate was added to this reaction mixture. This reaction mixture was stirred for 24 hrs. Methanol was evaporated under reduced pressure to leave white solid in the flask. To this 10 ml of ultrapure water was added and the white solid was dissolved in water. This mixture was transferred in a 1000 Da molecular weight membrane and was exhaustively dialyzed against ultrapure water to remove relatively smaller molecular weight compounds. This mixture was then flash frozen in a scintillation vial and the water was lyophilized to live white fluffy solid behind. Polymer was then characterized with GPC

*Poly(galactaramidodiethylenemethylguanine) GGme***:** 150 mg (0.556 mmol) of Compund 6 was weighed out and was added to 2 ml of methanol. To this 400 µl (5 x 0.556 mmol) of triethylamine (TEA) was added. This mixture was stirred for 15 minutes until a homogeneous mixture was obtained. To this mixture 132.4 mg (0.556 mmol) of dimethyl *meso*-galactarate was added. This reaction mixture was stirred at room temperature for 48 hrs. 5 ml of ultrapure water was added to this reaction mixture to dissolve any precipitated solids. This mixture was transferred in a 1000 Da molecular weight membrane and was exhaustively dialyzed against ultrapure water to remove relatively smaller molecular weight compounds. This mixture was then flash frozen in a scintillation vial and the water was lyophilized to leave sticky white solid behind. Polymer was then characterized with GPC

Poly(L-tartaramidodiethylenemethylguanine) TGme: 150 mg (0.556 mmol) of compound 6 was weighed out in a 5 ml round bottom flask (RBF). 1 ml of methanol was added to this RBF. 400 µl (5 x 0.556 mmol) of triethylamine was added to this mixture and stirred for 15 min to obtain a homogeneous mixture. To this reaction mixture 99.1 mg (0.556 mmol) of dimethyl L-tartarate was added and the reaction mixture was stirred for about 3 minutes to observe Dimethyl L-tartarate to dissolve. The reaction mixture was then stirred for 120 hrs and then methanol was evaporated under reduced pressure to leave white solid behind. 5 ml of ultrapure water was added to this reaction mixture to dissolve any precipitated solids. This mixture was transferred in a 1000 Da molecular weight membrane and was exhaustively dialyzed against ultrapure water to remove relatively smaller molecular weight compounds. This mixture was then flash frozen in a scintillation vial and the water was lyophilized to leave sticky yellowish solid behind. Polymer was then characterized with GPC

Poly(galactaramidodiethyleneguanine) GG: 100 mg (0.393 mmol) of compound 7 was weighed out in a RBF and to this 2 ml of methanol was added. To this 275 µl (5 x 0.393 mmol) of triethylamine (TEA) was added. This mixture was stirred for 15 minutes until a homogeneous mixture was obtained. To this mixture 94.0 mg (0.393 mmol) of dimethyl *meso*-galactarate was added. This reaction mixture was stirred at room temperature for 48 hrs. 5 ml of ultrapure water was added to this reaction mixture to dissolve any precipitated solids. This mixture was transferred in a 1000 Da molecular weight membrane and was exhaustively dialyzed against ultrapure water to remove relatively smaller molecular weight compounds. This mixture was then flash frozen in a scintillation vial and the water was lyophilized to leave sticky white solid behind. Polymer was then characterized with GPC

Poly(L-tartaramidodiethyleneguanine)TG: 150 mg (0.59 mmol) of compound 7 was weighed out in a 5 ml round bottom flask (RBF). 1 ml of methanol was added to this RBF. 425 µl (5 x

0.59 mmol) of triethylamine was added to this mixture and stirred for 15 min to obtain a homogeneous mixture. To this reaction mixture 105.5 mg (0.59 mmol) of dimethyl L-tartarate was added and the reaction mixture was stirred for about 3 minutes to observe Dimethyl L-tartarate to dissolve. The reaction mixture was then stirred for 120 hrs and then methanol was evaporated under reduced pressure to leave off-white solid behind. 5 ml of ultrapure water was added to this reaction mixture to dissolve any precipitated solids. This mixture was transferred in a 1000 Da molecular weight membrane and was exhaustively dialyzed against ultrapure water to remove relatively smaller molecular weight compounds. This mixture was then flash frozen in a scintillation vial and the water was lyophilized to leave sticky yellowish solid behind. Polymer was then characterized with GPC.

5.3.4 Polymer characterization

The molecular weight, and polydispersity were characterized with Viscoteck GPCmax equipped with a $GMPW_{XL}$ column coupled to a triple detector (static light scattering, viscometry and refractive index). A solution of 0.5 M sodium acetate in 80:20 water to acetonitrile was used as mobile phase. pH of the mobile phase was adjusted to pH 7 by adding acetic acid. Sample prep was done by dissolving about 2 mg of polymer sample in 1 ml of mobile phase, and injected onto the column (100 μl) and eluted at 0.6 ml/minute.

5.3.5 Polyplex characterization

Gel electrophoresis: The binding between GG, GGme, GT and GTme polymers and DNA is tested by gel electrophoresis under 60 V for 60 minutes. Ethidium bromide (0.6 μg/ml) contained agarose gel (0.6 % w/v) was made with pure agarose, 10 mg/ml ethidium bromide solution and 1X TAE buffer. Plasmid DNA (pCMV-*lacZ*) was diluted into 0.1 mg/ml stock solution with Gibco nuclease-free water. Different guanidine polymers are dissolved in Gibco nuclease-free

water to make *N/P* 50 (N = number of guanidine groups on polymer, P = number of phosphate groups on DNA) stock solution. Then different polymer solutions with different concentration (*N/P* 0 to 50) were made by diluting polymer stock solution. 10 μl polymer solution was then added into 10 μl DNA solution to form polyplexes at different *N/P* ratios and incubated for 60 min before adding 2 μl loading buffer (Blue Juice). 15 μl solution of each sample was loaded to the gel for testing.

Dynamic Light Scattering: Polyplexes at different Polyplex sizes were measured at 633 nm on a Zetasizer (Nano ZS) dynamic light scattering instrument (Malvern Instruments, Malvern, UK). Polyplexes (*N/P* 2 to 30) were formed by incubating each aqueous polymer solution (150 μL in H_2O) with pCMVβ (150 μL, 0.02 μg/ μL in H_2O) for 40 min. The particle size of polyplexes was characterized by with a detection angle of 173° in triplicate in water at 25 °C with and the average size and standard deviation are reported for each polyplex solution.

Transmission Electron Microscopy: Polymer-pDNA complexes were prepared at *N/P* = 20 as described above for the dynamic light scattering studies. Samples (5 μL of the polyplex solution in water) were applied in duplicate to 400-mesh carbon-coated grids (EMS, Fort Washington, PA) and incubated for 60 s. Excess liquid was removed by blotting with kimwipe. Samples were negatively stained with uranyl acetate (2%, w/v) for 90 s and again blotted with kimwipe. TEM images were recorded with a JEOL JEM-1230 transmission electron microscope operated at 60 kV.

5.3.6 Cell Culture Experiments

HeLa (human cervix adenocarcinoma) cells are purchased from ATCC. Cells were cultured in Dulbecco's Modified Eagle Medium (DMEM) with 10 % fetal bovine serum (FBS) and 1 % antibiotics in 5 % CO_2 at 37 ^{o}C. All the experiments used identical passage of cells and same

batch of reagents; all samples were prepared with Gibco nuclease-free water and all materials were autoclaved or treated under UV light for 15 min to make results reproducible.

Luciferase Assay in Serum-free Medium: HeLa cells were cultured in a 24-well plate with a density of $5x10^4$ cells/well and incubated for 24 hours prior to transfection. 150 μl GG, GGMe, TG, TGMe, **G1**, **T1**, poly-L-arginine and glycofect^{TM} were added into 150 μl luciferase DNA (0.02 mg/ml) at *N/P* ratio 5, 10, 15, 20, 25 and 30 at room temperature. A 60-minute incubation time was given before 600 μl serum-free medium (Opti-MEM) was added. HeLa cells were washed with 0.5 ml PBS and 300 μl polyplex solution (containing 1 μg DNA and different amount of polymer) was added to cells in each well. Untranfected cells and cells transfected with DNA only were used as negative controls. Experiments were done in triplicate. Four hours after transfection, 800 μl 10% FBS DMEM solution was added to each well. Twenty-four hours after transfection, medium was replaced with 1 ml 10% FBS DMEM solution in each well. Forty-eight hours after transfection, cells were washed with PBS and lysed with cell culture lysis buffer (Promega). Bio-Rad DC protein assay kit was used to determine the amount of protein in cell lysates. For luciferase activity, cell lysates were analyzed with luciferase substrate. Luminescence was measured over 10 s with a luminometer (GENios Pro, TECAN US, Research Triangle Park, NC).

MTT Assay: HeLa cells were cultured in a 24-well plate with a density of $5x10^4$ cells/well and incubated for 24 hours prior to transfection. 150 μl GG, GGMe, TG, TGMe, **G1**, **T1**, poly-L-arginine and glycofect^{TM} were added into 150 μl pCMV-*lacZ* DNA (0.02 mg/ml) at *N/P* ratio 5, 10, 15, 20, 25 and 30 at room temperature. A 60-minute incubation time was given before 600 μl serum-free medium (Opti-MEM) was added. HeLa cells were washed with 0.5 ml PBS and 300 μl polyplex solution (containing 1 μg DNA and different amount of polymer) was added to cells

in each well. Untranfected cells and cells transfected with DNA only were used as negative controls for cytotoxicity. Experiments were done in triplicate. Four hours after transfection, 800 μl 10% FBS DMEM solution was added to each well. Twenty-four hours after transfection, cells were washed with 0.5 ml PBS. Then 0.5 ml 0.5 mg/ml MTT in 10% FBS DMEM solution was added to each well. After incubated at 37 ^{o}C for 1 h, cells were washed with 0.5 ml PBS and lysed with 600 μl DMSO. An aliquot of 200 μl cell lysate was loaded to a 96-well plate for colorimetric measurement. Samples were measured with a spectrophotometer (GENios Pro, TECAN US, Research Triangle Park, NC) with wavelength 570 nm. Cell viability profiles were characterized by the absorbance. Cell viability of transfected cells was normalized to that of untransfected cells.

Flow Cytometry: HeLa cells were cultured in a 6-well plate with a density of 2.5x10^5 cells/well and incubated for 24 hours prior to transfection. 250 μl GG, GGMe, TG, TGMe, **G1**, **T1**, poly-L-arginine and glycofect^{TM} were added into 250 μl Cy5 (excited at 633 nm) labled pCMV-*lacZ* DNA (0.02 mg/ml) at *N/P* ratio 10 and 25 at room temperature. A 60-minute incubation time was given before 1 ml serum-free medium (Opti-MEM) was added. HeLa cells were washed with 1 ml PBS and 1.5 ml polyplex solution (containing 5 μg DNA and different amount of polymer) was added to cells in each well. Untranfected cells and cells transfected with DNA only were used as negative controls for cellular uptake. Experiments were done in duplicate. Two hours after transfection, cells were rinsed with PBS several time to remove polyplexes bound to cell membrane. 1 ml 10% FBS DMEM was then added to allow further endocytosis for 30 min. Four and half hours after initial transfection, cells were washed with PBS, trypsinized, pelleted, the supernants were removed, and cells were resuspended in PBS for fluorescent active cell sorting

(FACS) analysis. Cells were measured with a FACSCanto II (Becton Dickenson, San Jose, CA). Twenty thousand events were recorded.

5.4 - Results and Discussion

This study is an attempt towards understanding the structure-bioactivity relationship of earlier studied poly(glycoamidoamine)s (PGAAs). Chemical structure of repeat unit of PGAAs incorporates a carbohydrate moiety and secondary amines. PGAAs promote the binding with DNA due to the protonated secondary amines present as charge type on the polymer backbone. Here we have synthesized another polymer series, poly(glycoamidoguanine)s (PGAGs), analogues to the PGAAs with guanidine or methylguanidine as a charge type. The guanidine group has high pKa value of around 12.5 (dependant on the substituent) and are always protonated at physiological pH as compared to about 50% sencondary amines protonated at physiological pH in case of PGAAs (**T1**) [18]. As the subtle changes in the chemical structure [21, 22] of the delivery vehicle can have a high effect on the biological properties of the polymer, the different charge types in the PGAAs and PGAGs can show different binding affinity towards the pDNA and thus can affect the polyplex formation, cellular uptake of the polyplexes, its release from the endosome, release of the DNA in the nucleus which collectively can affect the transgene expression. Also, according to proton sponge hypothesis the PGAGs in the polyplexes wouldn't provide any buffering capacity in the endosome resulting in no endosomal release of the polyplexes. The transgene expression, if resulting from the luciferease assay will be an indication of refuting the proton sponge hypothesis.

5.4.1 Monomer and polymer synthesis

Poly(glycoamidoguanine)s (PGAGs) were designed based on the similar ammonolysis chemistry used before for the synthesis of PGAAs. The diamine with a guanidine moiety in the architecture is commercially not available and was designed from the Sambrook et al [23]. As shown in

scheme 5.1, mono-boc-protected ethylenediamine synthezed from the earlier reported procedure [24] was reacted carefully with thiophosgene at -78 ^{o}C in presence of diisopropylethylamine (DIPEA), the reaction mixture was warmed up to room temperature and then refluxed.

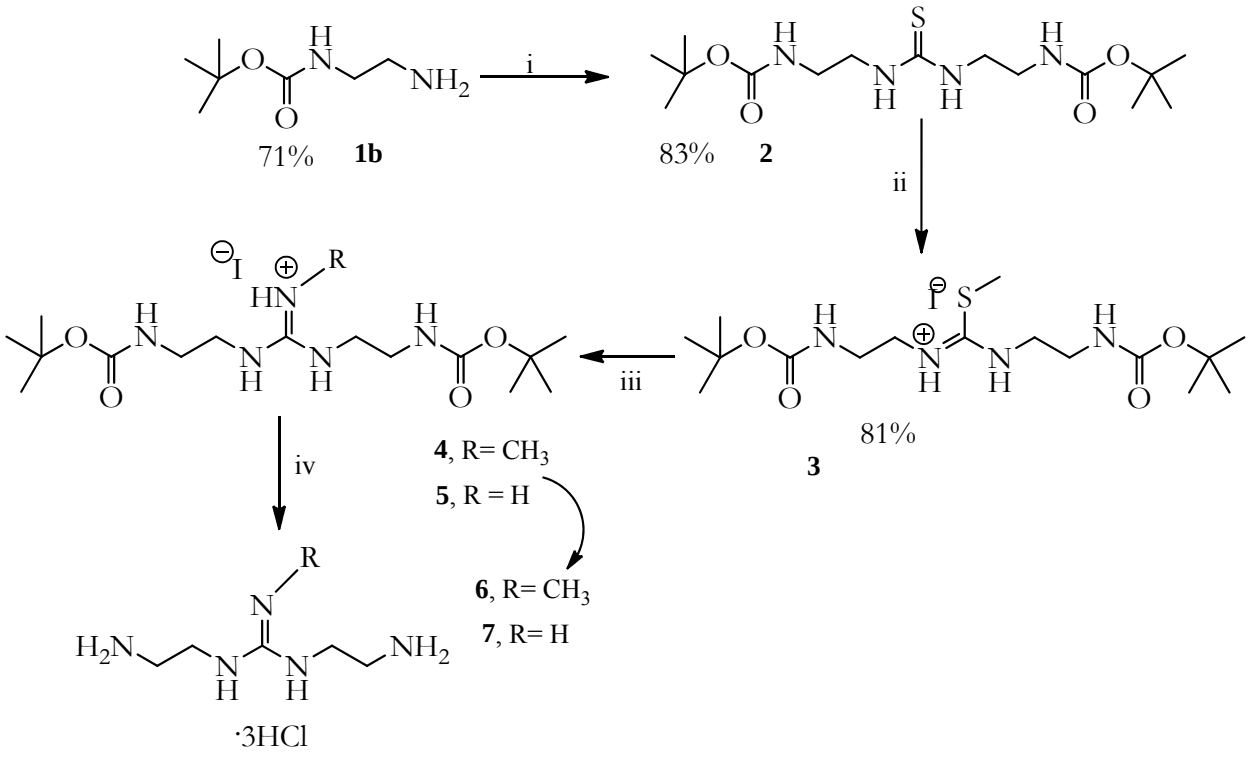

Scheme 5.1 Synthetic scheme for the synthesis of the guanidine containing monomers. i) Thiophosgene, DIPEA, -78 ^{o}C-reflux, $CHCl_3$ ii) methyl iodide, 50 oC, Acetonitrile. iii) 4.0 N methylamine (**4**) in THF, 6.0 N ammonia (**5**) in methanol. iv) TFA, ethanol (0.5 % HCl) wash

After purification a thiourea (**2**) compound was obtained and this compound was then reacted with methyliodide to result into methyl thiourea (**3**). The methyl thiourea was then treated with a nucleophile such as ammonia or methyl amine in order to get guanidine (**5**) or methyl guanidine (**4**) compound. Both the guanidine incorporating compounds were then treated with trifluoroacetic acid (TFA) in order to deprotect the amine groups by removing the boc groups. The final guanidine (**7**) or methyl guanidine (**6**) containing compounds were then dissolved in

ethanol and concentrated HCl was added to this solution and guanidine containing diamines with HCl salt were precipited out, dried and characterized.

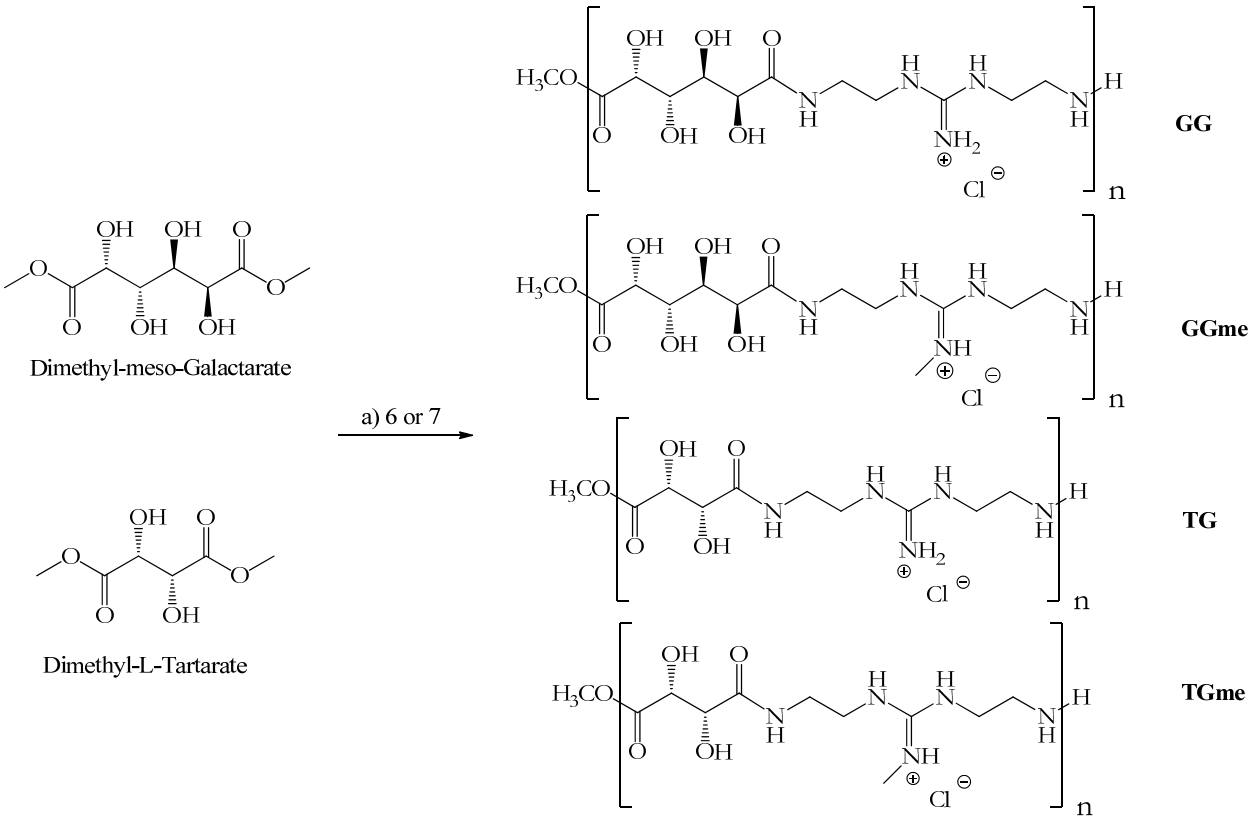

Scheme 5.2 Synthetic scheme for polymerization. a) TEAm MeOH

Step growth polymerization between diamines and dieaster as explained in the PGAAs synthesis was used for the PGAGs synthesis. The PGAG polymer series was synthesized using diamines incorporating guanidine (**7**) or methylguanidine (**6**) moieties with dimethyl *meso*-galactarate or dimethyl-L-tartarate to yield four different polymers. G and Gme were dissolved in methanol in presence of TEA and then reacted with dimethyl *meso*-galactarate for 48 hrs to synthesize the galactarate series. Similarly the tartarate series was synthesized by reacting G and Gme with dimethyl-L-tartarate in similar conditions for 120 hours. The reaction mixture was then dialyzed with 1000 kDa molecular weight membrane against ultrapure water in order to separate the low

molecular weight molecules and to get low polydispersed polymers. PGAG polymer series was then characterized with gel permeation chromatography (GPC) and different batches of PGAGs were used to obtain the degree of polymerization in the range four to five. Although a very small degree of polymerization of around five (oligomers) was obtained for this series which due to the nature of the monomer and the precipitation of the polymer from the reaction mixture.

Table 5.1 Different guanidine and amine containing polymers

Polymer	**Mw (kDa)**	**Mw/Mn**	**n**
GG	1.3	1.2	4
GGme	1.3	1.3	4
TG	1.3	1.2	5
TGme	1.4	1.2	5
G1	1.3	1.3	5
T1	1.1	1.3	4

The PGAAs with one secondary amines with either galactarate or tartarate moieties (**G1** and **T1**) were resynthesized to get similar DP in order to see the effect of the charge center on the binding with pDNA and the biological activity of the polyplexes. Table 5.1 shows the different polymers synthesized and the degree of polymerization of the corresponding polymers.

5.4.2 Polyplex characterization

Gel Electrophoresis Shift Assay: After the synthesis of the PGAGs series, its binding with the pDNA was characterized using gel electrophoresis assay in order to observe the inhibition of pDNA migration with increased *N/P* or polymer ratio. Different polyplexes with increasing *N/P*

ratio from zero (pDNA only) to 30 were prepared by adding the appropriate concentration of polymer solution to pDNA solution and incubating the mixture solution for 60 minutes to form the complexes. As observed in Figure 5.3 at *N/P* zero (pDNA only) the DNA migration towards the positive electrode is observed. The increase in the polymer ratio influences the binding of polymer with pDNA and decreases the pDNA migration towards the positive electrode.

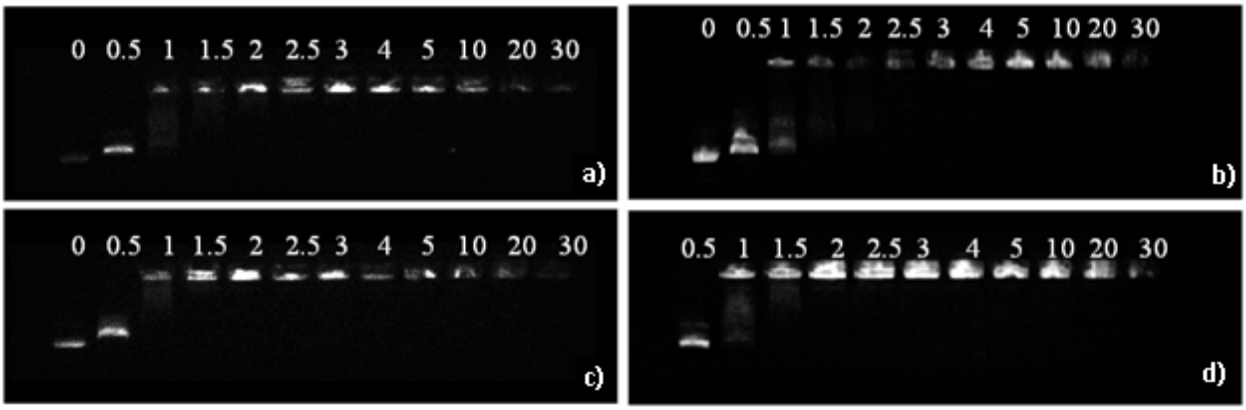

Figure 5.3 Gel electrophoresis shift assay for the PGAGs complexed with pDNA in different *N/P* ratios from 0 (pDNA only) to 30. a) shows retardation of DNA migration implying binding of polymer GGme with pDNA at *N/P* 2. b) shows the binding of polymer TGme at *N/P* 2.5. c) shows the binding of polymer GG with pDNA at *N/P* 1.5 d) shows the binding of polymer TG at *N/P* 2.

The Figure 5.3 shows that all the PGAGs bind the pDNA at the *N/P* ratio 2.5 or less as compared to the amine containing polymers **G1** and **T1** which show the retardation of the DNA migration at around *N/P* 10 exhibiting higher affinity of the guanidine containing polymers (PGAGs) towards the pDNA binding over amine containing polymers (PGAAs). Galactarate based guanidine containing polymers (GG *N/P* = 1.5, GGme *N/P* = 2) bind pDNA at a lower *N/P* ratio as compared to the tartarate based polymers (TG *N/P* = 2, TGme *N/P*=2.5) implying role of higher number of hydroxyl groups in galactarate moiety may have role in the increased binding affinity. Also, the PGAGs with methyl guanidine group exhibit lower binding affinity with pDNA over the PGAGs with guanidine group which implies that there might be less binding

interaction as with increased substituents on the guanidine moiety contributing to increased sterics. However, all PGAGs show higher binding affinity with pDNA and completely retard the migration of the DNA on the gel electrophoresis at lower (2.5 or less) *N/P* ratio as compared to the PGAAs (**G1** and **T1**) which show complete retardation of the DNA at *N/P* around 10.

*Polyplex size***:** The gel shift assay shows that the PGAGs are capable of binding with pDNA at lower *N/P* ratio. It is then important to know the size of the polyplexes and charge on the polyplex surface as this is previously has been studied to affect the cellular uptake of the polyplexes and further biological activity. The characterization of the polyplexes for its size was done using the dynamic light scattering (DLS) at *N/P* 2 to 30 (Figure 3.5). It was observed that all the PGAGs show stable polyplex formation at the *N/P* ratio 5 and above. The polyplexes average size at *N/P* ratio 2 was about a micron and was not reproducible. The polyplex size at *N/P* 5 was reproducible and was in the range from 70-300 nm for all the polymers in PGAG series although the polyplex size reduced to about 70 nm at *N/P* 10 and showed a very small error bar. Further increase in the *N/P* ratio did not result in further compaction of the polyplexes and the polyplex size attains the plateau after *N/P* 10. The transmission electron micrograph (Figure 5.4 f) for GGme at N/P 20 also supports the polyplex size ~70 nm. G1 and T1 are the when characterized for the particle size shows particle size of about 500 nm at higher N/P ratios. This is due to the fact that both PGAAs and PGAGs are short polymers and lack the cooperativity effect for the binding with pDNA as compared to longer polymers. But in case of PGAAs with secondary amine as a soft charge center which may not assist enough binding at lower N/P ratio. On the other hand the PGAGs are protonated at the physiological pH and thus have higher charge density and thus provide higher affinity towards the binding with pDNA.

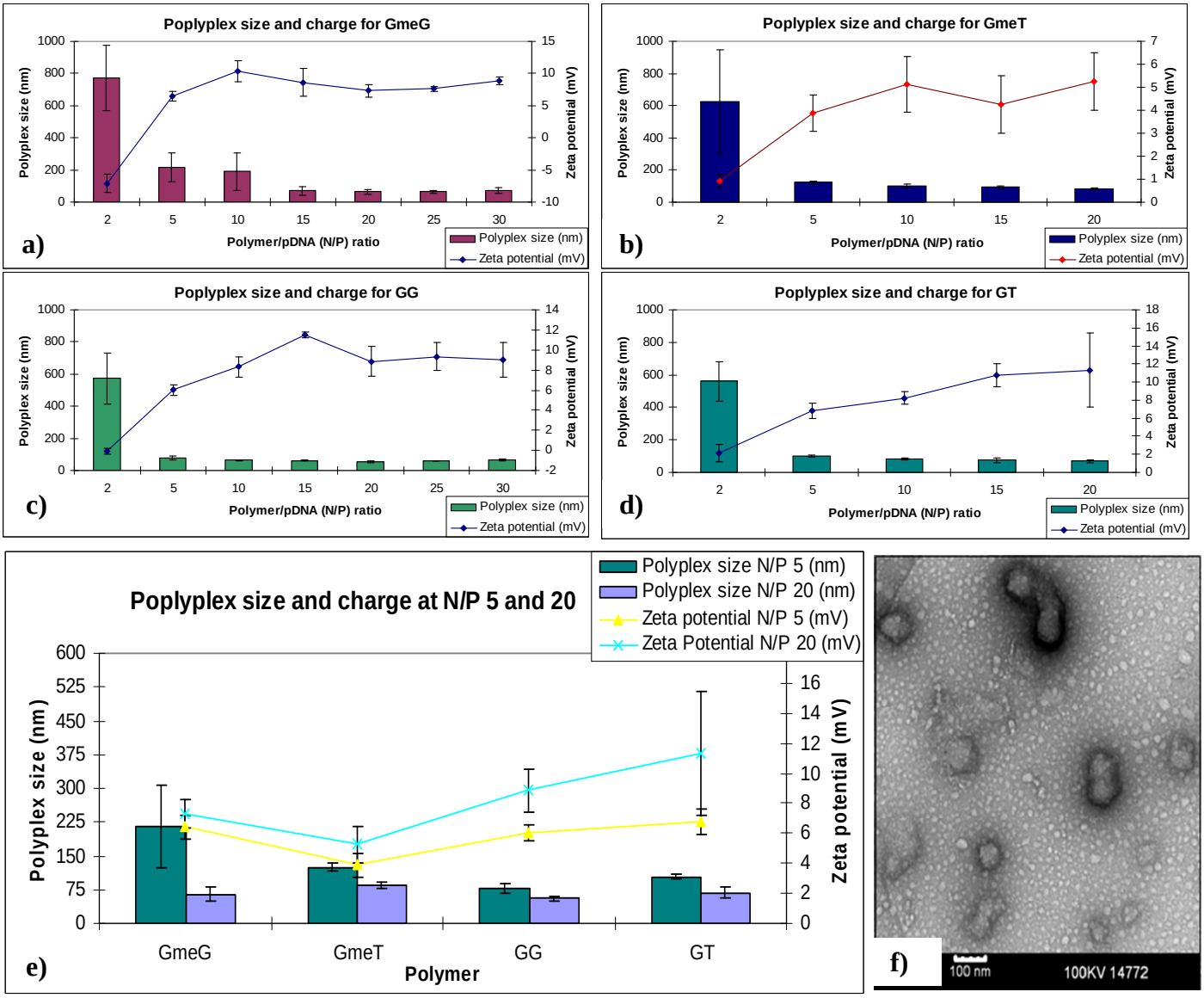

Figure 5.4. The polyplex size of the poly(glycoamidoguanine) polymer series when complexed with pDNA at different *N/P* ratio from 0 (pDNA only) up to 30 (increasing the polymer ratio) and then incubated for 40 minutes. a) The polymer GGme shows polyplex formation at *N/P* 2 although the size of the polyplexes formed is not reproducible and indicates that the polyplex formed are not stable. At *N/P* 5 the polymer shows polyplex of size ~200 nm and the size further reduces for ~70 nm at *N/P* 15 and higher. Zeta potential reveal similar trend and shows positive zeta potential around between *N/P* 2 and 5 and higher. Zeta potential also attains a plateau after *N/P* ratio 10. b), c), d) similar trends and show formation of stable polyplexes for TGme, GG and GT at *N/P* 5 and above. e) Representation of the all four PGAGs complexedwith pDNA at *N/P* 5 and 20 and shows that at *N/P* 20 polymers form smaller polyplex size of ~70 nm and also have positive charge on the suface. f) A transmission electron microscopy image of the GGme polymer complexed with pDNA at *N/P* 20 and shows that the polyplexes formed are around ~70 nm

Zeta potential: As shown in Figure 5.4 the zeta potential of the PGAG polymers in the aqueous solution results in the positive surface charge on the polyplexes. The zeta potential measurement show that the PGAG polyplexes formed at *N/P* ratio five show positive value and it increases as the *N/P* ratio increased to 10 but attains a plateau similar as the particle size. It is interesting to find both particle size and the zeta potential attains a plateau after N/P about 10 and is an indication that the polyplexes formed are thermodynamically stable at N/P 10 and there is no further effect of additional polymer on the polyplexes in the solution.

5.4.3 Cellular uptake and transgene expression studies

In order to study the cellular uptake of the PGAGs (GG, GGme, GT, GTme) based polyplexes, flowcytometry assay was carried out to investigate both, the number of cells that are positive for Cy5-labeled pDNA and the average intensity of Cy5 florescence in the cells. PGAG polyplexes were formed at *N/P* 10 and 25 and HeLa cells were incubated with each polyplex solution for 2 hours. Before characterization of the cells positive for Cy5 fluorescence, the cell surface bound polyplexes were washed with PBS in order to get the accurate characterization. The cells were then incubated with polyplexes and for 2 hours of transfection the cells were trypsinized and pelleted before its analysis with the FACS. The analyzed data as shown in the Figure 5.5 for per cent cells positive for the Cy5 fluorescence and the mean fluorescence intensity is represented in Figure 5.5. Only 20 % of the cells were positive for the Cy5 fluorescence in negative control (DNA only). Both the polymer series PGAGs and PGAAs show increase in the uptake of the DNA by HeLa cells and about 90 % of cells are positive for the Cy5 fluorescence for the PGAGs (except . It is also interesting to note that, PGAGs show similar cellular uptake of pDNA as the positive control Glycofect^{TM} and show higher cellular uptake than the other analogues PGAAs (**G1** and **T1**). The increased cellular uptake in case of PGAGs over PGAAs may be because of the guanidine groups present on the polymer backbone which may provide PGAGs an artificial

transduction domain (ATD). ATD provided by the guanidine groups have been shown to be responsible for the cellular uptake of the macromolecules in to the cells [20]. This is an important aspect of this delivery vehicle as the guanidine groups on the backbone of the polymers not only assists in the polyplex formation but also can assists in the cellular uptake making it a smart delivery vehicle.

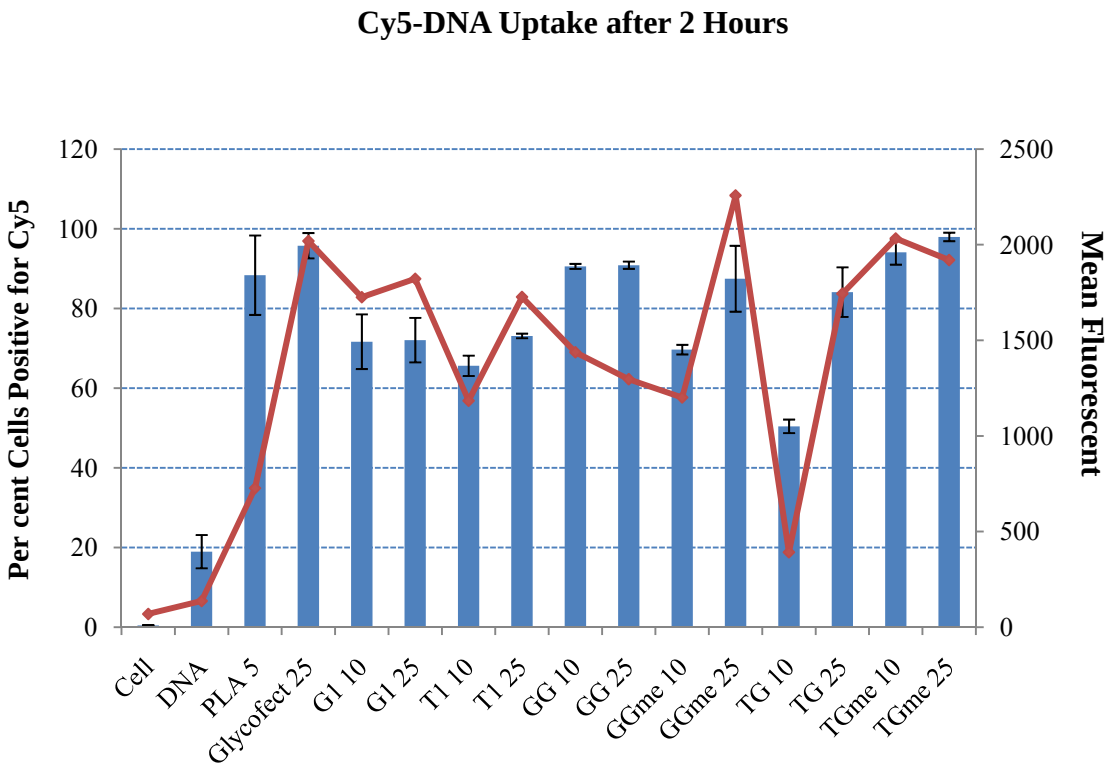

Figure 5.5 Cellular uptake of Cy-5 labeled PGAG and PGAA polymer series complexed with pDNA at *N/P* ratio 10 and 25 in HeLa cells. Cells only and DNA only are used as negative controls. Glycofect^{TM} (*N/P* 25) was used as positive control. Poly-l-arginine (PLA) was also used as another positive control as this is a guanidine containing commercially available polymer. The bars represent the per cent cells positive for Cy-5 fluorescence and line represents mean fluorescence intensity of the cells.

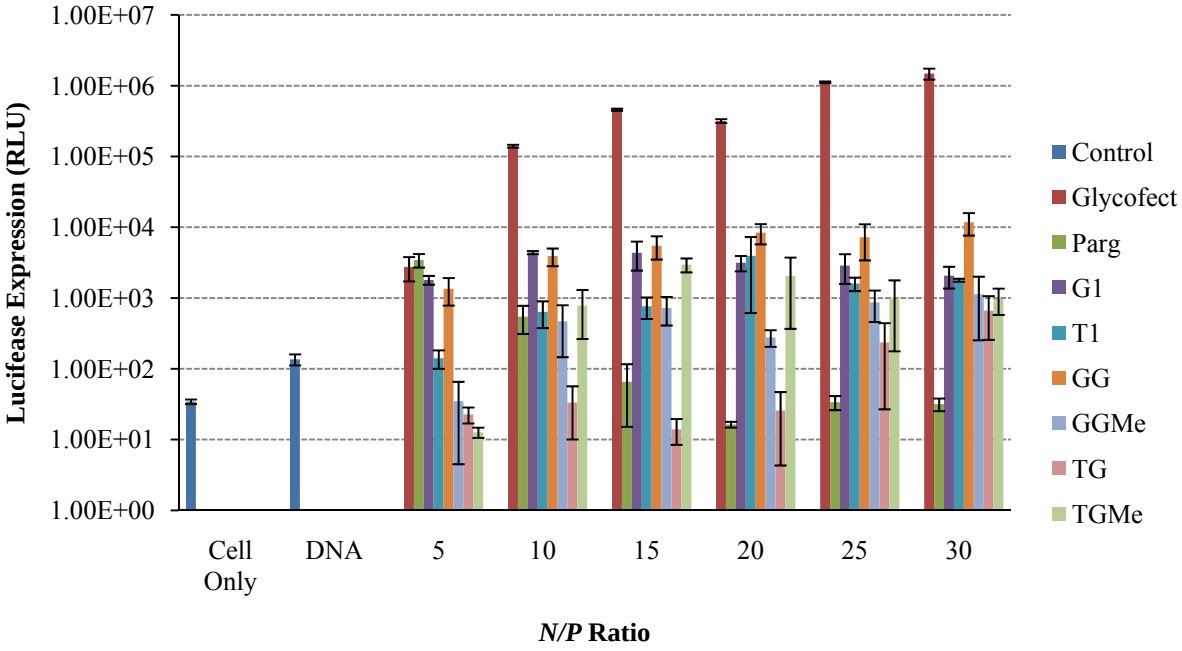

Figure 5.6 Luciferase gene expression observed with polyplexes formed with PGAG, PGAA series and Glycofect, poly-L-arginine (positive controls). The polyplexes are formed at different *N/P* ratios from 5 to 30. The gene expression values are shown as relative light units (RLU). The data is reported as the mean standard of deviation of three replicates.

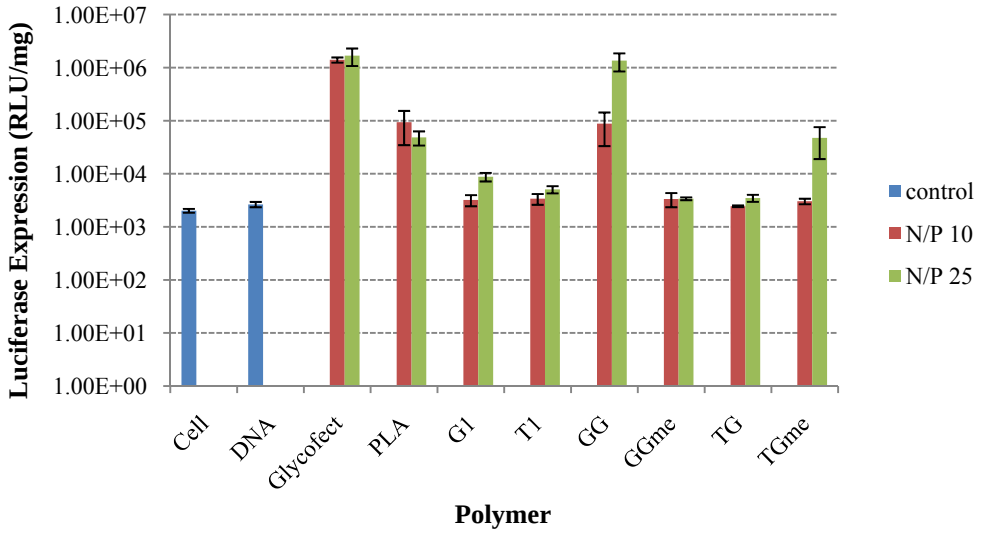

Figure 5.7 Luciferase gene expression observed with polyplexes formed with PGAG, PGAA series and Glycofect, poly-L-arginine (positive controls). The polyplexes are formed at *N/P* ratio 10 and 25. The gene expression values are shown as relative light units per milligram of protein (RLU/mg). The data is reported as the mean standard of deviation of three replicates.

Luciferase reporter gene expression assay were carried out in order to characterize how efficiently guanidine containing polymers can deliver pDNA to HeLa cells, and is quantified by the amount of luciferase gene expression of cells for each polymer. The luciferase assay carried in the serum (Figure 5.6) shows that PGAGs increase the luciferase with increase in the *N/P* ratios from 5 to 30. Within all *N/P* ratios, 10 and 25 are the most representative results. Compared to low molecular weight **G1** and **T1**, GG, GGme and TGme have similar gene expression level. However, TG barely showed gene expression at *N/P* ratio 10, and showed a lower expression level at *N/P* ratio 25 compared to other guanidine containing polymers, **G1** and **T1**. It is also interesting that GG has a higher gene expression level than GGme, while, a reverse trend was observed for the tartarate based guanidine containing polymer (TGme better than TG). Glycofect^{TM}, as a positive control for gene expression, showed much higher gene expression at all *N/P* ratios. Poly-L-arginine (PLA) showed decreasing expression level due to its high cytotoxicity. For gene expression studies done in serum medium at *N/P* 10 and 25 (Figure 5.7), the protein assay shows that all polyplexes are non-toxic. For expression results, Glycofect^{TM} showed highest and similar gene expression results. While **G1**, **T1**, GGme and TG barely showed any luciferase expression. It is noticeable that GG shows increasing luciferase expression from *N/P* 10 to 25. Also, at *N/P* 25, GG gave a competitive result compared to Glycofect^{TM}.

Cell viability of the all the polymers were characterized by MTT assay with HeLa cells. As shown in Figure 5.8, both PGAG and PGAA series exhibit a non-toxic behavior and more than 90 % of the cells are viable at all the *N/P* ratio from 5 to 30 over the 48 hours of transfection. The positive control Glycofect^{TM} shows the similar high non-toxic behavior as the PGAGs. Poly-L-Arginine (PLA) is a commercially available polymer which incorporates guanidine group in the each repeat unit as pendant and also have been studied as the DNA delivery vehicle in the

previous studies as shown in the literature. In this study PLA was shown to be very toxic and it shows about 80 % cell viability at *N/P* ratio 5 and the cell viability drastically decreased to about 16 % as the *N/P* ratio increased to 20 and above. In addition, the guanidine containing polymers used as the DNA delivery vehicle in the literature also show a very toxic behavior. The incorporation of the carbohydrate group in addition to the guanidine group in each repeat unit in case of PGAGs results in very low toxicity.

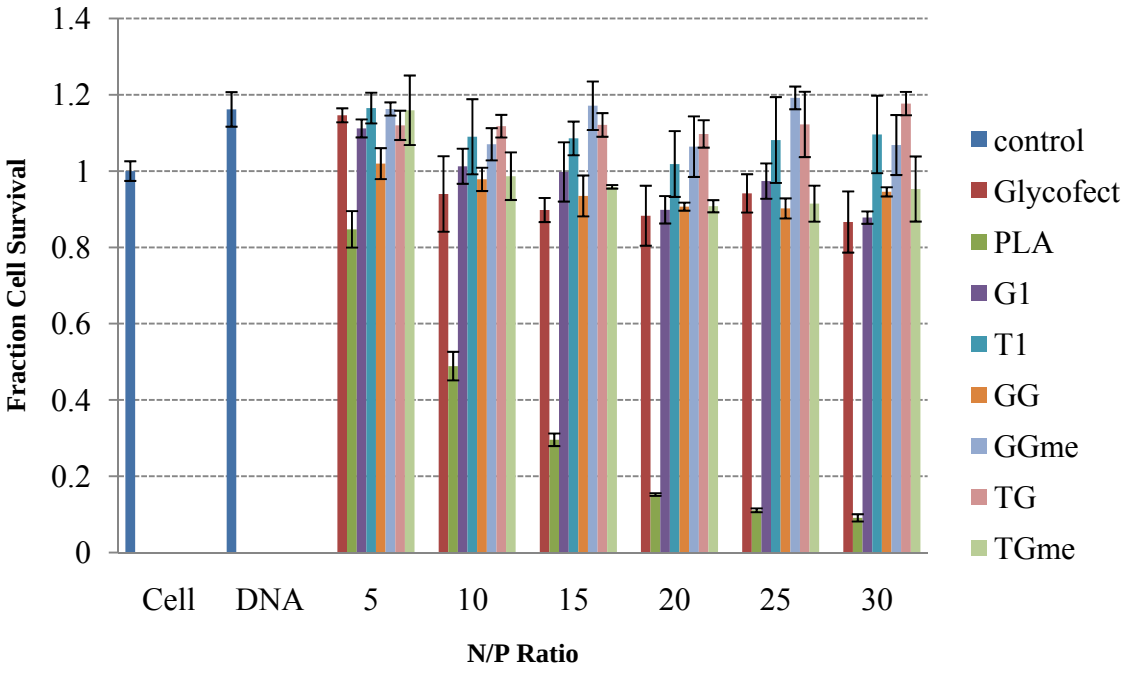

Figure 5.8 Fraction of cell survival in HeLa cells transfected with polyplexes formed with pDNA and each Poly(glycoamidoguanine)s (PGAGs) and PGAAs, Glycofect, and poly-L-arginine at different *N/P* ratio from 5 to 30 in the absence of serum. The fraction cell survival is normalized to the untransfected cells. DNA only was also used as the positive control.

5.5 Conclusions

Poly(glycoamidoamine)s (PGAAs) synthesized before show high pDNA delivery in non-toxic manner in mammalian cell lines. This series is rationally designed to incorporate one oligoamine and carbohydrate unit in the repeat unit. In order to design new materials, it is important to

understand the reasons for the high efficiency of the delivery vehicles. For this purpose, we are interested in synthesizing second generation PGAAs to understand the structure-bioactivity of the delivery vehicles. Lee et al. in past have shown that increase in the number of secondary amine in the repeat unit of PGAAs does not further increase the transgene expression but increases the toxicity [2]. In this study we have synthesized a analogues series of polymers poly(glycoamidoguanine)s (PGAGs), which contain guanidine as a charge type as compared to the amine as charge type in the PGAAs. As guanidine group is protonated at the physiological pH, incorporation of the guanidine groups in the polymer chain was assumed to have different affinity towards pDNA. The polyplexes from PGAGs show binding at low *N/P* ratio and form ~100 nm particles when complexed with pDNA as characterized from gel electrophoresis shift assay and DLS and the results are consistent with the previously reported guanidine containing polymers [25, 26]. The previously reported guanidine containing polymer in the literature show high toxicity although incorporation of the carbohydrate unit attached to the guanidine moiety via amide bond in the PGAGs make the polyplexes absolutely non-toxic as characterized from the MTT assay.

PGAGs show high cellular uptake in the HeLa cells as compared to the amine containing analogues (**G1** and **T1**). The higher cellular uptake of PGAGs can be attributed to the guanidine groups on the polymers as the guanidine groups can assists the polyplex endocytosis as reported earlier [25, 26]. The higher cellular uptake of PGAG polyplexes than PGAAs only results in the comparable transgene expression PGAGs with PGAAs, suggesting barrier to the nuclear transport of PGAG polyplexes. A delivery vehicle which can provide barrier to the transport of the polyplexes to the nucleus can be efficiently used as a siRNA delivery vehicle. Also, PGAGs do not provide any buffering capacity to the polymers as the guanidine groups are hard charges on the polymer backbone. PGAG polyplexes, according to proton sponge hypothesis should not

escape the endosomes although the comparable transgene expression of PGAGs to PGAAs suggests that the PGAG polyplexes escape the endosome and are released in the cytoplasm and are transported to the nucleus.

5.6 - Useful NMRs and mass spectrum

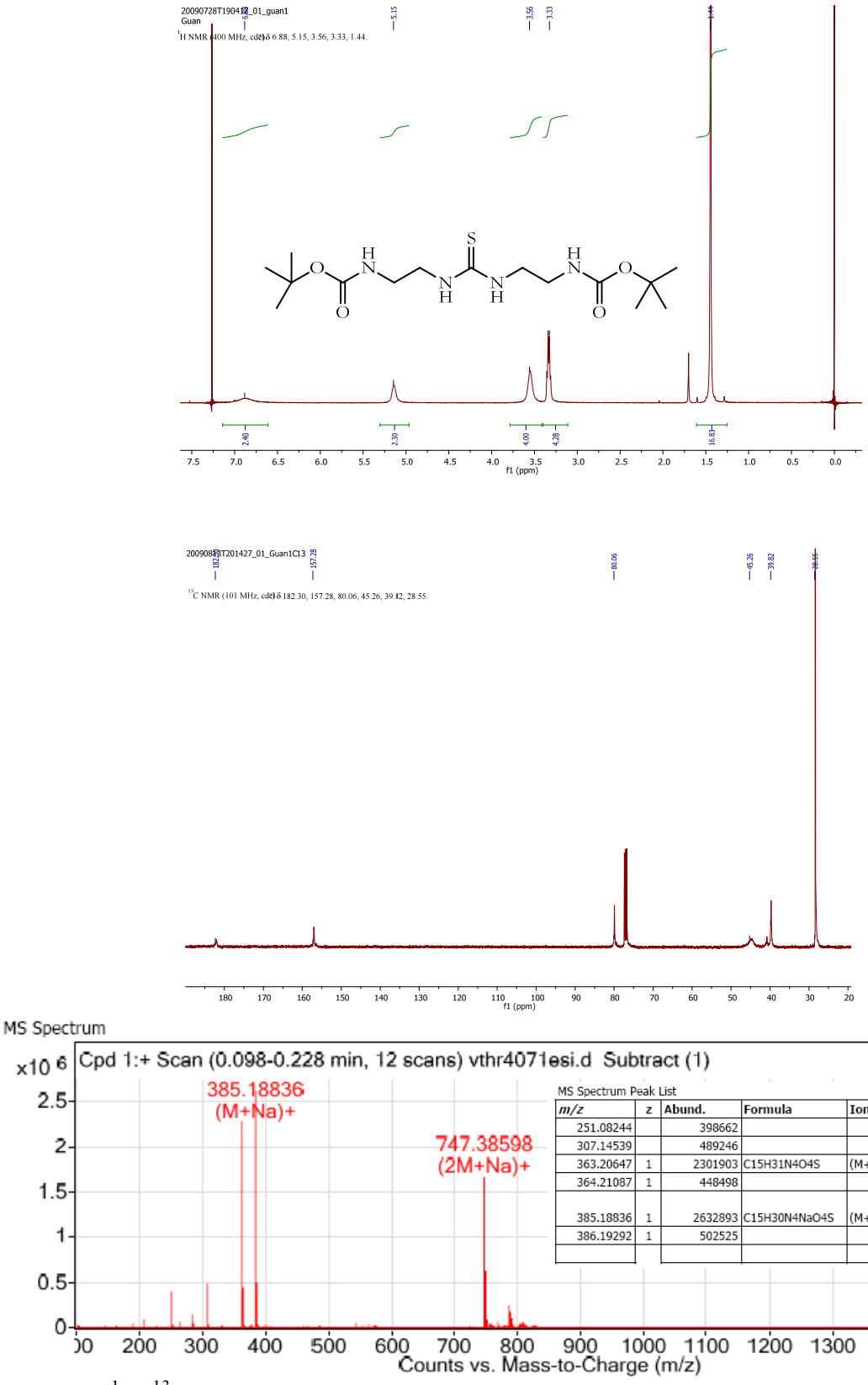

MS Spectrum Peak List

m/z	z	Abund.	Formula	Ion	Diff(ppm)
251.08244		398662			
307.14539		489246			
363.20647	1	2301903	C15H31N4O4S	(M+H)+	1.15
364.21087	1	448498			
385.18836	1	2632893	C15H30N4NaO4S	(M+Na)+	0.94
386.19292	1	502525			

Figure 5.9 ^{1}H, ^{13}C NMR and ESI-MS for 2

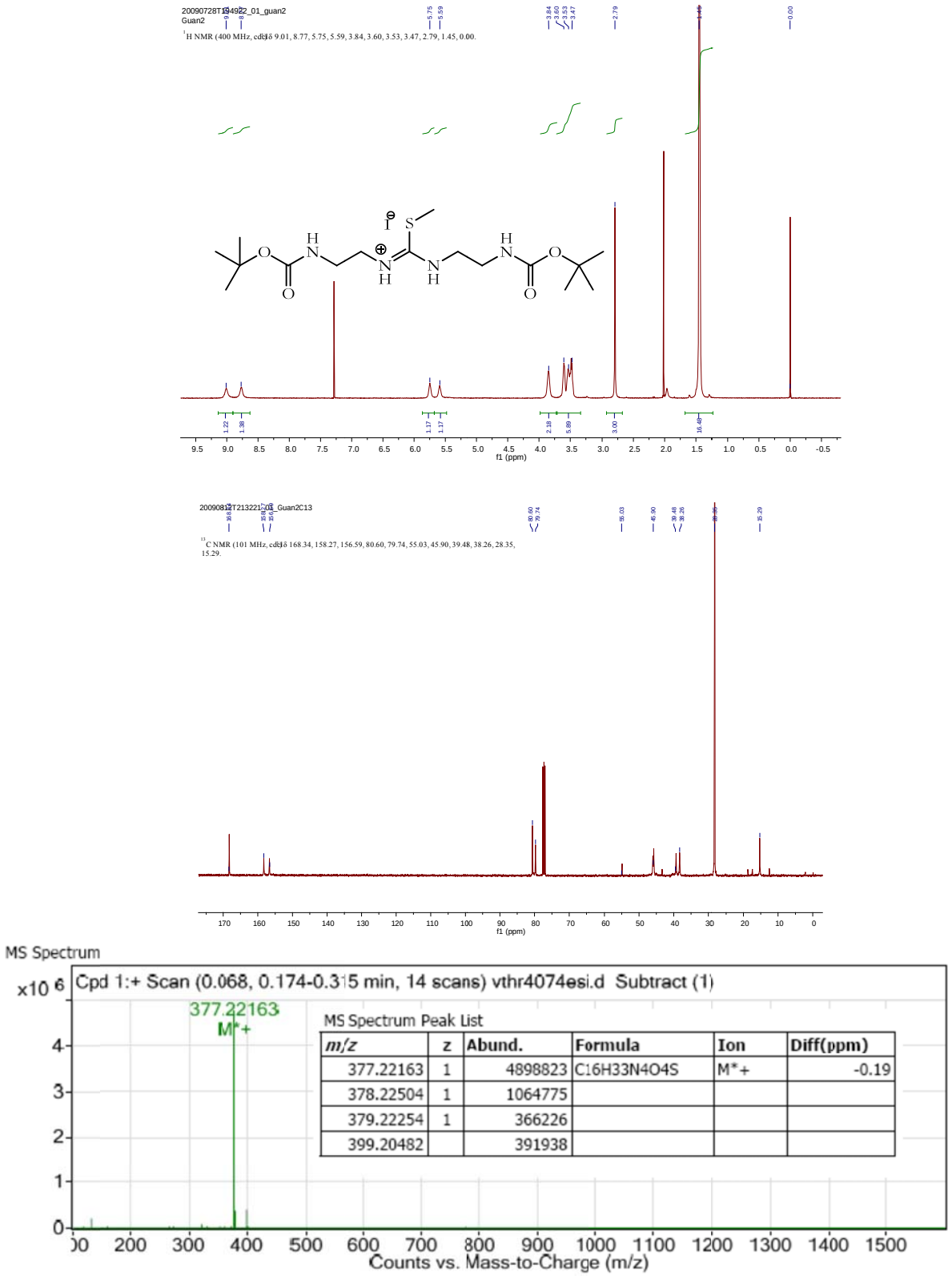

Figure 5.10 ^{1}H, ^{13}C NMR and ESI-MS for 3

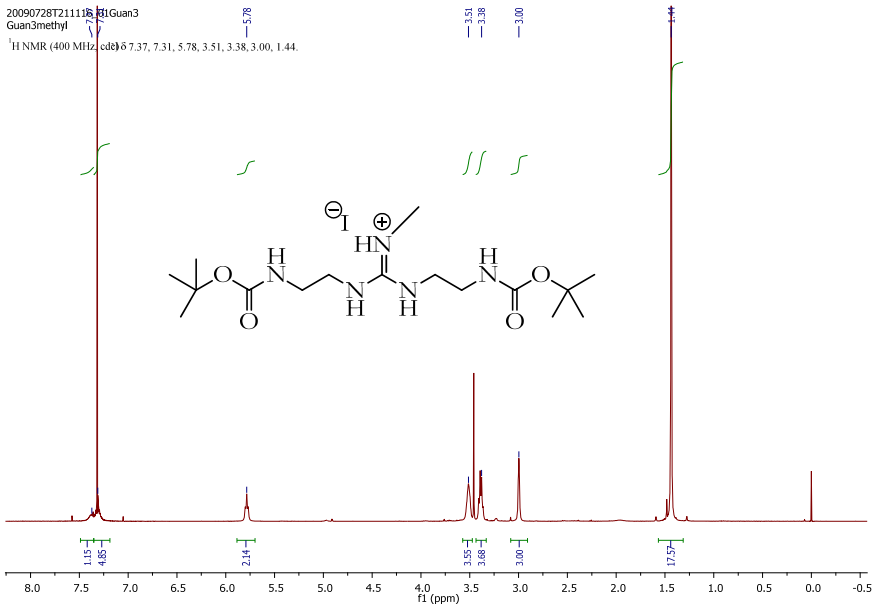

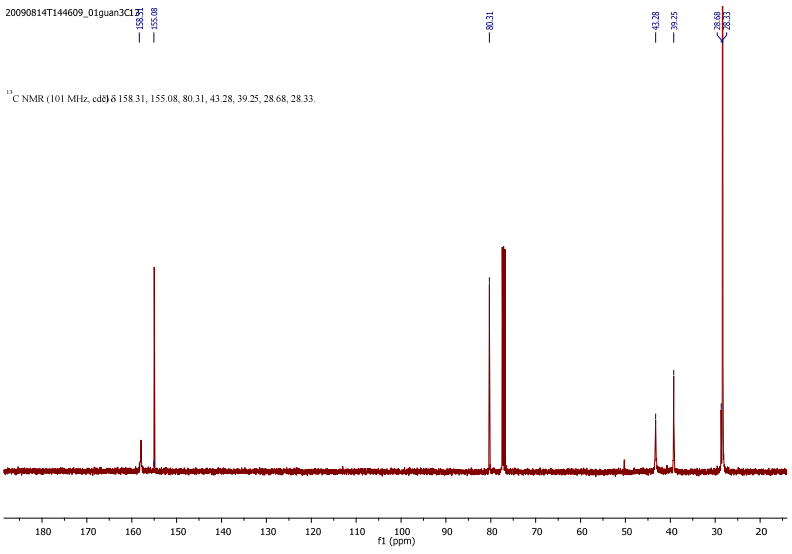

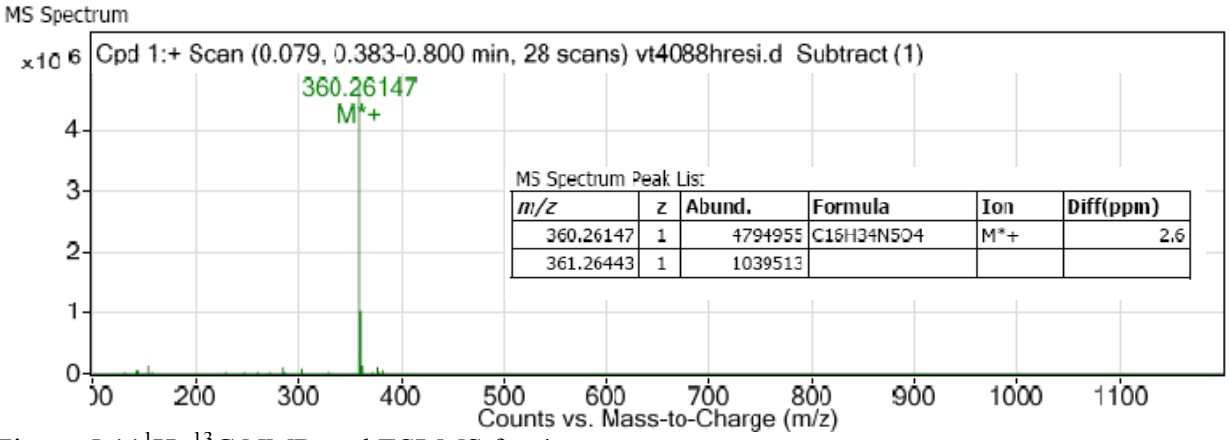

Figure 5.11 ^{1}H, ^{13}C NMR and ESI-MS for 4

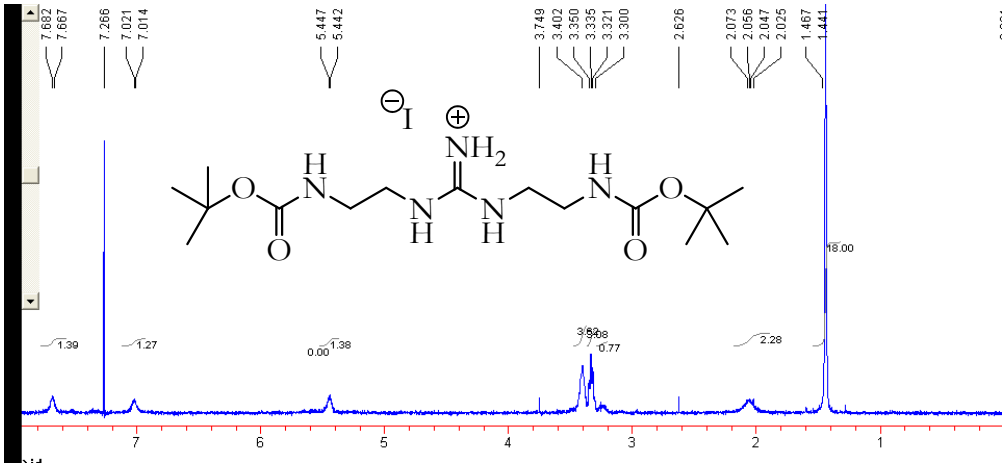

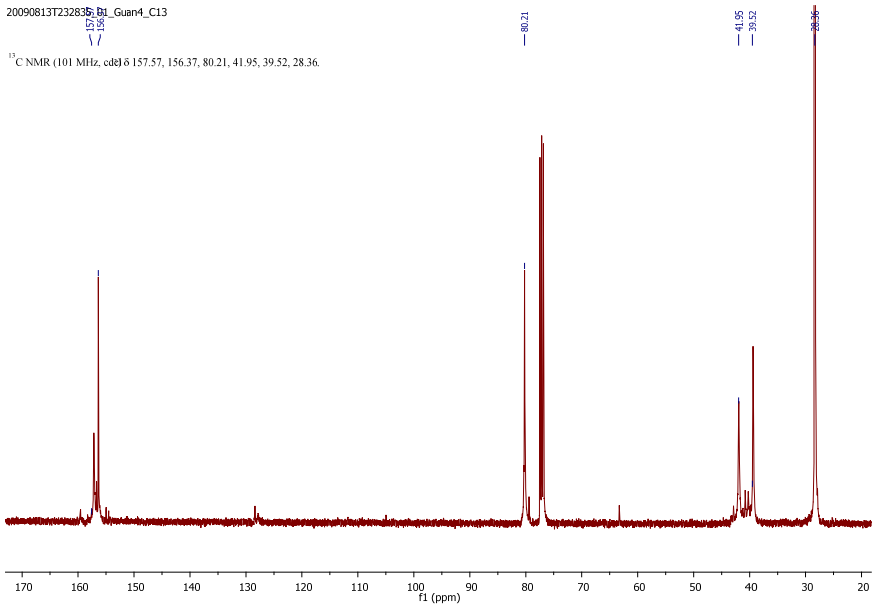

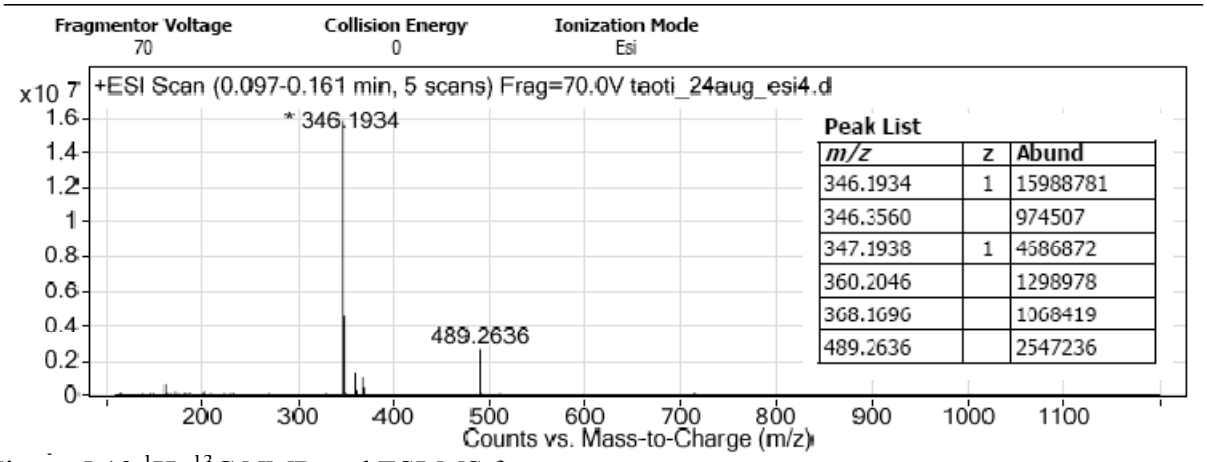

Figure 5.12 ^{1}H, ^{13}C NMR and ESI-MS for **5**

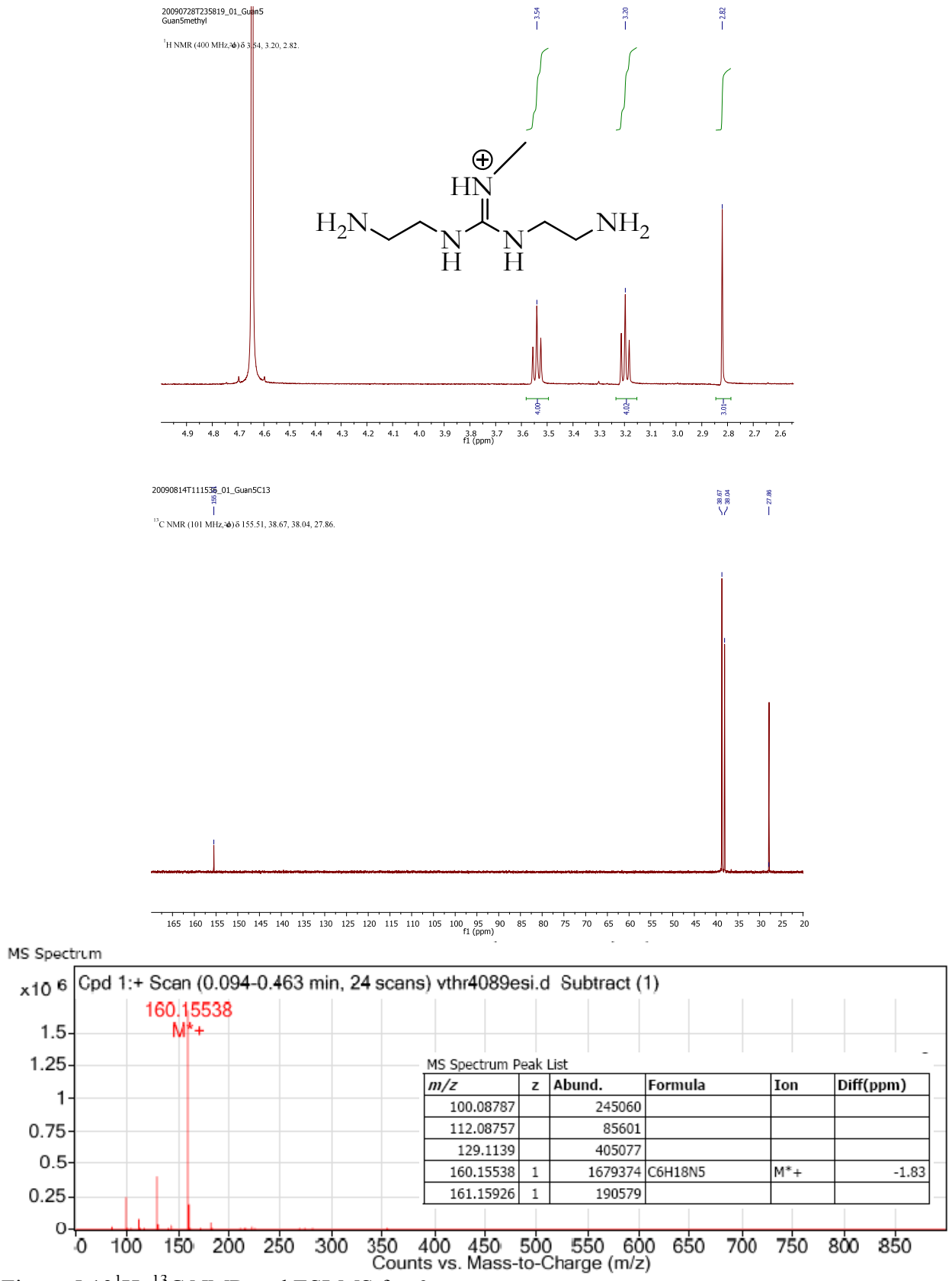

Figure 5.13 ^{1}H, ^{13}C NMR and ESI-MS for 6

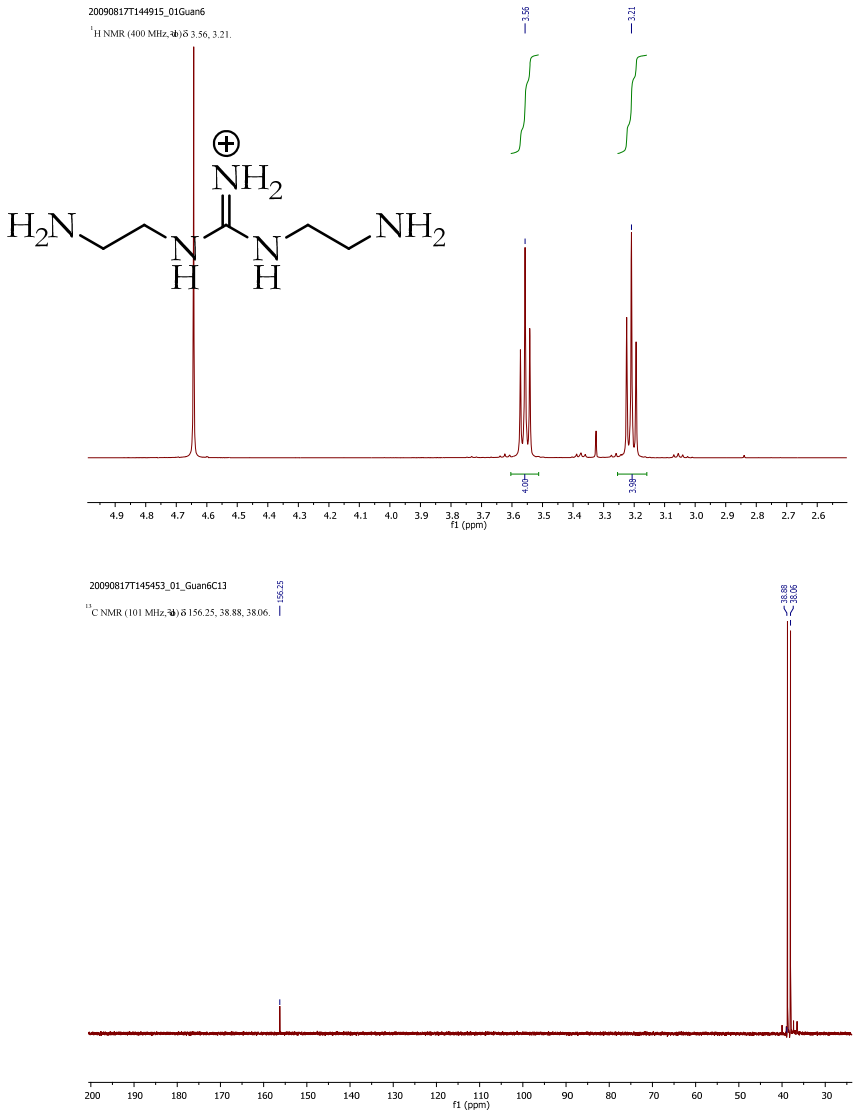

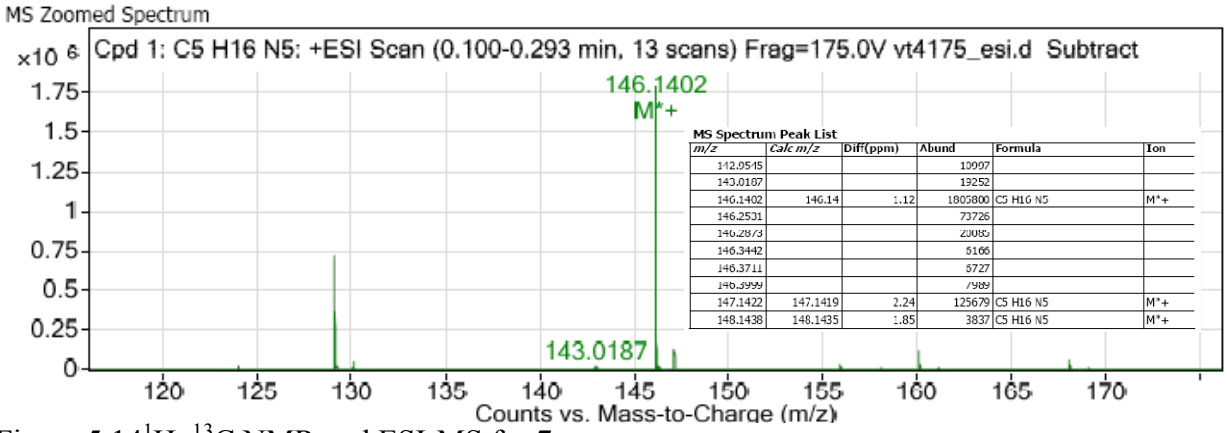

Figure 5.14 ^{1}H, ^{13}C NMR and ESI-MS for 7

5.7 - References

[1] Davis ME, Zuckerman JE, Choi CHJ, Seligson D, Tolcher A, Alabi CA, Yen Y, Heidel JD, Ribas A. Evidence of RNAi in humans from systemically administered siRNA via targeted nanoparticles. NATURE 2010;464:1067-1070.

[2] Lee CC, Liu Y, Reineke TM. General structure-activity relationship for poly(glycoamidoamine)s: The effect of amine density on cytotoxicity and DNA delivery efficiency. Bioconjugate Chemistry 2008;19:428-440.

[3] Liu Y, Reineke TM. Hydroxyl stereochemistry and amine number within poly(glycoamidoamine)s affect intracellular DNA delivery. J. Am. Chem. Soc. 2005;127:3004-3015.

[4] Liu YM, Wenning L, Lynch M, Reineke TM. New poly(D-glucaramidoamine)s induce DNA nanoparticle formation and efficient gene delivery into mammalian cells. Journal of the American Chemical Society 2004;126:7422-7423.

[5] Liu YM, Wenning L, Lynch M, Reineke TM. Gene delivery with novel poly(1-tartaramidoamine)s. Polymeric Drug Delivery I: Particulate Drug Carriers, vol. 923. 2006. p.217-227.

[6] Liu Y, Reineke TM. Degradation of Poly(glycoamidoamine) DNA Delivery Vehicles: Polyamide Hydrolysis at Physiological Conditions Promotes DNA Release. Biomacromolecules 2010;11:316-325.

[7] Taori VP, Liu YM, Reineke TM. DNA delivery in vitro via surface release from multilayer assemblies with poly(glycoamidoamine)s. Acta biomaterialia 2009;5:925-933.

[8] Allende D, Simon SA, McIntosh TJ. Melittin-induced bilayer leakage depends on lipid material properties: evidence for toroidal pores. Biophys. J. 2005;88:1828-1837.

[9] Yang L, Harroun TA, Weiss TM, Ding L, Huang HW. Barrel-stave model or toroidal model? A case study on melittin pores. Biophys. J. 2001;81:1475-1485.

[10] Fattal E, Nir S, Parente RA, Szoka Jr FC. Pore-forming peptides induce rapid phospholipid flip-flop in membranes. Biochemistry 1994;33:6721.

[11] Medina-Kauwe LK, Xie J, Hamm-Alvarez S. Intracellular trafficking of nonviral vectors. Gene Therapy 2005;12:1734-1751.

[12] Gabrielson NP, Pack DW. Acetylation of polyethylenimine enhances gene delivery via weakened polymer/DNA interactions. Biomacromolecules 2006;7:2427-2435.

[13] Behr JP. The proton sponge: a trick to enter cells the viruses did not exploit. CHIMIA International Journal for Chemistry, 51 1997;1:34-36.

[14] Boussif O, Lezoualc'h F, Zanta MA, Mergny MD, Scherman D, Demeneix B, Behr JP. A versatile vector for gene and oligonucleotide transfer into cells in culture and in vivo: polyethylenimine. Proceedings of the National Academy of Sciences of the United States of America 1995;92:7297.

[15] Liu Y, Reineke TM. Poly(glycoamidoamine)s for gene delivery. Structural effects on cellular internalization, buffering capacity, and gene expression Bioconjugate. Chem. 2007;18:19-30.

[16] Liu Y, Wenning L, Lynch M, Reineke TM. New poly(D-glucaramidoamine)s induce DNA nanoparticle formation and efficient gene delivery into mammalian cells. J. Am. Chem. Soc. 2004;126:7422-7423.

[17] Liu YM, Reineke TM. Poly(glycoamidoamine)s for gene delivery: Stability of polyplexes and efficacy with cardiomyoblast cells. Bioconjugate Chemistry 2006;17:101-108.

[18] Prevette LE, Kodger TE, Reineke TM, Lynch ML. Deciphering the role of hydrogen bonding in enhancing pDNA-Polycation interactions. Langmuir 2007;23:9773-9784.

[19] McLendon PM, Fichter KM, Reineke TM. Poly (glycoamidoamine) Vehicles Promote pDNA Uptake through Multiple Routes and Efficient Gene Expression via Caveolae-Mediated Endocytosis. Molecular Pharmaceutics:259-302.

[20] Kolonko EM, Pontrello JK, Mangold SL, Kiessling LL. General Synthetic Route to Cell-Permeable Block Copolymers via ROMP. J. Am. Chem. Soc 2009;131:7327-7333.

[21] Reineke TM, Davis ME. Structural effects of carbohydrate-containing polycations on gene delivery. 1. Carbohydrate size and its distance from charge centers. Bioconjugate Chemistry 2003;14:247-254.

[22] Reineke TM, Davis ME. Structural effects of carbohydrate-containing polycations on gene delivery. 2. Charge center type. Bioconjugate Chemistry 2003;14:255-261.

[23] Sambrook MR, Beer PD, Wisner JA, Paul RL, Cowley AR, Szemes F, Drew MGB. Anion-templated assembly of pseudorotaxanes: importance of anion template, strength of ion-pair thread association, and macrocycle ring size. J. Am. Chem. Soc 2005;127:2292-2302.

[24] Lucas RL, Benjamin M, Reineke TM. Comparison of a Tartaric Acid Derived Polymeric MRI Contrast Agent to a Small Molecule Model Chelate. Bioconjugate Chem 2008;19:24-27.

[25] Kim T, Lee M, Kim SW. A guanidinylated bioreducible polymer with high nuclear localization ability for gene delivery systems. Biomaterials 2009.

[26] Funhoff AM, van Nostrum CF, Lok MC, Fretz MM, Crommelin DJA, Hennink WE. Poly (3-guanidinopropyl methacrylate): a novel cationic polymer for gene delivery. Bioconjugate Chem 2004;15:1212-1220.

Chapter 6

Future Directions

6.1 - Introduction

This dissertation attempts to contribute to the scientific community, specifically interested in the advanced biomaterials. This chapter is devoted to the detailed research and applications that can be derived from the science explored here.

6.2 - Exploring the hydrolysis phenomenon in the galactarate based compounds.

As motioned in the chapter 3, *meso*-galactarate based polymers such as **G4** also show degradation. The degradation of few key *meso*-galactarate based models have been studied as a part of this dissertation and the observed hydrolysis of these key models are different in comparison with the tartarate based models. Model **a** shows hydrolysis on both sides in contrast to one side hydrolysis observed in model **d**. Model **b** does not show any hydrolysis in contrast to hydrolysis observed in model **e**. In case of galactarate based models, c shows very slow hydrolysis, in contrast, tartarate based analogue **f** do not show any hydrolysis over 500 hours.

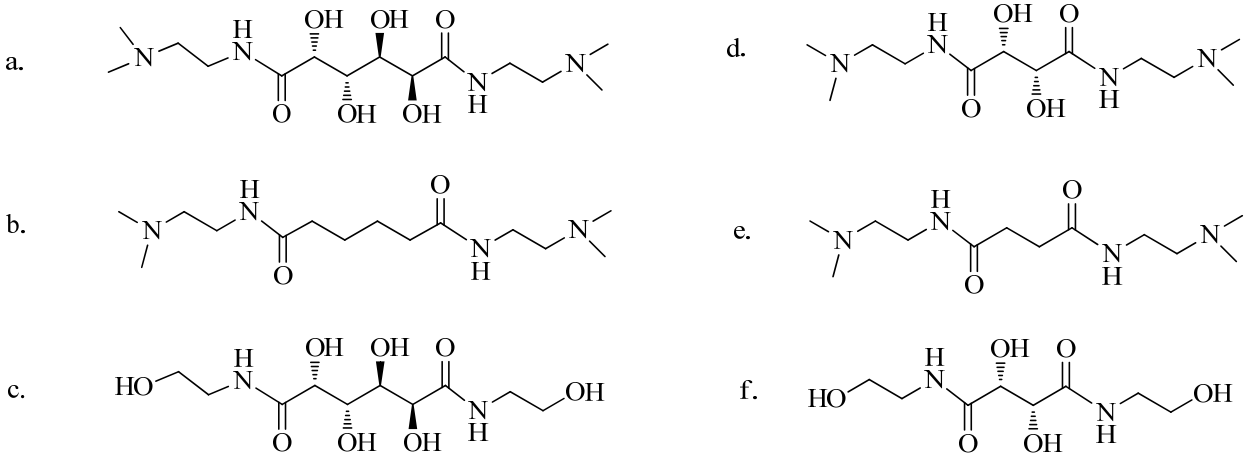

Figure 6.1 Structures of small models based on galactarate and adipate in comparison with small model based on tartarate and succinate models. 1) Model **a** shows hydrolysis on both sides in contrast to one side hydrolysis observed in model **d**; 2) Model **b** does not show any hydrolysis in contrast to hydrolysis observed in model **e**; 3) In case of galactarate based models, **c** shows very slow hydrolysis, in contrast, tartarate based analogue **f** do not show any hydrolysis. Observation are based upon the time period of 500 hours.

The results imply that the amide hydrolysis mechanism for the galactarate based models is different as compared to the other amide hydrolysis studied in this dissertation and it is important to explore this interesting chemistry also. Figure 6.2 shows different models that can be studied for its hydrolysis as explained for the tartarate based compounds. The results from this study can give insights into the design of new experiment in order to understand the mechanism. This mechanism upon understood can be applied in various systems for better designs.

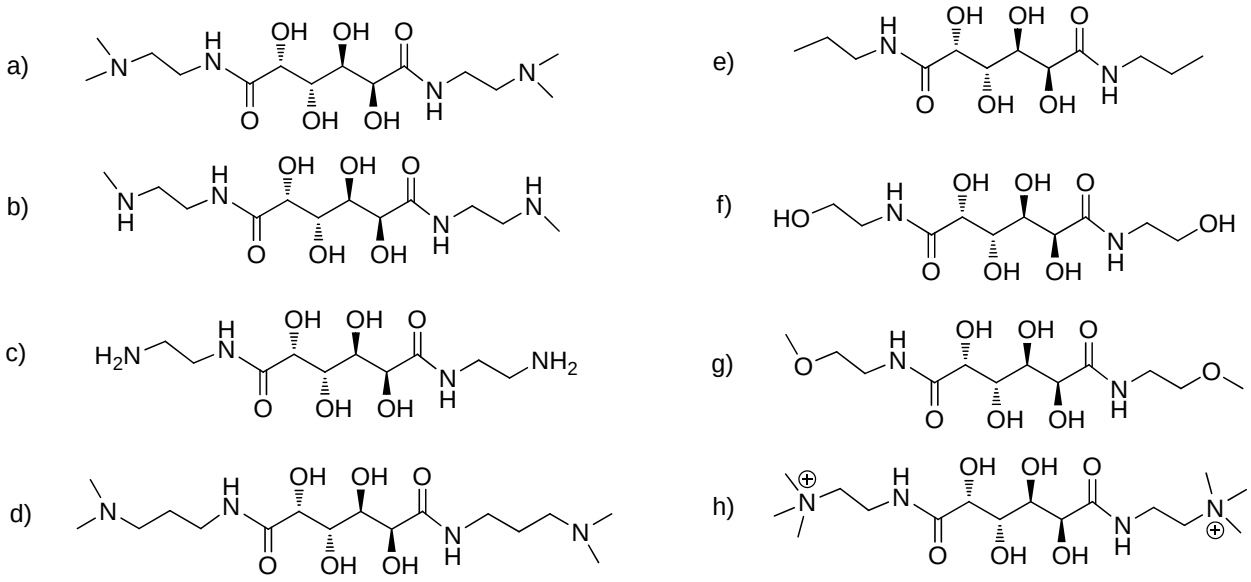

Figure 6.2 Structures of galactarate based small molecule models with varying functionality with respect to the amidic nitrogen in the models

6.3 - New controlled depolymerizing systems in the physiological conditions

Auto Lysing Intramolecular Amide Substrates (ALIAS) are interesting subset of the biomaterials and one of the significant discovery from this dissertation. The chemistry explained in this dissertation can be used to make new polymeric system which can be depolymerized in a very controlled fashion from the terminal ends to produce one small molecule. This systems can be used in the for the controlled release of therapeutics in the biological systems.

As shown in Figure 6.1 dimethyl-L-tartarate can be reacted with ethylenediamine to give tartarate based hydroxylated nylons. These nylons are linear polymers.

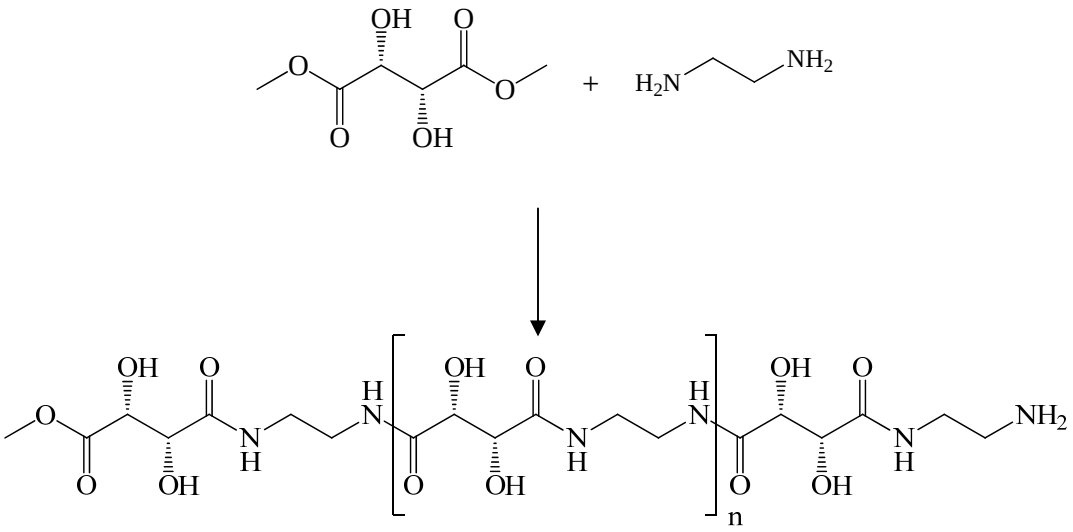

Figure 6.3 Tartarate based hydroxylated nylons (THN)

End capping THN with ester or any other functionality except the amines: The ends of these polymers can either be capped with esters functionality such as lactate or glycolate to yield a non degradable polymer.

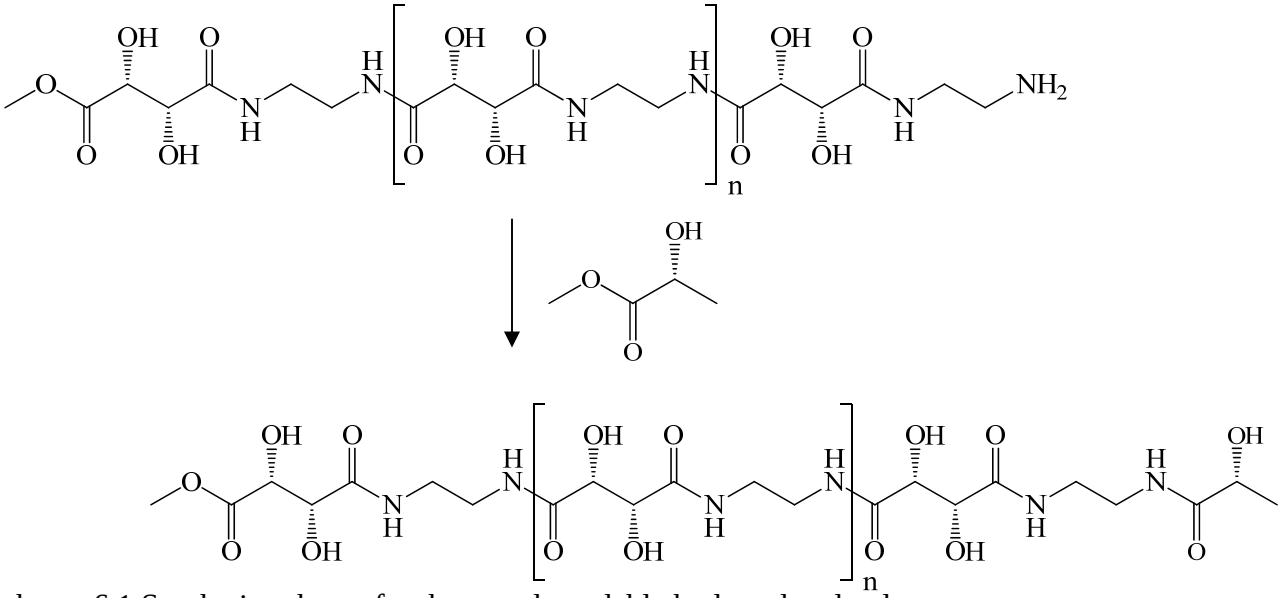

Scheme 6.1 Synthetic scheme for the non-degradable hydroxylated nylons

Self immolating polymers:

Self immolating polymers are a very interesting concept due to its ability to depolymerize [1]. Depolymerization is a very elegant process utilized by the biological systems in order to break down the long chain protein into its amino acids. Also depolymerization can occur in two different ways.

Random degradation: In case of polyesters the hydrolysis can start at any ester bond which will break the polymer into small molecules at random sites on the backbone.

Controlled depolymreization: A straight chain polymer with zero degree of branching if starts degrading at the ends to give two small molecules and the new polymer with two reduced repeat unit with terminal ends which are capable of introducing the same chemistry to degrade the polymer can produce the self immolating polymer

End capping THN with amine functionality

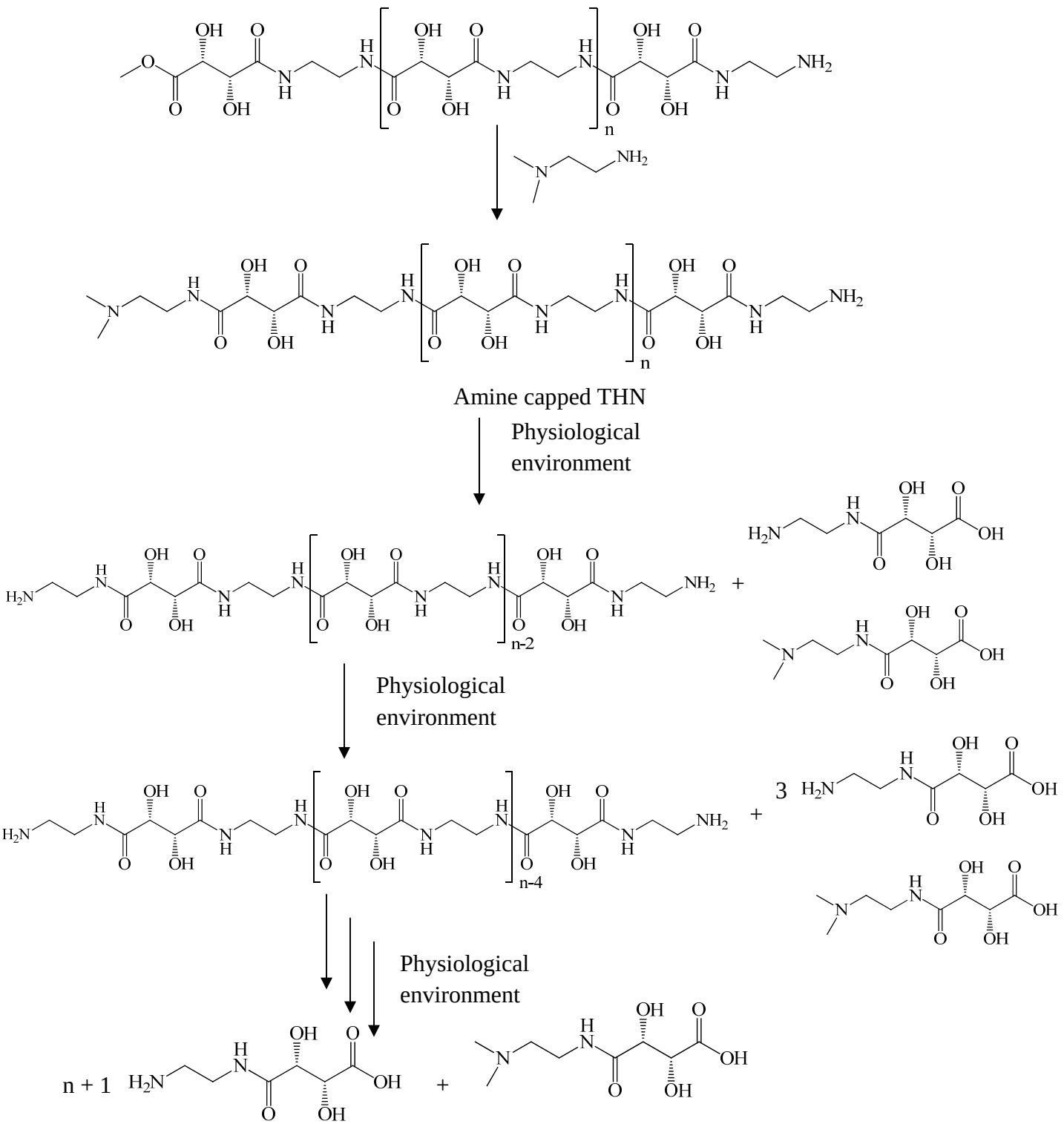

Scheme 6.2 Synthesis and mechanism of self immolating hydroxylated nylons

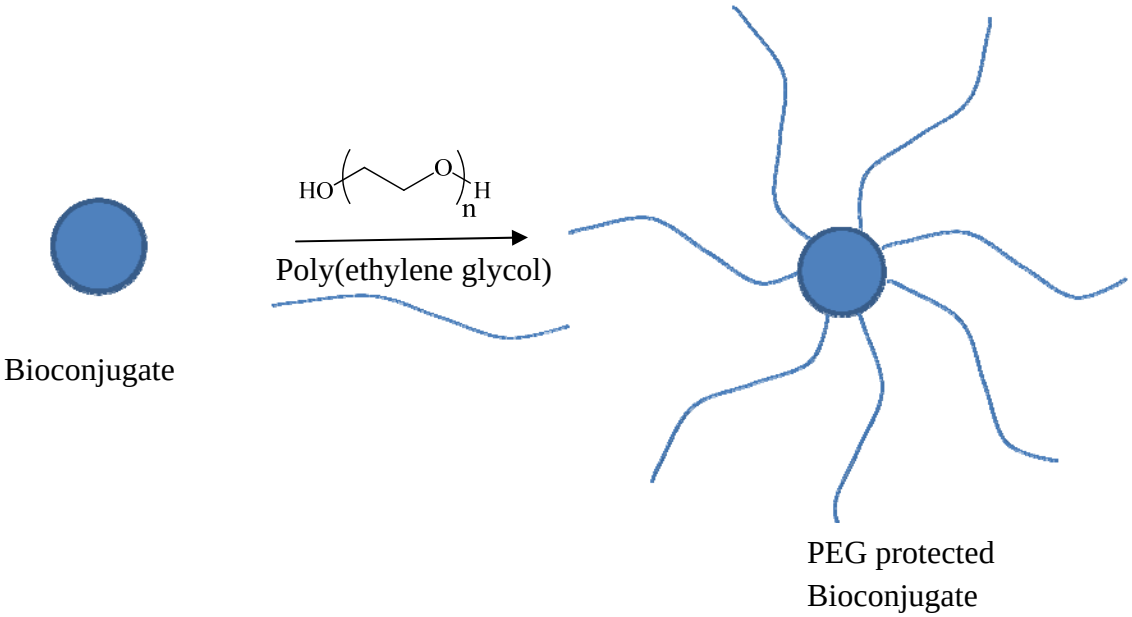

Figure 6.4 Bioconjugates protected with PEG groups in order to increase the therapeutic efficiency

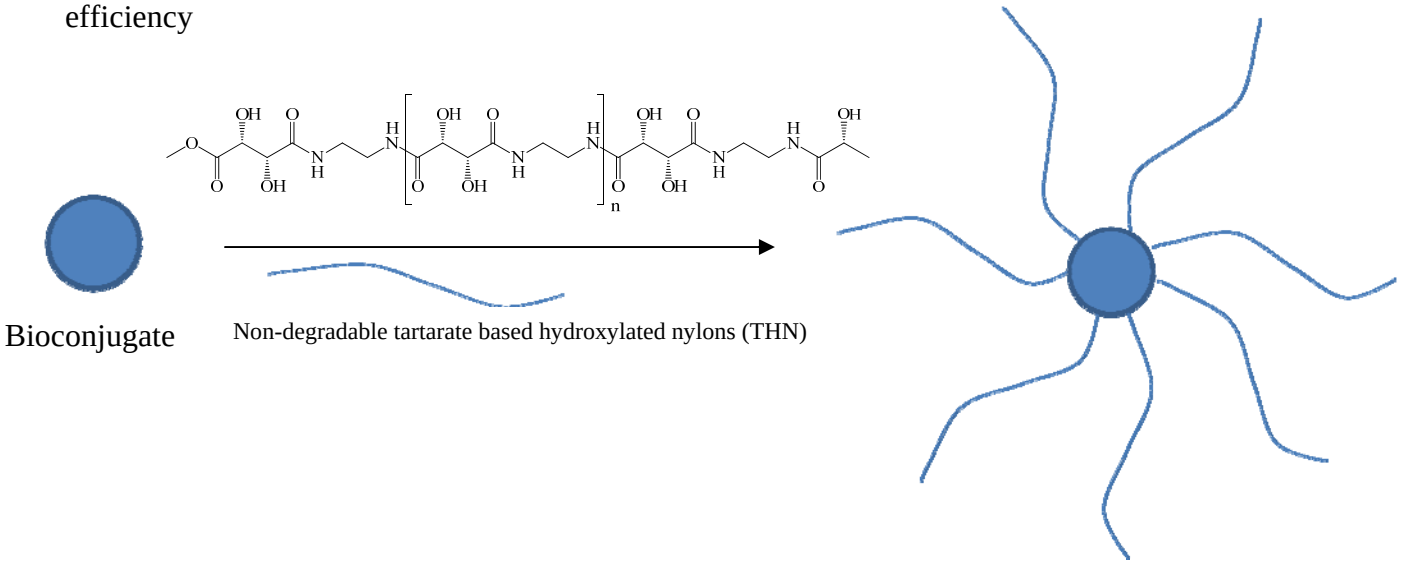

Figure 6.5 Bioconjugates protected with THN

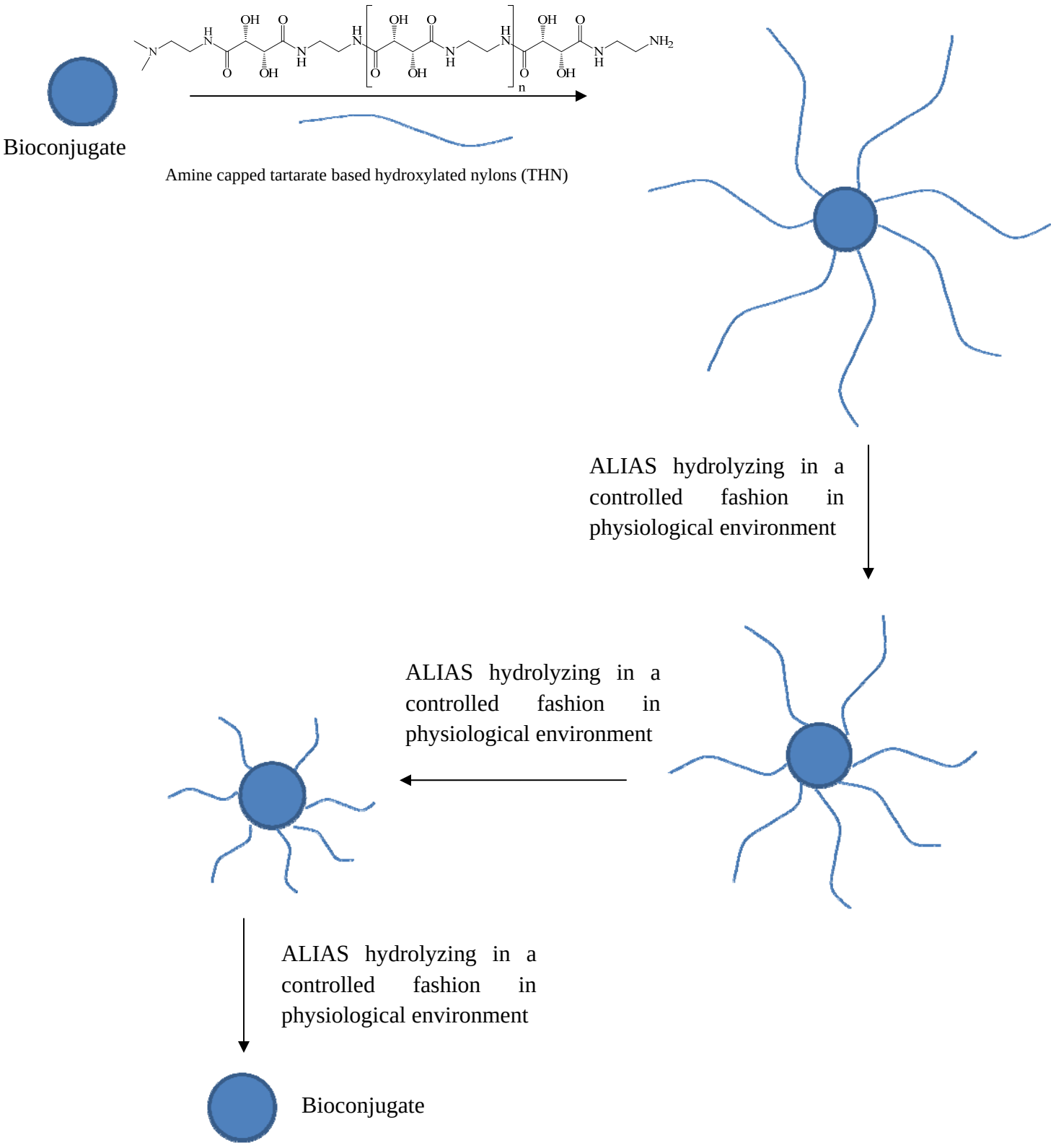

Figure 6.6 self immolating polymer to increase the protection of the bioconjugates as well as the increasing the bioavailability of the bioconjugates in the controlled fashion

As shown in the above Figures and Schemes, a self immolating hydroxylated nylon has a potential of controlled depolymerization . Depolymerization can further controlled by using different starting materials such as 1,3-diaminopropane instead of ethylenediamine. This property can have numerous applications. one of the most important application is depicted in the Figure 6.6 and Scheme 6.2, where these polymers can be used to protect the bioconjugates from getting cleared from the reticuloendothelial system (RES) but also provides ability for these polymers to depolymerize to increase the bioavailability of the bioconjugates.

6.4 - References

[1] Wang W, Alexander C. Self-Immolative Polymers. Angewandte Chemie International Edition 2008;47:7804-7806.